DTU Mechanical Engineering
Department of Mechanical Engineering

Natural convection cooled LEDs

Modeling measurements and experimental setup for natural convection cooled LEDs

Student
Hjalmar Danielsen
s134156

Supervisors
Associate Professor Niels Aage
Senior Researcher Boyan Stefanov Lazarov

Co-Supervisor
Associate Professor Knut Erik Meyer

Department of Mechanical Engineering
Technical University of Denmark
Date: 28/02-2017

Abstract

Light emitting diodes (LED) are one of the most energy efficient light sources on today's market, yet only 5%-40% of the electricity consumed goes towards light production. The remaining part goes to producing waste heat. The warmer the LED junction becomes, the worse it performs. With natural convection cooling at the LED through the use of heat sinks, higher performance can be achieved and electric power saved.

This project optimizes heat sink geometry as a natural convection cooler by assessing the FEM software Comsol's ability to predict heat transfer in and around an LED heat sink. Finding a valid methodology in Comsol will enable companies to better optimize the performance of a heat sink, saving time and money in the process. In this project, experimental temperatures of an aluminum heat sink in vertical, horizontal, and 45° positions were compared to temperatures conducted in Comsol simulations. The experiments were conducted with power inputs of 1 watt, 2 watts, 3 watts, 4 watts, and 5 watts. The lowest temperature difference found between experiment and simulation was at the 2 watts vertical HS position. Here, the experimental ΔT(difference between ambient temperature and temperature at heat sink junction) and the same measurement in the simulation were only 0.02℃ apart, at 11.08℃ and 11.099℃, respectively. The greatest difference was 1.61℃ at 5 watts vertical heat sink position. This time, the experiment had a temperature of 23.8℃ and the simulation of 22.193℃. The best performing Comsol model was on average 0.52℃ from the experimental temperatures. In conclusion, the model resembles the experiments well, but that there is room for improvement.

Lastly, optimization of the tested heat sink was investigated in Comsol. The study showed that extending the fins by 20 mm improved performance by 4.9%, and increasing the number of fins from 16 to 18 improved the performance by 1.6%. However, there is uncertainty with these measurements when the fins are, on average, 2.35℃ lower in the experiments than in the simulations.

Preface

This thesis is submitted in fulfillment of the requirements for obtaining my Bachelor of Engineering degree in Mechanical Engineering at the Technical University of Denmark (DTU). The project has been carried out at the Department of Mechanical Engineering at DTU during the period August 29th 2016 - February 28th 2017. The main supervisors on the project were Associate Professor Niels Asge and Senior Researcher Ph.D. Boyan S. Lazarov, and the co-supervisor was Associate Professor Knud Erik Meyer.

First of all, I would like to thank Niels and Boyan for their their support, valuable input, and patience. It has been a privilege to work with two extremely talented and clever engineers, in addition to also being wonderful people.

Next, I would like to thank the MEK workshop for producing the heat sink and for answering all my questions. Also, thanks to Comsol support and DTUs Computer Center Support (HPC) for great guidance. I am really impressed by the outstanding support Comsol provides their customers.

Finally, I would like to express my gratitude to my friends and family for their support. Special thanks to my parents who always are there for me, and to Caroline Eves for her love, support, and encouragement, as well as being my proofreader during this work.

This paper is targeted to an audience with limited knowledge of heat transfer, fluid mechanics and LEDs in general. My own knowledge of the subjects at the start of this project was basic, my only interaction with LEDs and lamps being turning them on and off. I had taken a class in Heat transfer and was enrolled in a Fluid Mechanics class while writing this thesis, helping to broaden my understanding of the underlying physics behind LEDs. Throughout the project, I have been able to explore how heat transfer occurs in LEDs, both in the solid parts and the fluids surrounding the LED.

Before this project, I had no experience working with Comsol and the theory behind the program. The self-teaching was frustration at times when the software did not give the results desired, but with help from Comsol support, I managed to obtain results that reflect/predict the real life experimental results relatively well. My understanding of what is happening behind the displayed results has also improved significantly.

All of the results obtained were found through Comsol simulations over Thinlinc. At the initial stages of this project, Thinlinc was totally new to me, but with help from DTUs HPC support, I was able to get some experience with the program. In the end I was able to submit and run several simulations at a time at DTUs supercomputers (High Performance computers).

An abbreviation list of abbreviations used a lot can be seen in the Appendix A.1.

Contents

1 Introduction

Within the past few decades, research regarding the technology of light, heat, and the interaction between the two, has increasingly become an important subject in the field of mechanical engineering. Light is so much more than just being able to see, it is an important factor in human lives. Light is information on a TV, knowledge learned from computers, energy from the sun, and the beauty of the rainbow. We rely on light to brighten our world, both through man-made and natural sources. Simply put, we humans use light everywhere and for everything. All around the world, engineers are trying to develop the coolest, cheapest, even healthiest lighting to optimize energy efficiency and provide the most eco-friendly lighting options.

Changes in climate have been happening since before humans walked on earth, but the change in the global temperature we see today is remarkable. The global temperature is rising faster than ever because of the emission of greenhouse gasses like CO2, predominantly caused by humans. The world's leaders and governments are beginning to realize the negative impact of CO2 emissions and the damage they can cause [2]. To combat this issue, the first-ever universal, legally binding global climate deal was agreed upon in December 2015 at the Paris Climate Conference (COP21). 195 countries agreed to limit the rise of the global temperature well below 2 degrees above pre-industrial levels within the next century [3, 4].

The European Union has been on the front lines of fighting the issue of global warming, setting targets as early as in 2007 [5]. In 2009, these targets were enacted into legislation. The European Union has committed to a 20% reduction of greenhouse emissions by 2020 compared to the levels in 1990, where 20% of energy should come from renewable sources and the energy efficiency should show an improvement of 20% [6, 7]. To reach these goals, new research and technology is vital, focusing on using fewer chemicals, reusable materials, and more efficient and renewable energy usage. These technological developments will take major strides in lighting up the world with as few negative effects on the environment as possible.

More efficient lighting can reduce the use of electricity significantly, as lighting represents 19% of the electricity consumption worldwide and 14% within the EU [8, 9]. The EU Commission is trying to change these statistics and has implemented regulations to reduce the use of halogen lamps and inefficient incandescent light bulbs and move towards using solid-state lighting (SSL). These regulations will improve the energy efficiency of lighting, taking major steps towards attaining the 2020 goals [10]. SSL is the most energy–efficient and versatile light technology in today's market. 70% of the energy used on lighting today can be reduced by combining SSL with intelligent light management systems, including sensors and timers [8]. SSL is low maintenance with an extremely long lifespan, saving money for both the customer and public authorities. A unique component about SSL is the absence of electrical filaments, plasma, and gas. Instead, light-emitting diodes are used as the source of illumination. Examples of SSL are semiconductor light-emitting diodes (LEDs), polymer light-emitting diodes (PLED), and organic light-emitting diodes (OLED) [9, 11].

LED lights feel cool to the touch because they do not produce heat in the form of infrared radiation. However, this does not mean that LEDs do not produce heat at all. In reality, 60-95% of the electricity consumed is going to heat production generated within the LED device itself [12]. Not only is this a huge waste of energy, but increased LED junction temperature also reduces light output and lifespan of the LED. At temperatures above 125°C, the lifespan of the LED shortens dramatically [13]. Cooling is necessary for the LED to function properly. While the LED light is influential new technology, there is still potential for improvement and optimization of the design and function of the LED.

The project presented in this thesis addresses the heat transfer and cooling of LEDs. There are two types of cooling, forced and natural cooling, both of which can be introduced in LEDs. In forced convection, the fluid motion is driven by a fan, pump, or atmospheric winds. This results in high thermal dissipation and easily controlled cooling. The problem with forced cooling is that the cooling objects use additional energy and are noise polluting. Natural cooling, on the other hand, is the phenomenon in which density-gradients make fluid motion due to temperature differences. This means that the cooling happens automatically wherever there is a difference in temperature between solid and fluid [14]. Natural convection has no noise pollution and has no additional energy consumption, and is therefore the preferred alternative. The cooling effect depends on the difference in temperature, and how well a heat sink can distribute the heat through as much surface area as possible.

Many previous studies have aimed at optimizing natural cooling by modifying the design of the structure of the object of interest. For optimization of heat sinks in electric cooling, structural optimization techniques, such as size and configuration optimization, are often used. Morrison [15] used a downhill simplex method and empirical correlations to optimize plate fin heat in natural convection, with fin spacing, fin thickness and black plate thickness as variables. Bahadur and Bar-Cohen [16] considered pin height, diameter and spacing as variables, when they optimized staged pin fin heat sinks for natural convection cooled microprocessors applications using simplified models.

One of the first industries to use LED technology and conduct research regarding the cooling of LEDs was the automobile industry, further proving that there are many practical uses for such technological advances. Jang and Shin [17] studied the thermal performance of LED arrays for automotive headlamps with a novel cooling system as a function of the circulating speed of cooling air, the input power, and the number of fins. Zhao, Cai, Wang, Li and Zhang [18] did a study on conventional plate-fin heat sink and novel cooling device integrated with heat conductive plates for the application in high-powered LED headlights. This was an experimental based analysis with computations using the CFD software FloEFD.

The study conducted is based on the Hypercool project, a cooperation between the Mechanical Department at the Technical University of Denmark (DTU) and AT-lighting. AT-lighting is a high bay lighting design company that started this project with the goal of creating new organiclooking heatsinks for LEDs. DTU's task was to use topology optimization to design new heat sinks and learn more about natural LED cooling, in addition to testing luminaire designs that AT-lighting engineered. Two bachelor theses and several articles have been written regarding the Hypercool project. Nissen [19] did experimental verification on an axial symmetric “cup” in Comsol and tested geometries provided by AT-lighting. Arenfeldt [20] also investigated two complex cooling fins provided by AT-lighting, but mainly focused on the validation of the CFD software Star-CCM+ as a tool to predict heat velocity development over the cup design. The Mechanical Department at DTU has also taken an alternative approach, by looking at topology. Alexandersen, Andreasen, Sigmund, and Aage [21, 22] used steady-state incompressible Navier-Stokes equation coupled with the thermal convection-diffusion equation through the Boussinesq approximation for density-based topology optimization of three-dimensional heat sink designs cooled by natural convection.

1.1 Structure of thesis

The purpose of this thesis is to validate the FEM software Comsol Multiphysics as a tool to predict the junction temperature of a natural convection cooled non-axial symmetric heat sink. 1) The validation examination is done through experimental verification, where Comsol simulation results are compared to real life experiments(seen in Figure 1.1 . As in Alexandersen's studies [21, 22], Navier-Stokes equation coupled to the thermal convection-diffusion equation through Boussinesq approximation in Comsol will be used. Laminar flow is assumed. The experiments are carried out on a non-axial symmetric aluminum fin heat sink that is coupled with a heat-conducting resistor. The experiment was conducted in horizontal, vertical and 45 degree positions. The use of a valid tool to calculate effects of complex heat sinks will make conducting real life experiments unnecessary, in addition to ensuring cheaper, easier, and more efficient analysis of complex heat sinks. 2) Thought comparisons, the simulation model used for the verification will be investigated to see if it can be improved . Lastly, 3) the optimization of the designed fin heat sink is explored using Comsol by changing fin height, diameter and the number of fins.

This thesis is divided into chapters dealing with individual topics. Chapter 2 is a short introduction to light, LEDs and the Hypercool project, followed by explanation of modeling and manufacturing of heat sink in chapter 3. Chapter 4 explains the experimental setup (Figure 1.1), before heat transfer theory is presented in chapter 5. Chapter 6 covers the theory and setup of the heat transfer simulation in Comsol. In chapter 7, the results for both experiments and comsol are presented, before we compare and discuss the results found in chapter 8. The report ends with a summary and conclusion in chapter 9 and some perspective on possible future works in chapter 10.

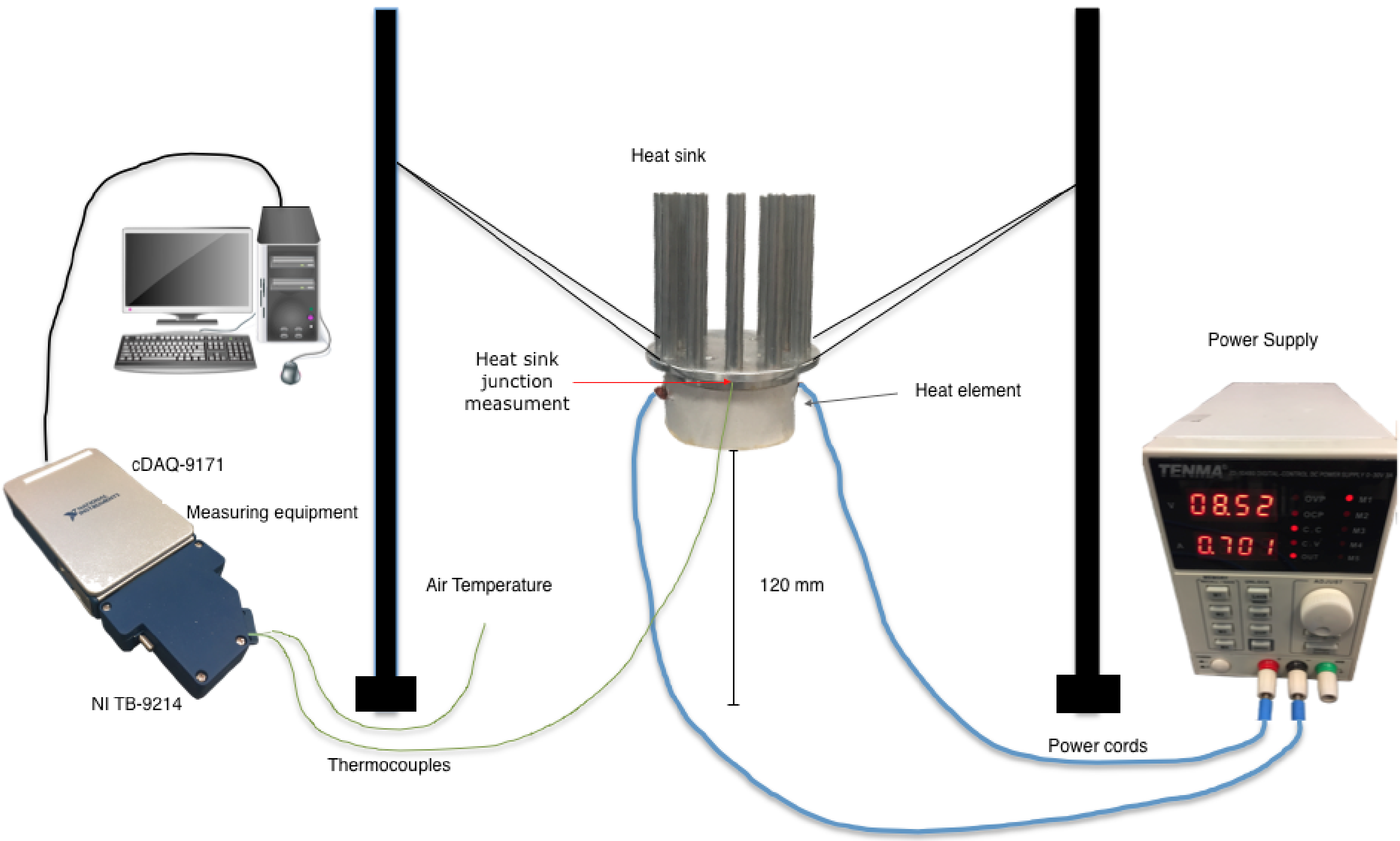

Figure 1.1: LED bulb

2 Light, LEDs and Project Hypercool

2.1 Light

Light brings joy and comfort into our lives whether it comes from the sun, the glow of a candle or gazing at stars from a distant galaxy. Without the light and heat from the sun, life on earth would cease to exist. Man-made light is one of the most groundbreaking inventions ever, taking many different forms and we use it to learn, explore, navigate, and communicate. The story of light explains the development of human life, and how mankind has been able to evolve, resulting in modern day society [23]. It all started with wooden fires and developed into oil lamps and candles using cow fat and later, whale fat. Today, we use electricity and have technologically advanced lamps like compact fluorescent lamps (CFL), fiber optic lighting systems, and light emitting diodes (LED). We get as much light as we want with the simple a flick of a switch. However, the science behind light is a bit more complex [24].

When we talk about light, we usually talk about visible light, which is defined as having a wavelength between 400 and 700 nanometers [25]. However, physics defines light as a spectrum of electromagnetic waves of any wavelength [26, 27]. This means infrared, radio waves, ultraviolet, microwaves, gamma rays, and X-rays, as seen in Figure 2.1, are all different forms of light which can not be detected by the human eye. Electromagnetic energy, which is made up of photons, travels in waves at a constant velocity and is absorbed and emitted in small energy packets. A wave of photons is characterized by velocity, frequency, wavelength, and amplitude. The velocity is the speed of light in a vacuum, while frequency is the rate of complete cycles/waves per second. Wavelength is defined as the distance between peaks, and amplitude is the distance from one peak to another [28].

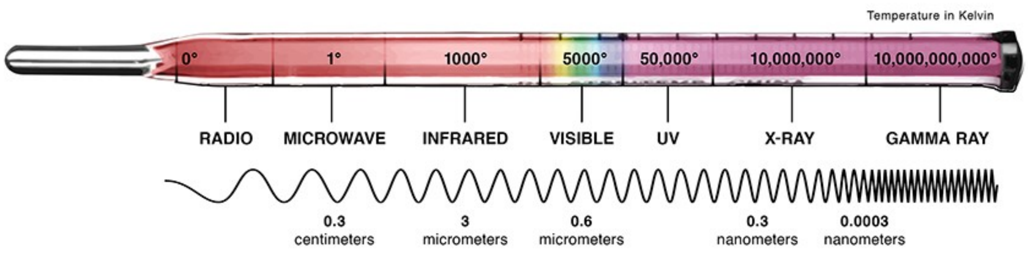

Figure 2.1: Light-waves

All forms of light travel at the same speed of approximately 300,000 kilometers per second. Light is the fastest-known entity in our universe with the ability to circle the Earth 7.5 times in one second. As light travels, it can be absorbed, reflected, blocked, and bent. For example, light can be absorbed by objects it touches, warming a stone or human skin with the sun's infrared light. Light can also be reflected off of a mirror, blocked when a shadow occurs, or bent when traveling between different mediums such as air and water [1].

The SI unit for luminous intensity is candela (cd). Luminous intensity is not a measure of light energy, but rather the brightness itself. This measurement is obtained by weighing the emitted power in a particular direction by the luminosity function of light. The luminosity function is standardized model that accounts for the fact that the human eye is more sensitive to some wavelengths of light than others [29].

2.2 LEDs

LEDs, or light-emitting diodes, are extremly versatile, come in many shapes and forms, and can be used in multitude ways in everyday life. We use them in everything, from commercial freezers to TV-screens. LEDs are gradually taking over traditional radiation sources because of their high-energy efficiency, high luminance, long lifespan and because they are cheap to produce [30].

LEDs are a particular type of diode that produce light when electrical current passes through them [29]. Like other diodes, the LED is a small chip consisting of two elements of processed material called P-type semiconductors and N-type semiconductors. The P-type semiconductor, or anode, is positively charged, while the N-type semiconductor, or cathode, is negatively charged. The region between the anode and cathode where they are in direct contact is called the P-N junction or bandgap [31]. Particles that carry the current, known as electrons, and holes flow into the junction from electrodes with different voltages. Energy will be released when an electron meets a hole, and falls into a lower energy level. The energy is released as a light particle, the photon. In most diodes, this energy is released as heat, but in LEDs, the energy dissipates as light.

The photon energy and bandgap determines the wavelength, in other words, the light color. The photon energy depends on the semiconductor material in the diode, as different semiconductor materials with different bandgaps produce different colors of light. For example, LEDs made out of indium gallium nitride (InGaN) make green, blue, or ultraviolet light, while gallium phosphide LEDs (GaP) make yellow or green light [32]. The most common colors are red, blue, and green. "White" LEDs do not actually exist. To create the white LEDs we have in our homes today the RGB color model is used, in which red, green and blue light are added togther to produce other colors, as seen in 2.2. To creat white, usually blue LEDs mixed or covered with phosphor, which converts the color to white [33].

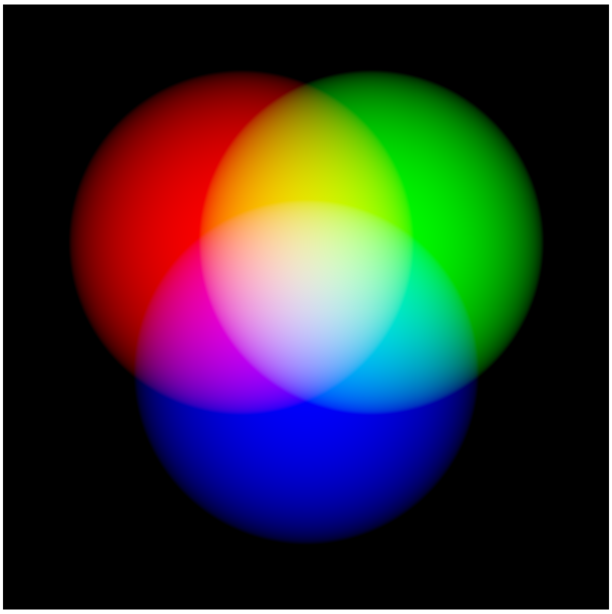

Figure 2.2: RGB color model [34]

Brightness, on the other hand, depends on how much current is available for the LED. The LED will always dissipate as much power as it is allowed to draw, and will destroy itself if it draws too much. Therefore, resistors are often used to limit the amount of current surging through the LED, easily controlling the brightness by adjusting the current. The brightness or luminous intensity can range from ten to tens-of-thousands of millicandela. For example, a good flashlight has a luminous intensity of around 20,000 mcd, while a TV is around 100 mcd [29].

Not all the energy produced at the bandgap goes to lighting. Instead, a portion of it is dissipated as heat. 60-95% of the electricity consumed by LEDs is going to heat production [12]. However, LED lighting systems do not radiate heat the way incandescent or halogen light bulbs do. Heat is produced within the LED device itself and must therefore be drawn away from the LED to prevent the light from overheating and burning out. This is typically accomplished using a heat sink, which basically is a chunk of heat conducting material with large surface area. The job of the heat sink is to absorb the waste heat produced and transfer as much as possible to the surrounding environment [33, 29]. The design of the heat sink is vital for lifespan, light output, and optimal performance of the LED. Studies have shown that the light output gradually decreases when junction temperature increases from room temperature to 100℃. In terms of lifespan, the LED will degrade by 75% when the junction temperature reaches approximately 70℃ [35]. Therefore, the heat sink's ability to effectively draw and release heat away from the LED is a key component to optimizing energy efficiency of the bulb.

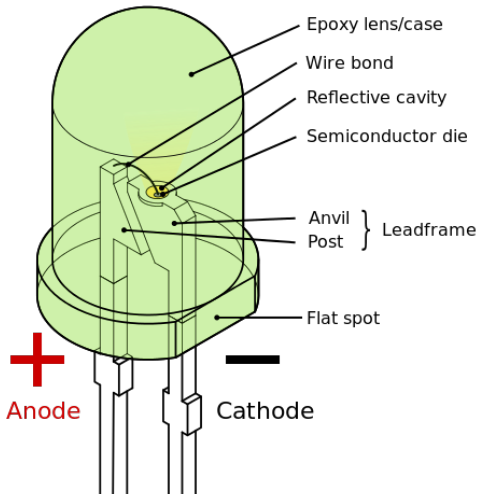

Figure 2.3: LED bulb

2.2.1 Why LEDs? LEDs vs CFLs and Incandescent Bulbs

LEDs differ in several ways from regular light bulbs. Incandescent bulbs use electricity to heat a metal filament until it glows, using 90% of the energy on heat and only 10% of the energy on producing light [33]. Compact fluorescent lighting (CFL), on the other hand, produces ultraviolet light and heat when electric current flows between electrodes placed at each end of a tube containing gas. On the inside of the CFL, there is a phosphorous coating and when the UV light strikes the coating, it is transformed into visible light.

The is no doubt that LED lighting is one of the most durable, efficient, versatile, and long lasting light bulbs on today's market. Studies have shown that a 15 W LED lamp emits the same quantity of luminous flux as a standard 100 W incandescent lamp and a 23 W CFL. LED lamps are also cheaper than both CFL and incandescent lamps if looking at the big picture. While a CFL costs $5-19 in the USA, an LED lamp costs $50-160 but lasts 9-10 longer and uses 2-3 times less energy than the CFL. LEDs have an average lifespan of 50,000 h with the overall operational cost for a LED lamp being 1.62 times cheaper compared to CFL and 6.46 times cheaper compared to incandescent lamps [24]. Additionally, LEDs are the only kind of lamp without mercury, which is known to be a major health threat.

2.3 Project Hypercool

The Hypercool project is a cooperation between the Department of Mechanical Engineering at the Technical University of Denmark and the design company, AT-lighting. AT-lighting started this project with the goal of creating beautiful organic looking heat sinks for LEDs with integrated natural convection. When DTU joint the project, making the optimal heat sink improving passive cooling for LED's became a additional goal . AT-lighting made several 3D-printed luminaires, which have integrated natural convection in a beautiful geometrical shape, incorporating the cooling technology as a part of the design. In the future, this technology will be an important part of cooling for all kinds of machines and, in some cases, will replace the active cooling used in computers and other technologies.

AT-lightning is composed of two designers, Jacob Willer Tryde and Alexandra Alexiou. Tryde and Alexiou created 3D-printed luminaires and asked DTU to research how to optimize the passive cooling of LEDs. Since then, students and faculty at DTU have tested AT-lighting's luminaires as well as designed their own more optimal luminaires. In addition to the design of luminaires, the mode of manufacturing has also been researched, investigating the difference between molded heat sinks and 3D printed heat sinks has also been tested.

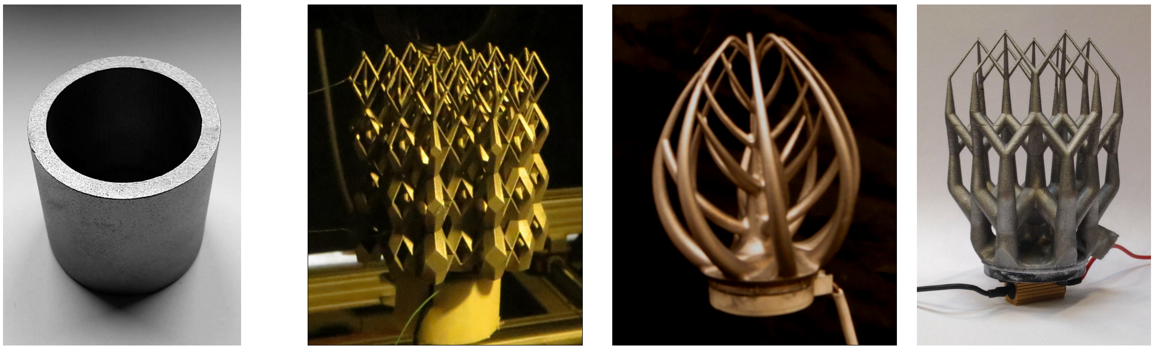

(a) The Cup **(b)** Cooling Fins **(c)** The Tulip **(d)** The Crown

Figure 2.4: Heat sink designs

The Cup, shown in figure 2.4a, has been the test subject on several different occasions. It was the test subject when Brit S. Nissen [19], in the spring of 2015, compared FEM simulations from Comsol with real life experiments. In this experiment, the natural convection velocity was the main focus. The Cup was modeled as a 2D axial symmetric domain, and Comsol found a maximum velocity of 0.18 m/s, while the real life experiments showed a maximum velocity of 0.17 m/2. Nissen explains that the difference is a result "of the surrounding influence on the experimental results and since the numerical model is as a 2D axial symmetric domain it cannot detect any asymmetry in the flow" [19].

In another bachelor project [20], student Frederik Arenfeldt used the CFD software STAR-CCM+. Again, the Cup was used for comparison with velocity as the main focus. The maximum velocity of the simulation was 0.291 m/s compared to 0.286 m/s in the real life experiment. Arenfeldt's conclusion was that the simulation accurately describes the natural convection of a heated cylinder.

In an experiment where the temperature was measured between the heat sink and a mounted 80 W LED, showed that the Cooling fins (Figure 2.4b) outperforms the Tulip (Figure 2.4c. The temperature for the Tulip was 74.5°C, while 50.6°C for the Cooling fins [19]. In another study[20], Infrared images revealed that the Crown (Figure 2.4d) have a better heat distribution from the bottom to top then the Tulip. In a horizontal position the tulip reached 52°C while the crown reached 49°C when 5 watts was used to heat the cooling fins. Temperatures were 54.3°C for the Tulip and 53.5°C in vertical position, again showing that the crown performs better. A 3D printed cup was also compared to a molded cup to see if there was any difference in the heat conduction. When exposed to 5.2 W, the 3D printed cup had velocities 12% higher than the molded cup.

The most comprehensive work was conducted by Joe Alexandersen and the Mechanical Department at DTU. As previously mentioned, Alexandersen used the steady-state incompressible Navier-Stokes equation, coupled to the thermal convection-diffusion equation through the Boussinesq approximation to do a density-based topology optimization of heat sink designs [21, 22]. The designs found thought simulation can be seen in Figure 2.5. Some of the designs has been manufactured, tested, proven to be the best optimized heat sinks to lead heat away from an LED.

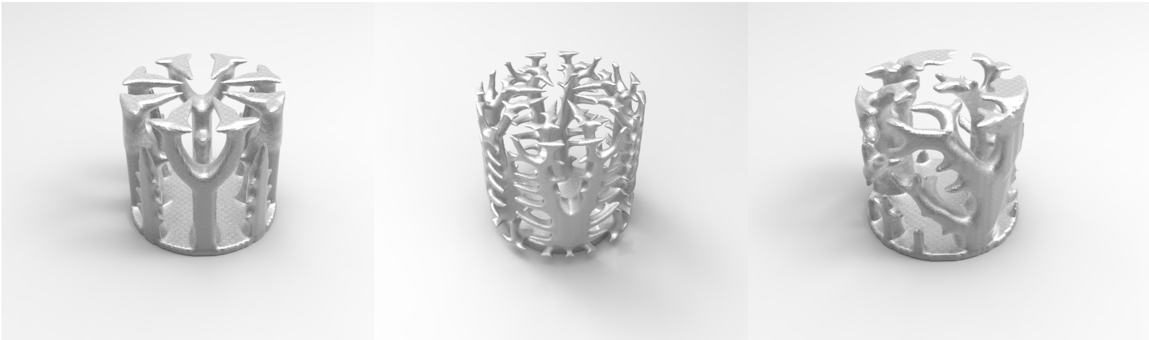

(a) **(b)** **(c)**

Figure 2.5: Renderings of topology optimized heat sink designs

3 Modeling and Manufacturing

3.1 Modeling

A new heat sink was made for this particular verification of Comsol. Joe's topology designs were used as inspiration (see Figure 2.5), since they are the most optimal heat sinks in the Hypercool project. In manufacturing a new, homegrown heat sink, the goal was to make a simplified version of Joe's design. It was important that the design was:

- simple, easy and quick to manufacture
- not axial symmetric
- possible to create and simulate in Comsol
- constructed with the same form and dimensions as the other heat sinks in the Hypercool project (height of 60 mm and a diameter of 65 mm)
- consistent with the experimental setup and functionality

One of Joe's designs is a plate with 8 fins that resemble large trees. They have a thick trunk that divides into several thinner branches. There are two kinds of fins, one that is 60 mm high and spreads towards the center at the top, and one that is smaller and looks like a 2D Christmas tree. The bigger fins also have much thicker, oval trunks, that start closer to the center of the plate. The placement of these two fins alternates as a unique part of the heat sink design.

Using Joe's design as a baseline, a new and simpler heat sink was created. In the new design, Joe's alternating fins were replaced with simple rods, each with a constant diameter and height of 5.98 mm and 60 mm, respectively. Due to the fact that the new fins do not branch out as they did in Joe's design, there was a lot of extra space on the heat sink plate. Therefore, in the new design, the extra space was used for additional fins. Eight fins were added, making a total of 16 fins. 12 of the fins were placed equidistantly in a circle with diameter of 53mm, while four of the fins were placed closer to the center of the plate in a circle with diameter of 37mm. The inner fins were also equidistant and aligned with four of the outer fins, trying to get the same effect as the thicker oval fins in Joe's design.

The machine drawings for the new model were made in the CAD program, SolidWorks. First, the fins and plate were designed separately as 3D components with features like sketch, extrude, and smart dimensions, before they were assembled. Then, 2D engineering drawings were made for each part of the heat sink and brought to DTU's mechanical workshop, where technicians manufactured it. The engineering drawings can be seen in Appendix B Figures B.1, B.2, and B.3.

3.2 Manufacturing

In terms of manufacturing, there were also a few differences between the new design and Joe's design. Joe's design was 3D printed, but that was not an option for the new model due to economic and time restraints. The heat sink needed to be fast and easy to produce in the DTU workshop, so instead of making a one piece product, 16 individual fins and one plate were made and later assembled. With this method, complex manufacturing techniques were avoided.

The fins, Figure B.1, were cut from long a cylindrical rod with the diameter specified in the engineering drawings. Workshop technicians cut the fins to the right length and chamfered the edges.

The plate, B.2, was cut out of a bigger plate at precisely the right dimension, before the plate was chamfered, and polished to get smoother corners and sides. The holes were drilled with a tolerance that was smaller than the diameter of the fins, in addition to two M3 holes with thread. These holes were made so that the heat sink could be attached to the rest of the experiment setup.

To fasten the fins to the plate, the fins were cooled down and the plate was warmed up. When you warm up a material it expands, and vis versa with cooling. So the diameter of the fin shrunk slightly and the holes in the plate got bigger. Technicians were then able to press the fins into the holes of the plate. When both the fins and the plate reached the same temperature, the fins became firmly fixed, creating an interference fit. The manufactured heat sink can be seen in Figure 3.1 below

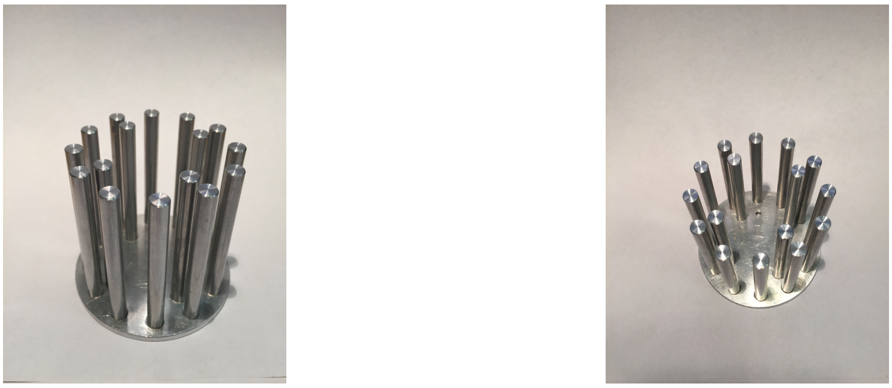

(a) **(b)**

Figure 3.1: Manufactured heat sink from the side (a) and top (b)

4 Experiment setup

This project consists of two types of testing, the real-life experimental testing and the simulated experimental testing using Comsol software. This chapter will focus on the methodology behind the real life experiments, the various components needed to conduct the experiment, and how they are set up. The total experimental setup will look like this

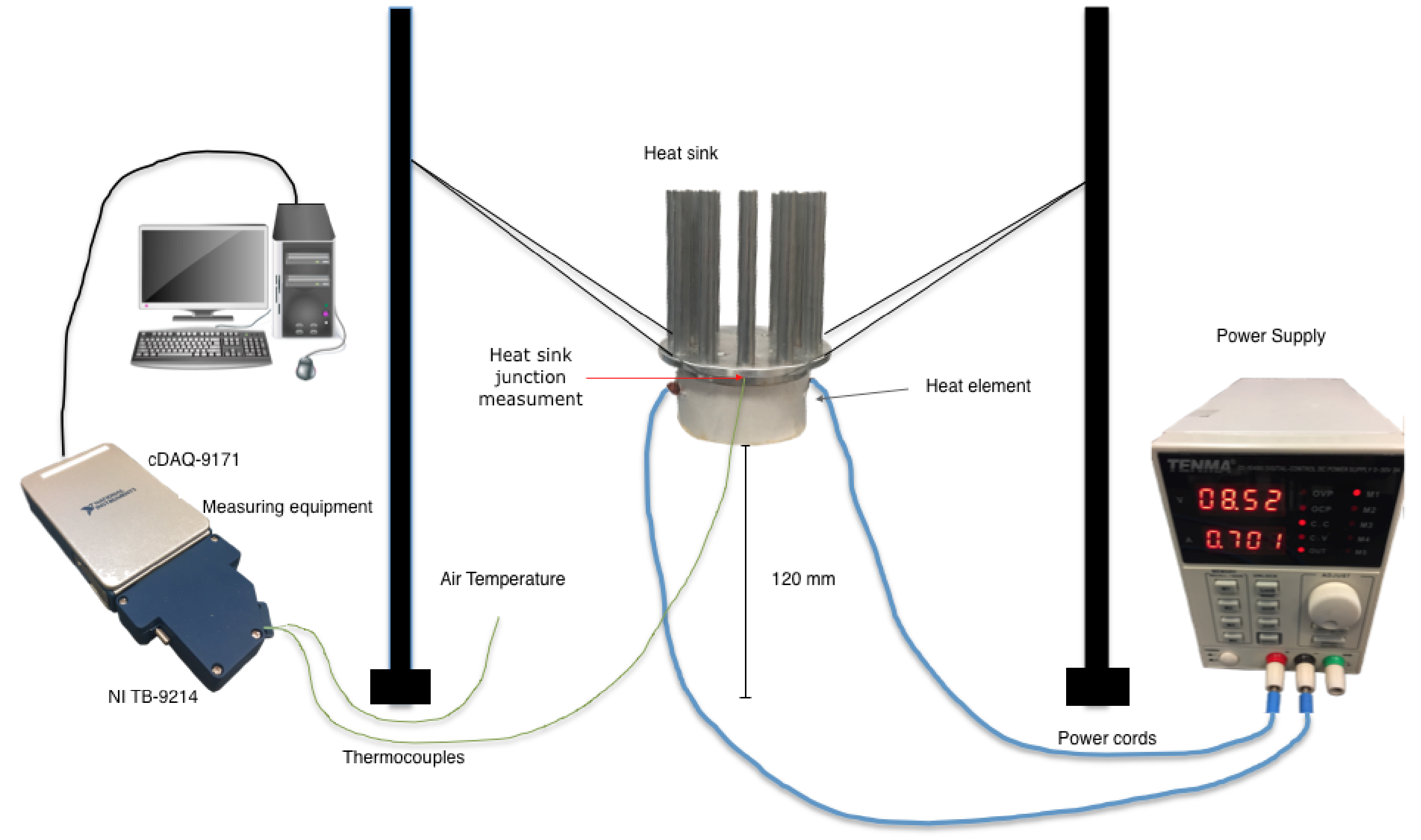

Figure 4.1: Experimental setup

The heat sink, as seen in (Figure 3.1, is the main component of the testing procedure and was attached to the heat element. The heat element (Figures 4.1) and 4.2a), which generates heat, is a construction made out of three parts, a resistor, an aluminum plate, and thermal isolation foam. An electric cable was attached to either side of the resistor, which was then placed on top of the aluminium plate. Tape was put around in the edge of the plate creating a cylindrical shape. Then, the cylinder was filled with SikaBoom S isolation foam, which posses material properties that can be seen in table 6.1. The heat element was constructed to allow the heat generated by the resistor to flow towards the aluminum plate and the heat sink.

Before attaching the heat element to the heat sink, a thermocouple was placed between the two aluminum plates in a small groove, as seen in Figure 4.2a. A thermocouple is a device that measures temperature via a cable with a wired loop of conducting material inside. One end of this wire loop was welded together, making a junction where the temperature is measured, and was placed between the two plates. The other end of the thermocouple was attached to voltage-measuring equipment. The conductor loop was in a plastic insulated cable to minimize exposure to environmental effects. When there was a change in temperature at the heat sink, voltage was produced, which was then transported through the wired junction of the thermocouple and interpreted by the measuring equipment. In the center of the heat element plate was a divot made for the thermocouple junction. Tape was placed around the thermocouple junction, as seen in Figure 4.2b, to prevent contact between the conducting material of the wire and the aluminum plates of the heat sink unit. Aluminum also is a conducting material and will generate extra voltage during any temperature increase. Taping the junction ensured that the voltage generated was originating solely at the thermocouple junction.

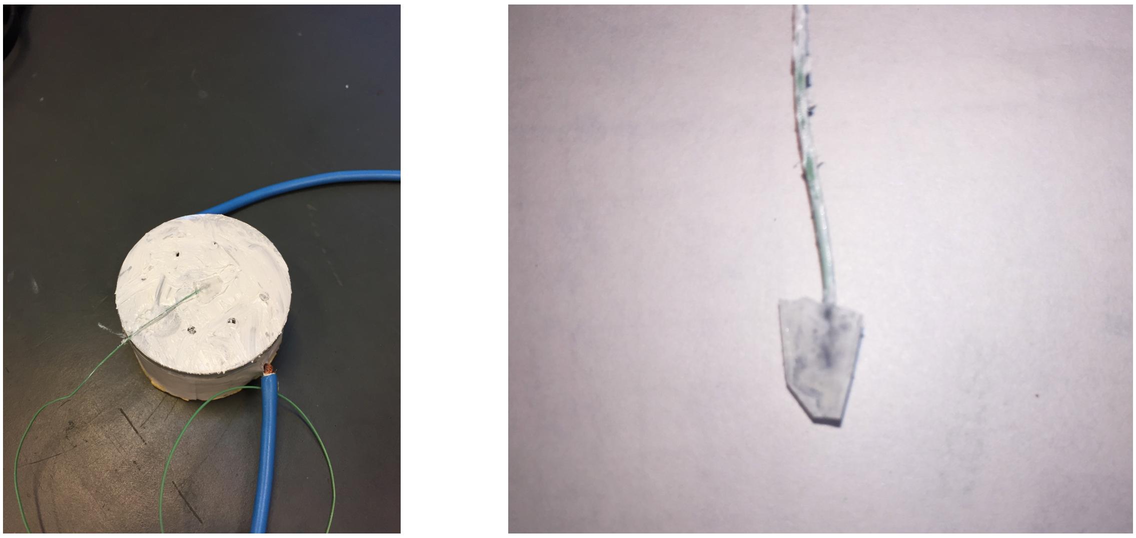

(a) Thermal grease on top of heat element with thermocouple in place

(b) Thermocouple with tape

Figure 4.2

There were two M3 holes in both the heat element plate and the heat sink plate. The screws were inserted at the thermal isolation side and were barely seen on the heat sink side of the unit. However, there were still gaps between the two aluminum plates because the natural surface roughness of the material. To prevent air pockets and maximize heat transfer, a thin layer of Dow Corning 340 heat sink compound(see Table 6.1 for properties), which is a kind of thermal grease, was lathered onto the aluminum plates. Thermal grease consists of a polymerizable liquid matrix and large volume fractions of electrically insulating, but thermally conductive filler.

When put the heat element and heat sink together it looks like this:

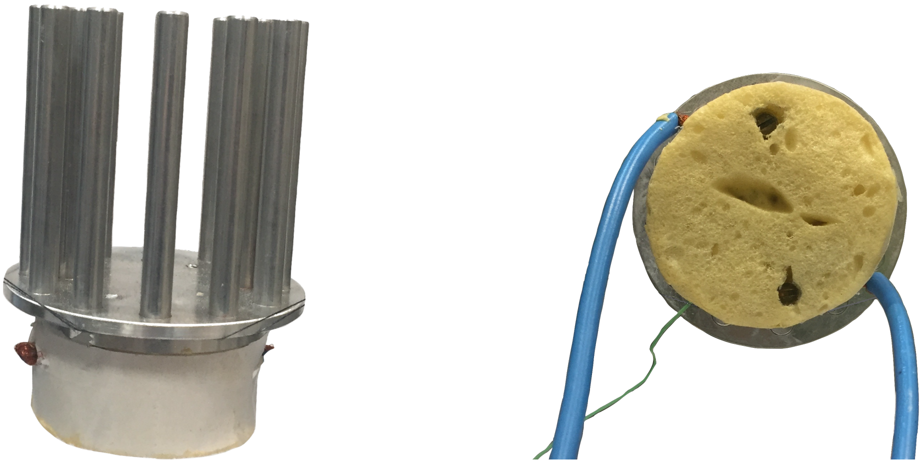

(a) (b)

Figure 4.3: Heat sink and heat element from the side (a) and bottom (b)

The heat sink unit was hung by a tread 120 mm above a desk to prevent it from being affected by anything other than the heat element and the surrounding air. There were two rods and the thread was used to tie the heat sink to both rods as illustrated in the Figures 4.1, 4.4, and 4.5.

In order to produce heat, the resistor needs electricity. The resistor is connected to a power supply via two cables, one at each end, creating an electric circuit. The power supply is a Tenma digital controlled DC power supply and regulates the amount of power supplied to the resistor, by either controlling the electric current or voltage. At the power supply, the voltage and amperage output use the following formula

$$P = I \cdot V \tag{4.1}$$

where the power output is calculated in Watts

The temperature was measured two places. In addition to the space between the heat sink and the heat element, the temperature was also measured in the surrounding air (Figure 4.1. A thermocouple was placed nearby the experimental setup so that the thermocouple was free in the air, away from any surfaces. The temperatures were measured by an NI TB-9214, which is an isothermal terminal block with measurement accuracy up to 0.45℃ [36]. Then, the measurements were sent to the cDAQ-9171, which controls the timing, synchronization, and data transfer to the computer [37]. The results were then displayed on the computer.

Picture of the experiment can be seen in the Figures 4.4, and 4.5 on next page.

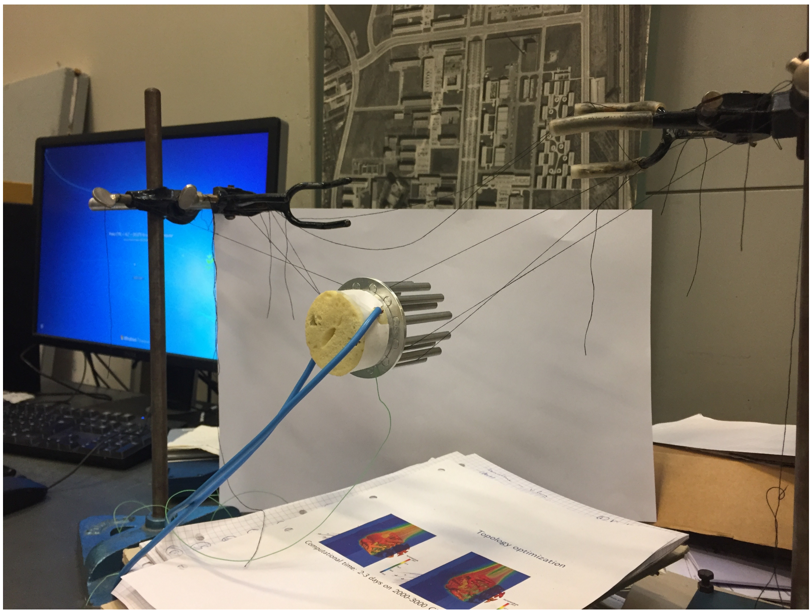

Figure 4.4: Picture of the experiment Horizontal position

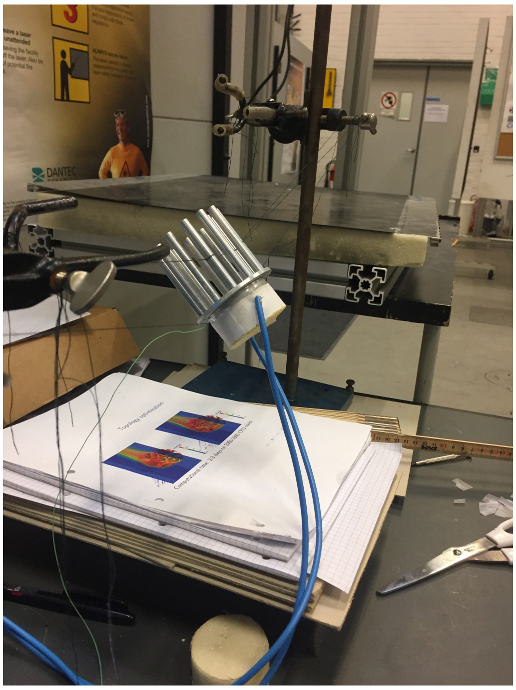

Figure 4.5: Picture of the experiment in 45° position

5 Heat Transfer Theory

In this chapter, the relevant heat transfer theory will be presented. The heat transfer theory was based on the book Fundamentals of Heat and Mass Transfer, written by Bergman, Lavine, Incropera and Dewitt [14], if nothing else is noted.

5.1 Heat Transfer

Heat transfer is all around us, though most of us do not even realize it. Let us say it is Tuesday morning and you are really tired. You need some caffeine to stay awake and focused, so you make some coffee. When the coffee is ready, it is 90°C, which is too hot to drink. What do you do? Most people know that the coffee will cool down over time, but what is really happening over the course of time to cause the coffee to cool down? Heat transfer is taking place.

Heat Transfer is defined as; *thermal energy in transit due to a spatial temperature difference.* In other words, heat transfer is transfer of energy in a way other than through work between a system and its surroundings. In our little coffee scenario, we would say that the coffee is transferring energy, or heat, to the cup that again is transferring energy to the surrounding air. The average amount of kinetic energy particles in the coffee are decreasing, while the cup both gains and loses energy from the warm coffee and the cold air surrounding the cup, respectively.

There are three different modes of heat transfer; 1) conduction, 2) convection, and 3) radiation, which will be explained in the upcoming sections.

5.2 Conduction

When a temperature gradient exists in a stationary medium, which may be a solid or a fluid, we use the term conduction to refer to the heat transfer that will occur across the medium. At high temperatures, molecules have a high velocity/vibration and a high molecular energy, causing them to collide more frequently with their neighbors. When molecules collide, energy transfers from the more energetic molecule to the less energetic molecule. Conduction will occur in the direction of decreasing temperature, which in our experiment means from the resistor via the heat element (HE) plate and the heat sink(HS) plate to the fins.

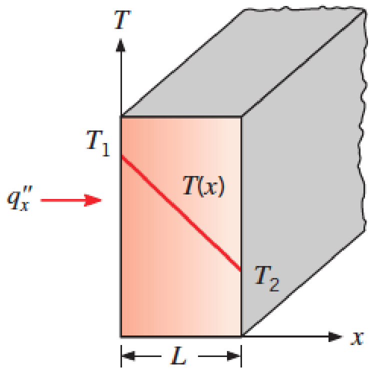

Figure 5.1: Heat transfer thought wall

Figure 5.1 above shows a uniform one-dimensional wall, where one side is warm and the other cold. For our heat sink this could be the aluminum plate, where the hot resistor is on one side and the cold ambient air is on the other side. In this case, Fouries's law could be used to calculate the amount of energy being transferred per unit time thought the wall in Figure 5.1

$$q''_x = -k\frac{dT}{dx} = \frac{q_x}{A} \tag{5.1}$$

Fourier's law tell us that the heat flux, q''_x (W/m^2), through the wall is the thermal conductivity, k, multiplied with the temperature gradient, $\frac{dT}{dx}$. Heat flux is heat transfer rate per unit area normal to the cross-section area A, in this case in the x direction. Thermal conductivity is the materials ability to conduct heat and has the unit W/(m·K). The minus sign in front of the equation is due to that heat is transferred in the direction of decreasing temperature.

In many cases, we assume steady-state conditions, under which the temperature has a linear distribution, as shown in figure 5.1. Fourier's law can expresses as:

$$q''_x = k\frac{T_1 - T_2}{L} \tag{5.2}$$

A more general statement for Fourier's law is

$$\mathbf{q}'' = -k\nabla T = -k\left(\mathbf{i}\frac{\delta T}{\delta x} + \mathbf{j}\frac{\delta T}{\delta y} + \mathbf{k}\frac{\delta T}{\delta z}\right) \tag{5.3}$$

Here we have recognized that the heat flux is a vector quantity. ∇ is the three dimensional vector differential operator and $T(x, y, z)$ is the scalar temperature field.

5.2.1 Thermal conduction, k

Fourier's law applies for all materials, regardless of their state. However, heat transfer varies with different materials due to varying material properties. In general, the thermal conductivity is much larger in solids than in fluids due to the much larger intermolecular spacing and more random molecular motion in fluids. In solids, like the aluminum in the HS, the thermal conduction relates to lattice vibration waves and the migration of free electrons, while in fluids, air in the experiment, thermal conductivity is directly proportional to density. A material's ability to transfer heat is measured as the thermal conduction constant, k. For solids, we express k as,

$$k = \frac{1}{3} C \bar{c} \lambda_{mfp} \tag{5.4}$$

where C is electron specific heat per unit volume, $\bar{c}$ is the mean electron velocity, and λ is the distance traveled by an energy carrier prior to a collision, also called mean free path. For liquids, we find k as,

$$k = \frac{1}{3} c_v \rho \bar{c} \lambda_{mfp} \tag{5.5}$$

where $\bar{c}$ is the mean molecular velocity and ρ is the material density and λ is the mean free path.

Aluminum has a thermal conductivity at about 237 $W/(m \cdot K)$, while airs thermal conductivity is at 22.3 $W/(m \cdot K)$. This means that the heat sink itself has a high heat transfer through the plate and fins, while the air around will not be good at transferring the heat away form the heat sink by convection. Luckily, i air heat is also transferred by convection and radiation.

5.3 Convection

Convection is energy transfer through advection, diffusion, or both. Advection refers to transport due to bulk fluid motion, while diffusion is random movement of molecules in liquids and gasses from a region of high concentration to a region of low concentration. Convective heat transfer occurs when a bounding surface and a fluid in motion are at different temperatures, like the surface of the heat sink and the ambient air surrounding it.

To calculate the amount of energy being transferred per unit time for heat convection we will use Newton's law of cooling.

$$q'' = h(T_\infty - T_s) \tag{5.6}$$

The cooling law states that the rate of which the temperature of a body changes is proportional to the difference in temperatures between the body itself and its surroundings. The equation can be used regardless of the nature of the convective heat transfer process, where T_∞ is the temperature of the fluid, T_s is the surface temperature, and q'' is the heat flux (W/m^2) given in section 5.2. The parameter h is the convective heat transfer coefficient and depends on the boundary layer condition.

Boundary layers

Boundary layers are an important component behind convective heat transfer between a surface and fluid flowing past it. There are two different boundary layers, velocity boundary layer and thermal boundary layer. **Velocity boundary layers** involve fluid velocity and how it is reduced when in contact with a solid wall, because of shear stress acting in planes parallel to the fluid velocity. Let us consider figure 5.2 Here we have a horizontal heated plate with a cold fluid above. The fluid varies from having a zero velocity at the wall (at y=0), to the the free stream velocity u_∞ further away from the wall. This transition region is the velocity boundary layer. The velocity boundary layer thickness is defined as where $u \leq 0.99u_\infty$.

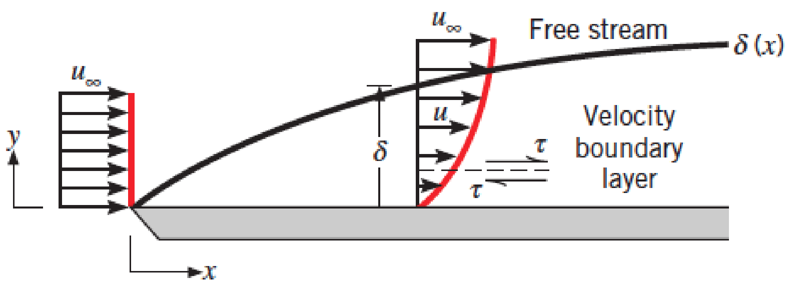

Figure 5.2: Velocity boundary layer

A **thermal transition layer** emerges if there is a difference in the temperature of the wall and the fluid. Fluid particles close to the plate achieve thermal equilibrium with the plate's surface temperature. These particles then exchange energy with the adjoining fluid layers and, as a result, temperature gradients develop in the fluid. The region where these temperature gradients occur is the thermal boundary layer. The thickness, δ_t in Figure 5.4b, is defined as the distance from the wall where $[(T_s - T)/(T_s - T_\infty)] \leq 0.99$. Near the surface, where the velocity is low, heat is mostly transferred by diffusion. Farther away from the wall, when we get closer to t_∞, the bulk fluid motion will contribute more and more in the heat transfer.

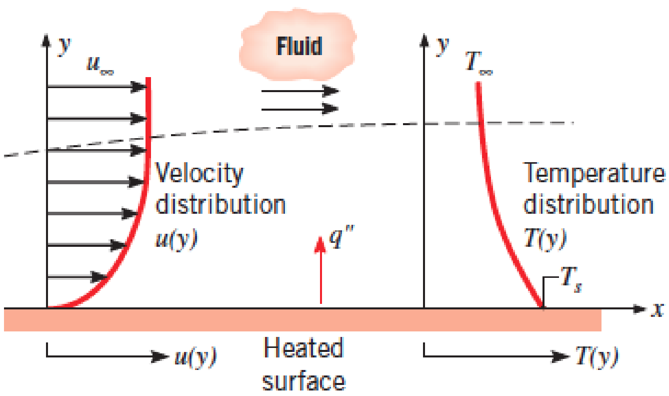

Figure 5.3: Boundary layers

Laminar and Turbulent flow

An essential step in the treatment of any convection problem is to determine whether the boundary layer is laminar or turbulent. Laminar fluid flow is highly ordered and streamlines along which particles move are easily identifiable. Turbulent flow, on the other hand, is highly irregular and is characterized by random, three-dimensional fluid motion. Laminar and turbulent flow conditions often occur at the same time, with the laminar section preceding the turbulent section. We decide if a boundary layer is laminar or turbulent by calculating Reynolds number (forced flow) or Grashof's number (natural convection). See section 5.10 for info and formulas.

5.3.1 Natural convection

As stated earlier, there are two types of convection, forced and natural. **Forced convention** is caused by external means, such as by a fan, pump, or atmospheric winds, while **natural convection** is induced by buoyancy forces induced due to density differences caused by temperature variations in the fluid.

In this thesis, the focus will be on natural convection. Free or natural convection is a situation in which there is no forced velocity, but still convection currents within the fluid. This happens when a body force acts on a fluid with density gradients. It has a gentle circulating pattern set up by buoyancy forces in a fluid usually stratified by a temperature gradient. The body force is usually gravitational.

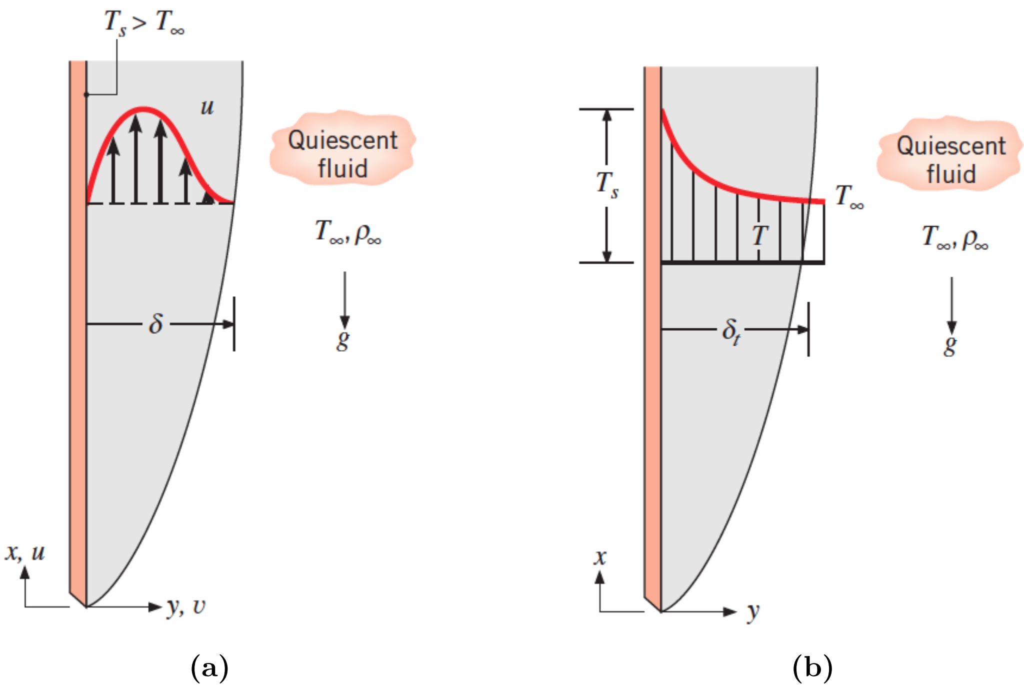

Figure 5.4: Natural convection boundary layers on heated vertical plate. (a) shows velocity boundary, while (b) shows thermal boundary

Consider the fins in the heat sink in vertical position. Each fin will be exposed to cold air, like in Figure 3.3. The temperature on the surface of a fin will drop, while the temperature of adjacent air will rise. There will be a thin layer of warmer air close to the fin. Heat will be transferred from this layer to the outer layers of air. The warmer adjacent air will have a lower density than the colder air. As a result, the warmer air will rise above the less dense cold air, and cause what we call the chimney effect or natural convection flow.

5.4 Radiation

Radiation is energy transferred by electromagnetic waves. All matter, in any form, with a temperature greater than absolute zero, emits thermal radiation energy. Electromagnetic radiation is generated by thermal energy of charged particles in matter. The emission may be attributed to changes in the electron configurations of the constituent atoms or molecules.

Stefan Boltzmann's law

Stefan Boltzmann's law describes the surface emissive power, E_b, and has the unit W/m^2. Surface emissive power is the energy released per unit area emitted from a black body in terms of its temperature. A black body is a body that absorbs all radiation that fall on its surface. Stefan Boltzmann's law for black bodies is

$$E_b = \sigma T_s^4 \tag{5.7}$$

where σ is the Stefan Boltzmann constant, $\sigma = 5.67 \cdot 10^{-8}\ W/(m^2K^4)$, and T_s is the absolute temperature of the surface (in Kelvin). The heat flux from a normal surface is described with a radiation property of the surface termed emissivity, e. Emissivity lays between 0 and 1 and describes how effective a surface is able to emit radiation relative to a black body, which has an emissivity of 1. Stefan Boltzmann's law for all surfaces is

$$E = \epsilon \sigma T_s^4 \tag{5.8}$$

In a situation where a small surface is completely surrounded by a bigger surface, there will be a net rate of radiation heat transfer per area

$$q''_{rad} = \frac{q}{A} = \epsilon\sigma(T_s^4 - T_{sur}^4) \tag{5.9}$$

from the small surface (T_s) to the bigger surface(T_{sur}). For many applications, it is convenient to express the net radiation heat exchange in the form

$$q_{rad} = h_r A(T_s - T_{sur}) \tag{5.10}$$

where h_r is the radiation heat transfer coefficient and can be calculated like this

$$h_r \equiv \epsilon\sigma(T_s + T_{sur})(T_s^2 + T_{sur}^2) \tag{5.11}$$

In relation to LEDs, it was already mentioned that LED don't produce much heat by radiation. In the HS there will be radiation between the fins and between the plate and the fins, but because of similar temperatures, and aluminum's low emissivity coefficient the radiation heat transfer will be small. Therefore, the radiation is neglected and not used in Comsol.

5.5 Thermal resistance (one-dimensional)

A thermal residence can be associated with the conduction of heat in the same way that an electric residence is associated with the conduction of electricity, through Ohm's law ($I = \frac{I}{R}$). This is shown when the heat transfer rate is expressed as

$$q = q''A = \frac{\Delta T}{R_t} \tag{5.12}$$

where A is the area normal to the direction of heat transfer, ΔT is the temperature difference and R_t is thermal resistance. Thermal resistance has the units K/W, and takes different forms for the three different modes of heat transfer.

Conduction:

$$R_{t,cond} = \frac{T_{s,1} - T_{s,2}}{q_x} = \frac{L}{kA} \tag{5.13}$$

Convection:

$$R_{t,conv} = \frac{T_s - T_\infty}{q} = \frac{1}{hA} \tag{5.14}$$

Radiation:

$$R_{t,rad} = \frac{T_s - T_{sur}}{q_r ad} = \frac{1}{h_r A} \tag{5.15}$$

where k is the thermal conduction, h is the convective heat transfer coefficient, and h_r is the radiation heat transfer determined from equation 5.11 where $T_{sur} = T_{inf}$.

Overall heat coefficient

It is possible to create an overall heat transfer coefficient when working with thermal resistance. This coefficient is called U and it can be found from

$$U = \frac{1}{Rtot \cdot A} \tag{5.16}$$

where

$$R_{tot} = \frac{1}{UA} = \sum R_t \tag{5.17}$$

The overall heat transfer coefficient can be used in an expression analogous to Newton's law of cooling

$$q_x \equiv UA\Delta T \tag{5.18}$$

It is often convenient to work with an overall heat transfer coefficient, when working with composite systems.

Parallel and series

R_{tot} is the total thermal residence and includes conduction, convection, and radiation. Composite wall may be in series-parallel configuration,

$$\text{In parallel:} \qquad \frac{1}{R_{tot}} = \frac{1}{R_a} + \frac{1}{R_b} \tag{5.19a}$$

$$\text{In series:} \qquad R_{tot} = R_a + R_b \tag{5.19b}$$

It is possible to look at the heat sink setup as a composite wall, where the resistor and aluminum plates are in series while, all the fins are in parallel.

Contact Resistance

Another important concept in composite systems is the contact resistance, $R_{contact}$. Between the aluminum plates in the HS and HE, there will be small gaps, like in Figure 5.5, causing a higher thermal resistance. The heat transfer will be largest at the contact spots due to conduction, and lower when the heat transfer goes through the medium as convection and/or radiation.

$$R''_{contact} = \frac{\Delta T}{q''_x} \tag{5.20}$$

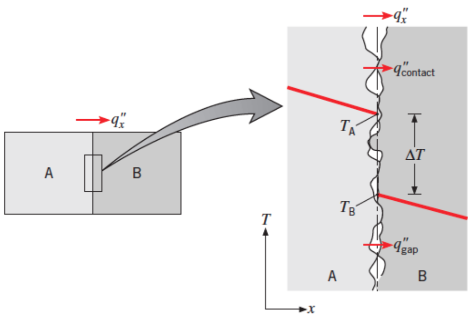

Figure 5.5: Thermal contact residence

Contact resistance, will also occur between the resistor and the aluminum plate, as well between the plate and fins. However, the resistance between the plate and the fins will be smaller because of the pressure at the contact surface in the interference fit (Section 3.2).

Cylinder and spheres

All the parts of the heat sink are cylinders. Cylindrical and spherical systems only experience temperature gradients in radial direction and may, therefore, be solved as one-dimensional problem.

Cylinder:

$$q_r = \frac{2\pi Lk(T_{s,1} - T_{s,2}}{\ln(r_2/r_1)} \tag{5.21}$$

$$R_{t,cond} = \frac{\ln(r_2/r_1)}{2\pi Lk} \tag{5.22}$$

Sphere:

$$q_r = \frac{4\pi k(T_{s,1} - T_{s,2}}{(1/r_1) - (1/r_2} \tag{5.23}$$

$$R_{t,cond} = \frac{1}{4\pi k}\left(\frac{1}{r_1} - \frac{1}{r_2}\right) \tag{5.24}$$

5.6 Heat Transfer from extended surfaces (fins)

By increasing the fluid velocity and/or reducing the fluid temperature, we can increase the heat transfer rate so that a LED can cool down faster. Both possibilities are somewhat inconvenient and impractical, due to the fact that both blowers and cooling elements use energy and space to increase the fluid velocity and reduce temperature. However, there is another option. Looking at Newton's law of cooling, we can see that increasing the surface area will give a higher heat transfer rate. Increasing surface area can be accomplished with a heat sink with extended surfaces or fins protruding into the surrounding fluid. Ideally, the base and tip of the fins should have the same temperature in order to maximize possible heat transfer exchange. This is not possible, since the direction of heat transfer from the boundaries is perpendicular to the principal direction of heat transfer in the solid. To minimize the temperature difference, the fin material should have a large thermal conductivity. All the equations in this section is based on the assumptions of steady state, constant material properties, no internal heat generation, one-dimensional conduction, uniform cross-section areal and uniform convection across the surface area. The general form of the energy for an extended surface is,

$$\frac{d^2T}{dx^2} + \left(\frac{1}{A_c}\frac{dA_c}{dx}\right)\frac{dT}{dx} - \left(\frac{1}{A_c}\frac{h}{k}\frac{dA_c}{dx}\right)(T - T_\infty) = 0 \tag{5.25}$$

where T_∞ is the air temperature, dAs is the surface area of the differential element, and Ac is the cross-sectional area of the fin.

However, there is no assurance that fins will help increase the heat transfer, when the fin itself represents a conduction resistance. To figure out if the fins are an assessment we can calculate the **fin effectiveness**. The formula for fin effectiveness is

$$\epsilon_f = \frac{q_f}{hA_{c,b}\theta_b} \tag{5.26}$$

where $A_{c,b}$ is the fins cross-section area at the base, h is the convection heat transfer, and $\theta_b = T_b - T_\infty$. The formula is defined as the ratio of the fin's heat transfer rate to the heat transfer rate that would exist without the fin.

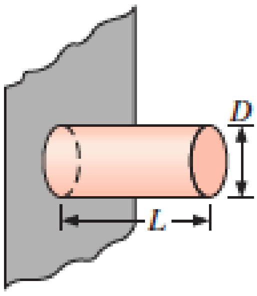

Figure 5.6: Pin fin

Fin efficiency n_f is how well a fin performs compared to how well it would perform if the whole fin had base temperature. The definition of fin efficiency is

$$\eta \equiv \frac{q_f}{q_{max}} = \frac{q_f}{hA_f\theta_b} \tag{5.27}$$

where A_f is the surface area of the fin. For a pin fin, formal is

$$\eta_f = \frac{\tanh mL_c}{mL_c.} \tag{5.28}$$

where $L_c = L + (D/4)$, and $m = (4h/kD)^{1/2}$ for a pin with circular cross-section. To find the overall efficiency (η_0) of an array of fins, the equation is:

$$\eta_0 = 1 - \frac{NA_f}{A_t}(1 - \eta_f) \tag{5.29}$$

or

$$\eta_0 = \frac{q_t}{q_{max}} = \frac{q_t}{hA_t\theta_b} \tag{5.30}$$

q_t is total heat rate from the surface area A_t associated with both the fins and the exposed portion of the base. N is number of fins in the array, each of surface area A_f. The thermal resistance of a fin array is expressed as:

$$R_{t,0} = \frac{\theta_b}{q_t} = \frac{1}{\eta_0 hA_t} \tag{5.31}$$

and is based on an inference between equation 5.30 and equation 5.12.

5.7 Conservation Equations

Let's consider Figure 5.7, a surface S surrounds an arbitrary frame in space with volume V. d**S** is a vector normal to a small patch on the surface S, which points outward by convection. A quantity Φ is made, which presents units of stuff per unit volume inside the frame. The only way to change the amount of Φ with time is by creating it within the volume or flux it though the surface. We can express the conservation of Φ for the volume as

$$\frac{d}{dt}\int_V \Phi dV = -\int_S \mathbf{F}\cdot d\mathbf{S} - \int_S \Phi\mathbf{V}\cdot d\mathbf{S} + \int_V H dV \tag{5.32}$$

where $\mathbf{F}$ is the heat conduction of Φ, $\Phi\mathbf{V}$ is the transport flux and H is a Φ source [38].

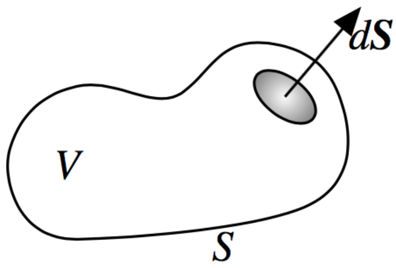

Figure 5.7: Arbitrary frame in space [38]

In this project, the control volume has to be divided into smaller differential control volumes (elements), as spatial variations within the control volume is at interest as well as time. In Comsol, the size of the elements is decided by the mesh explained in 6.1 and Appendix **??**.

By saying that we are not interested in anything smaller than the scale of the element and assuming that $\bar{\Phi}$ is defined for each element, the property of interest is now differentiable, and by using Gauss' theorem we can now replace the surface integrals

$$-\int_S \mathbf{F}\cdot d\mathbf{S} - \int_S \Phi\mathbf{V}\cdot d\mathbf{S} = -\int_V \nabla\cdot(\mathbf{F}+\Phi\mathbf{V})dV \tag{5.33}$$

Because volume and surface are fixed in a frame, we have that

$$\frac{d}{dt}\int_V \Phi dV = \int_V \frac{\delta\Phi}{\delta t}dV \tag{5.34}$$

which tells that the time derivative of the summed properties is equal to the sum of the local time.

Now we can substitute Eq. 5.33 and Eq.5.34 into Eq.5.32 and get

$$\int_V \left[\frac{\delta\Phi}{\delta t} + \nabla\cdot(\mathbf{F}+\Phi\mathbf{V}) - H\right]\delta V = 0 \tag{5.35}$$

because V is of arbitrary size and shape, and can only be satisfied if the term inside the square brackets is zero, we can express the general form for all conservation laws [38] as

$$\frac{\delta\Phi}{\delta t} + \nabla\cdot(\mathbf{F}+\Phi\mathbf{V}) - H = 0 \tag{5.36}$$

which is a partial differential equation that can be solved analytically or numerically for the different conservation equations. More about this in Chapter 6.

5.7.1 Conservation of Mass

The law of conservation of mass says that matter can not be destroyed nor created, hence $H = 0$. In other words, mass that enters a control volume has to be equal to the matter that leaves it. Density is the amount of mass per unit volume, $\Phi = \rho$, and mass flux can only change due to transport, $F = 0$. By substituting this into Eq. 5.35, we get that

$$\frac{\delta\rho}{\delta t} + \nabla \cdot (\rho\mathbf{V}) = 0 \tag{5.37}$$

The equation is called the continuity equation and must be satisfied at all points in the fluid.

5.7.2 Conservation of Energy

The law of conservation of energy states that the rate of energy entering a moving fluid control volume plus the heat added, must equal the work done by the fluid plus the energy leaving. This is expressed in the transport equation,

$$\frac{\delta\rho c_p T}{\delta t} + \nabla \cdot (\rho c_p T) = \nabla \cdot k\nabla T + H \tag{5.38}$$

where c_p is specific heat, T is temperature, k is the thermal conductivity. The equation is derived from Eq.5.35 where $\Phi = \rho c_p T$, $F = -k\nabla T$ and H is heat generated withing the fluid.

5.7.3 Conservation of Momentum

Conservation of mommentum or Newton's second law of motion states that, *"The sum of all forces acting on the control volume must equal the net rate at which momentum leaves the control volume"*[14].The equation can be derived the same way as the transport equation. However, the momentum is not a scalar field like the temperature, but a vector field. There are two ways of changing momentum in the elements; by adverting momentum or by exerting forces onto the element. The forces can be stress acting on the surface of the volume with local force $\mathbf{f} = \sigma \cdot d\mathbf{S}$ or body forces like gravity. Stress can be thought of as a flux force and we can therefore define $\mathbf{F} = -\sigma$. H is the body forces acting on the control volume, while Φ can we written as $\Phi = \rho \cdot \mathbf{V}$ as momentum per unit volume. The conservation of momentum equation is expressed as

$$\underbrace{\rho\left(\frac{\delta \mathbf{V}}{\delta t}+(\mathbf{V}\cdot\nabla)\mathbf{V}\right)}_{1}=\underbrace{\nabla\cdot\sigma}_{2}+\underbrace{H}_{3} \tag{5.39}$$

where, the left hand side of the equations(1) is the net rate of momentum flow. The terms on the right hand side correspond to net pressure force and the net viscous forces(2), and body force(3).

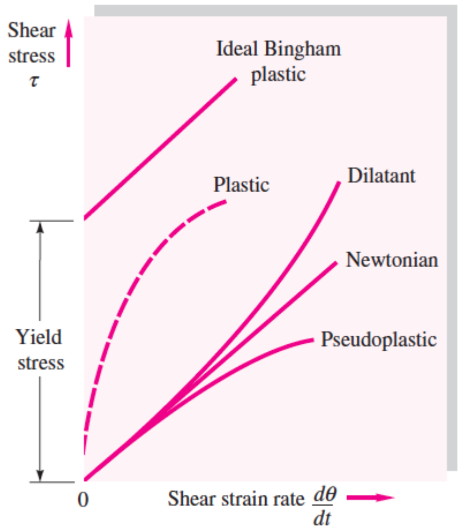

Figure 5.8: Newtonian fluid

Assuming that the stress as linear, Galilean invariant and that the fluid as isotropic, also called Newtonian fluid (Figure 5.8), an equation for a compressible fluid is derived. The following equation is also know as Navier-Stokes equation.

$$\underbrace{\rho\left(\frac{\delta \mathbf{V}}{\delta t}+\mathbf{V}\cdot\nabla textbfV\right)}_{1}=\underbrace{-\nabla p}_{2}+\underbrace{\nabla\cdot\left(\mu(\nabla\mathbf{V}+(\nabla\mathbf{V})^T\right)-\frac{2}{3}\mu(\nabla\cdot\mathbf{V})\mathbf{I}}_{3}+\underbrace{H}_{4} \tag{5.40}$$

where p is fluid pressure, $\mathbf{V}$ is fluid velocity, μ is the fluid dynamic viscosity, ρ is fluid density, g the gravity acceleration, and $\mathbf{I}$ is the identity matrix. The different parts of the equation is; (1) is the inertial forces, (2) is the pressure forces, (3) viscosity forces, and (4) the external forces applied to the fluid [39].

5.8 Boussinesq Approximation

The Boussinesq approximation is used to predict nonisothermal flow, such as natural convection, without solving Navier-Stokes equation for compressible fluids. The approximation states that density does not have an effect on the fluid field other than on the buoyancy term.For a incompressible fluid flow with on other body forces than gravity, the Navier-Stokes equation becomes

$$\rho_0 \left(\frac{\delta \mathbf{V}}{\delta t} + \mathbf{V} \cdot \nabla \mathbf{V} \right) = -\nabla p + \nabla \cdot \left(\mu (\nabla \mathbf{V} + (\nabla \mathbf{V})^T \right) - \frac{2}{3} \mu (\nabla \cdot \mathbf{V}) I) + F \tag{5.41}$$

and the modified continuity equation becomes

$$\nabla \cdot \mathbf{V} = 0 \tag{5.42}$$

Putting eq. 5.42] into eq. 5.41] gives us that the $\frac{2}{3}\mu(\nabla \cdot u)I$ term becomes zero. We also usually assume that the viscosity, μ is constant, giving that

$$\rho_0 \left(\frac{\delta \mathbf{V}}{\delta t} + \mathbf{V} \cdot \nabla \mathbf{V} \right) = -\nabla p + \mu \nabla^2 \mathbf{V} + F \tag{5.43}$$

As mentioned earlier, the Boussinesq approximation assumes that density variations have a fixed part and a part linear dependent on temperature,

$$\rho = \rho_0 - \beta \rho_0 \Delta T \tag{5.44}$$

where β is the thermal expansion coefficient. This gives the following Navier-Stokes equation for an incompressible fluid

$$\rho_0 \left(\frac{\delta \mathbf{V}}{\delta t} + \mathbf{V} \cdot \nabla \mathbf{V} \right) = -\nabla p + \mu \nabla^2 \mathbf{V} - \rho \beta (T - T_0) g \tag{5.45}$$

5.9 Boundary conditions

To solve the heat diffusion equation it is important to know the condition existing in the medium at the initial time and the physical conditions at the boundaries of the medium. It is also important to decide if the situation is time dependent. As earlier stated in Chapter 4, the heat sink was hung 120 mm above a desk. This desk was assumed to be at a constant temperature in the Comsol simulation, meaning that the desk is a Dirichlet condition expressed as

$$T(0, t) = T_s \tag{5.46}$$

The resistor was assumed to generate a constant surface heat flux,

$$-k \frac{\delta T}{\delta x}|_{x=0} = q_s'' \tag{5.47}$$

which also is called a Neumann condition.

The surface of the heat sink there will be obtained a surface energy balance

$$-k\frac{\delta T}{\delta x}|_{x=0} = h[T_\infty - T(0,t)] \tag{5.48}$$

In the simulations the initial temperature was set to 23℃, and it was solved as a time-dependent study. More about this is Chapter 6

5.10 Important numbers

Volumetric Heat Capacity

Transport and thermodynamic properties are the two categories of thermophysical properties that are necessary when analyzing situations of heat transfer. Thermal conductivity and kinematic viscosity are transport properties, while density and specific heat pertain to the equilibrium state of a system. The product ρc_p is the volumetric heat capacity $(\frac{J}{m^3K})$, which measures the ability of a material to store thermal energy.

Thermal Diffusivity

Another important property is the thermal diffusivity α. which measures a material's ability to conduct thermal energy relative to its ability to store thermal energy. Thermal Diffusivity can be calculated using the following equation:

$$\alpha = \frac{k}{\rho c_p} \tag{5.49}$$

Reynolds

Reynolds number is the ratio of inertia and viscous forces. It is used to predict whether the flow is laminar or turbulent during forced convection.

$$Re_x = \frac{\rho u_\infty x}{\mu} \tag{5.50}$$

For tubes, the flow is turbulent if Reynolds number is larger than 2300, and laminar if less. For immersed bodies the transition number is $5 \cdot 10^5$.

Prandtl number

The Prandtl number is the ratio of momentum to heat diffusivity. It is temperature dependent and is calculated like this:

$$Pr = \frac{c_p\mu}{k} = \frac{\nu}{\alpha} \tag{5.51}$$

Grashof's number

Grashof's number is a measure of the ratio between the buoyancy forces and the viscous forces acting on a fluid. The formula is

$$Gr_L \equiv \frac{g\beta(T_s - T_\infty)L^3}{\nu^2} \tag{5.52}$$

where β is the expansion coefficient, L is a characteristic length and ν is the fluid's viscosity. The number is used to characterize natural convection. The transition from turbulent flow occurs when Grashof's number is between 10^8 and 10^9.

Rayleigh Number

The Rayleigh number is the product of the Prandlt and Grashof's number, and describes the relative magnitude of the buoyancy and viscous forces in the fluid. Transition from laminar to turbulent flow happens when the Rayleigh number becomes more than 10^9.

$$Ra_L = Gr_L Pr = \frac{g\beta(T_s - T_\infty)L^3}{\nu\alpha} \tag{5.53}$$

where L is the characteristic length of the geometry, α is thermal diffusivity, β thermal expansion factor, ν kinematic viscosity, T_s surface temperature, and T_∞ ambient temperature

Nusselt number

Nusselt number provides a measure of convective heat transfer occurring at a surface. It is the ratio of convective that goes to conductive heat transfer, and is calculated using the following formula

$$Nu = \frac{h \cdot L}{k} \tag{5.54}$$

where h is the heat coefficient, L is the characteristic length and k is the thermal conductivity

6 Comsol Setup

The partial differential equation Navier-Stokes equation (section 5.7.3) is the heart of fluid flow modeling. Together, with a certain set of boundary conditions, the movement of a fluid in a given geometry can be predicted, including velocity and pressure at specific points. However, the Navier-Stokes equation only has a limited amount of known analytical solutions, so the more complex geometries have to be solved numerically [comsolNS]. In this report, the FEM software, Comsol, is used to calculate the numerical solutions for fluid flow and heat transfer in and around the heat sink. This chapter will explain how the geometry is built, what boundary conditions are used, and an overall background regarding how Comsol works.

6.1 Setup

The heat sink and heat element were built in 3D using a combination of modeling shapes like blocks and cylinders, transform commands like rotate and copy, and Boolean operations like difference, intersection, and union. A big rectangular box was built around the heat sink creating a control volume, which was set to a height of 450 mm and a length and width of 400 mm. The heat sink was equidistant from all four side walls and 120 mm from the bottom side of the box. Through several rounds of trial simulations, the air flow above the heat sink became more stable and realistic while test results became more accurate when simulating only half of the model rather than the model in its entirety. This also made the simulations quicker because they required less computational resources. Based on these observations, half of the geometry was used for the simulation portion of this project. The geometry and boundary conditions were modeled using parameters that were defined at the beginning to make "parameter" optimization simpler. The parameters can be seen in Appendix C.1, and the geometry created in Comsol can be seen in the Figures 6.1a and 6.1b

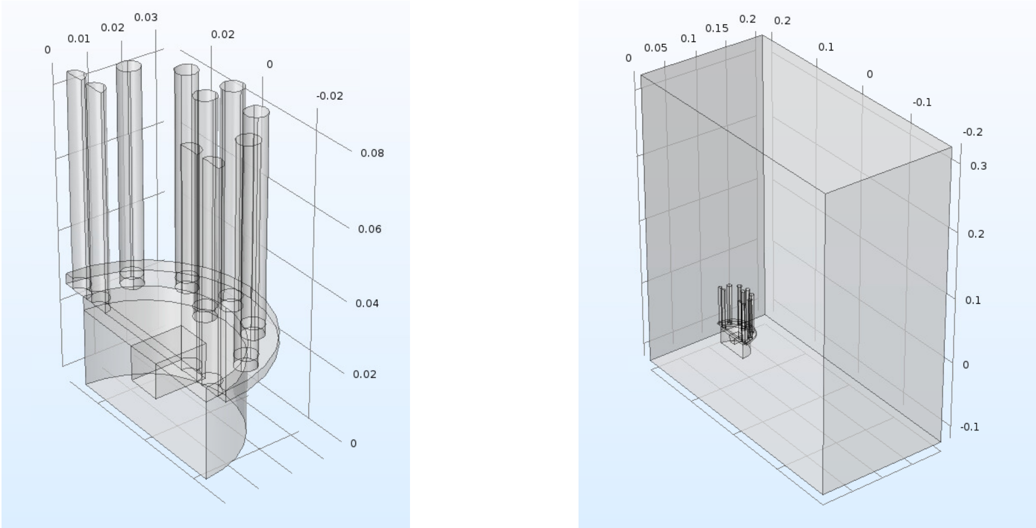

(a) Heat sink and heat element **(b)** Comsol geometry

Figure 6.1

After the heat sink geometry was created, various materials were added to different components. Aluminum was added to the heat sink and to the plate in the heat element. Carbon was added to the resistor, as seen in Figure 6.2a. Sikaboom s isolation foam was added to the area surrounding the resistor. Lastly, air was added to the box surrounding the heat sink. Most of the materials were obtained from Comsol's own material database, which by default, stores the properties of many common materials like air and aluminum. Less common materials, like SikaBoom, had to be defined manually. All the materials used, in addition to their material properties, can be seen in Table 6.1

	Thermal Conductivity $[W/mK]$ k	Density $[kg/m^3]$ ρ	Heat capacity $[J/(kgK)]$ c_p	Dynamic viscosity $[Pa \cdot s]$ η	Ratio of Specific Heat γ
Aluminum	238	2700	900		
Air	k(T[1/K])	rho(pA[1/Pa],T[1/K])	Cp(T[1/K])	eta(T[1/K])	1.4
Carbon steel [14]	60.5	7854	434		
SikaBoom S [40]	0.03	18	1800		
Paper [14]	0.180	930	1340		
Steel AISI 4340	44.5	7850	475		
Polysilicon	k(T[1/K])	2320	678		
Thermal Grease [41]	0.67				

Table 6.1: Material properties

The material settings determine how the material properties are interpreted when the mesh is formed and how the material behaves. A fluid like air will have properties that are defined only as functions of the current local state at each point in the spatial frame and for which no unique material orientation can be defined. On the other hand, solids have properties that change as functions of material orientation, strain, and other variables evaluated within the material frame. In a study of heat transfer and fluid flow, like this one, the used solids will have constant material properties, while air will have properties that depend on temperature and pressure. Airs functions for thermal conductivity, density, heat capacity and dynamic viscosity can be seen in Appendix C.2

Another important variable when using Comsol modeling is setting the boundary conditions. Three modules of boundary conditions were used; one concerning heat transfer, one concerning fluid flow, and one combining the two. In the heat transfer module, Comsol was told which domains were solids and which were fluids. Additionally, the heat source and the heat rate were defined (Figure 6.2a), and the initial temperature set to 23℃ throughout the whole model. The boundary conditions at the border of the control volume were also predetermined. The control volume was defined with open boundary conditions on three out of four sides in addition to the top borders, as seen in Figure 6.2b. Open boundary means that heat could flow in and out of the domain with a specified exterior temperature, which was set to 23℃. In contrast, the bottom border was set to a specific temperature to take into account that in the real life experiment, there was a table present. This table was assumed to have a constant temperature of 23℃ throughout the entire experiment. The last side of the box is where the half geometry was cut in two, and has a boundary condition set to symmetry. This indicates that the same results will occur on the mirrored side of the geometry and that there is no heat flux across this boundary.

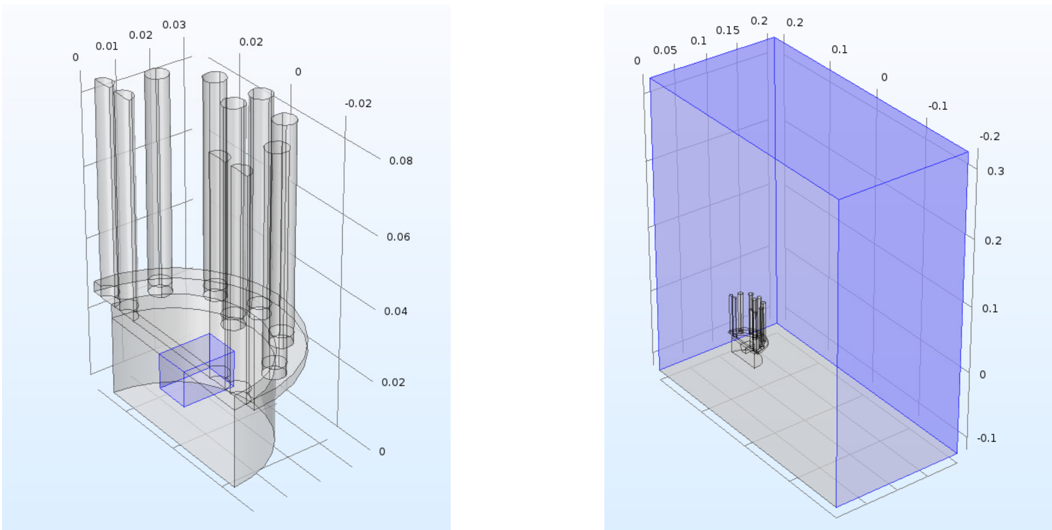

(a) Heat source (blue) **(b)** Open boundaries

Figure 6.2

The fluid flow module determines the nature of the air flow. Bassed on low air velocitys temperatures in Nissens [19] and Arentfelts [20] thesis, the flow is assumed to be laminar, meaning that the flow pattern is more predictable and that it will be easier to achieve good results. The flow was also assumed to be incompressible, meaning that the density of air is regarded as a constant. Based on previous experiments conducted,

[19],[20] temperatures did not rise above 50℃. This means that the density maximum would have a change of 0.15 kg/m^3, approving the assumption of incompressible flow. When incompressible flow is assumed Comsol will use Boussinesq approximation. $\frac{\delta u}{\delta t}$ and $\frac{\delta \rho}{\delta t}$ are part of these equations because this project is a time-dependent study.

In the laminar flow node, the initial velocity field was defined as 0 m/s in all directions. Symmetry was added to the cut side of the half geometry, but only the parts that are fluids. Open boundary conditions were added to same boundaries as in the heat transfer module (se Figure 6.2b). In the flow module, the open boundary condition means that fluids can enter and leave the control volume with an unknown velocity. Also, it means that there is a normal stress at the boundary, which in this project, is set to $f_0 = 0\ N/m^2$. Lastly, the bottom border and the heat sink surface was defined as walls with a no-slip boundary condition. In other words, the velocity of the fluid must be at the same velocity and in the same direction as these boundaries, hence the equation $u = 0\ m/s$.

The fluid flow depends on the temperature and is therefore coupled the heat transfer node through the Non-isothermal flow node. This node ensures that the same definition of the density is used in both modules. In the simulations conducted, the density was set to come from the heat transfer interface.

When creating a mesh, the problem that already is discretized in space and time is divided into small units of simple shapes. The physics-controlled mesh was used, which allows Comsol to generate a mesh based on the given geometry and boundary condition. This produces a mesh where the lines between the nodal points are a lot smaller near the surface of the heat sink than in the rest of the control volume. This is because the change in heat flux and acceleration of particles are largest near the surface. Meshes can be seen in Figure 6.4

As mentioned earlier, the simulations were conducted as part of a time-dependent study rather than a stationary study. This decision to use a time-dependent study was made after several rounds of trial simulations in a stationary-study producing non-converging results that were not following the expected flow pattern. The time-dependent study gave stable results when it ran for a sufficient amount of time. Therefore, the studies were conducted in a 45 minute time interval, calculating a solution each minute.

A explanation of all the Comsol features used and additional figures can be seen in Appendix C.3

6.2 Simulation program

There are three main goals of this project in regards to simulation. One is to discover the predictive accuracy and capabilities of Comsol when compared to real life experiments. This was done for the heat sink in three positions; vertical, horizontal and 45° position as seen in Figure 6.3.

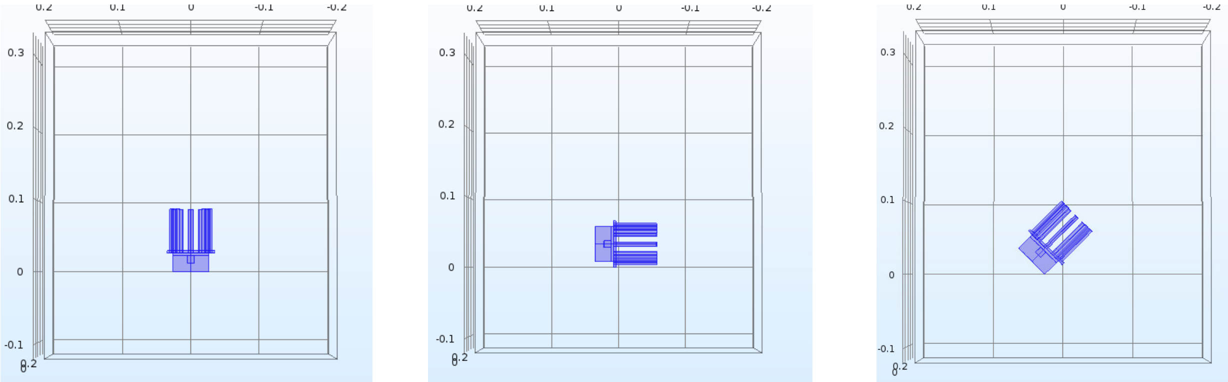

(a) Vertical Position **(b)** Horizontal Position **(c)** 45°Position

Figure 6.3

An additional goal was to investigate the effects of slight changes in experimental setup and/or design would alter results produced by Comsol. These slight changes might include making the model more realistic and complex by adding the electric cables, screws, or thermal grease. Differences in airbox dimension, resistor material, mesh, and flow nature were also simulated and compared. The goal is to make Comsol easier to use for others trying to solving natural convection problems, in order to achieve approximate, but realistic results. All simulations where done with 4 watts in a vertical heat sink position.

In the end, a parameter optimization study was conducted, investigating whether the heat transfer in the heat sink can be optimized by changing fin height, diameter, and number of fins. The total simulation program can be seen in table 6.2, 6.3 and 6.4, where the the red values represents the values used in the "final" Comsol model and is used in all the simulations.

Table 6.2: Vertification simulations

Input	Normal mesh	Fine mesh
Vertical	1W, 2W, 3W, 4W, 5W	1W, 2W, 3W, 4W, 5W
Horizontal	1W, 2W, 3W, 4W, 5W	1W, 2W, 3W, 4W, 5w W
45°position	1W, 2W, 3W, 4W, 5W	1W, 2W, 3W, 4W, 5W

Table 6.3: Comsol test

Input	Variables
More realistic model	Electric cables, Screws, Porous foam, Thermal grease and Tape, All together
Airbox dimension (mm) (heigth x length x width)	350x300x300, 450x400x400, 550x500x500, 650x600x600
Resistor material	Carbon, Aluminum, Steel, Polysilicon
Flow	Incompressible, Weakly compressible, Compressible
Geometry	Full(1), half (1/2), quarter (1/4)

Table 6.4: Parameter optimization

Optimize	Variables
Fin height	40 mm, 50 mm, 60 mm, 70 mm, 80 mm
Fin diameter	4 mm, 5 mm, 5.98 mm, 7 mm, 8.2 mm, 9 mm
Number of fins in outer circle	4, 8, 12, 16, 20
Number of fins in inner circle	0, 2, 4, 6, 8

All of the simulations were conducted with, what Comsol calls, a *normal* physics-controlled mesh, unless something else was specified. The reason for this was a time restriction. A coarse mesh requires less computational resources to solve and while it may give a less accurate solution, it still gives a good indication of how the simulations will vary when you change various parameters. A coarse mesh will also provide information regarding which parameters that are better than others. The different meshes can be seen in figure 6.4

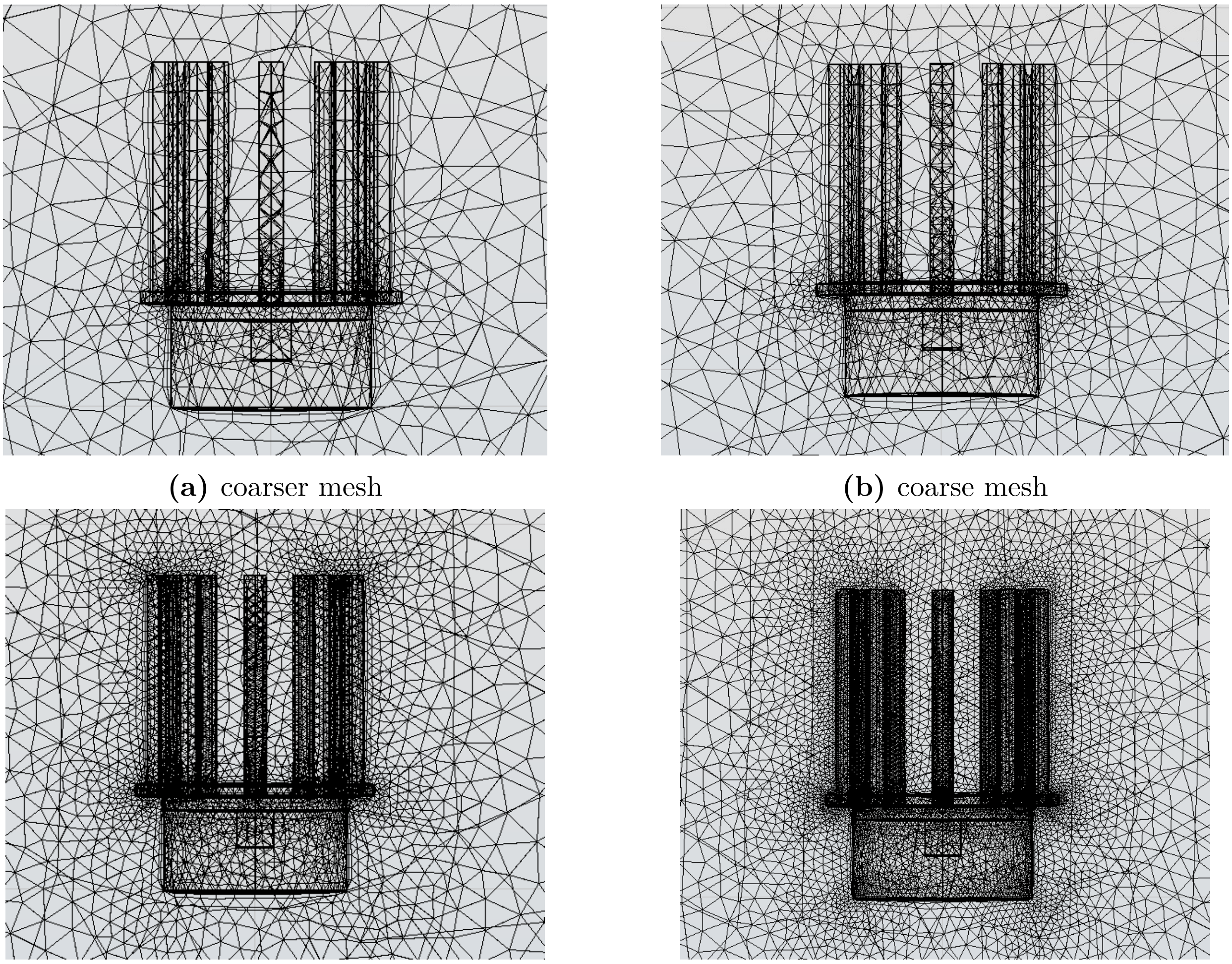

(a) coarser mesh **(b)** coarse mesh

(c) Normal mesh **(d)** Fine mesh

Figure 6.4: Meshes compared

7 Results

In this chapter, the results achieved in the experiences and simulations are presented with charts and numbers.

7.1 Experiments

After the experimental setup (Figure 4.1) was complete, the experiments were conducted with heat sink in a vertical position. During different trials of the experiment, the power supply was set to various wattages, ranging from 1-5 watts. Each wattage level tested was allotted two hours with the temperature measured each second. In the first set of experiments, the power was raised from 1 watt to 2 watts and so on, up to 5 watts. When 5W was reached, the power was set to 6W for approximately 30 minutes (reached approximately 50℃), before the same experiments were conducted, this time starting at 5W and ending at 1W. This complete set of experiments was completed with the heat sink in the vertical, horizontal, and 45 degree position. The temperature was measured at the heat sink junction, as seen in Figure 7.1. The temperature development for experiments with the heat sink in each of these positions was measured and can be seen in the Figures 7.2, 7.3, and 7.4

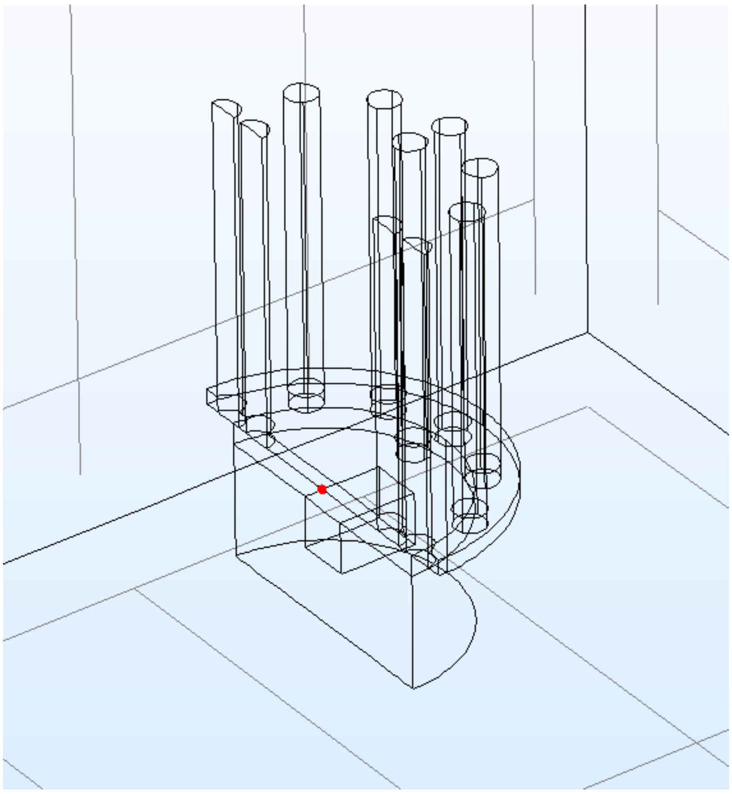

Figure 7.1: Red point is where the temperature was measured in Comsol(HS junction)

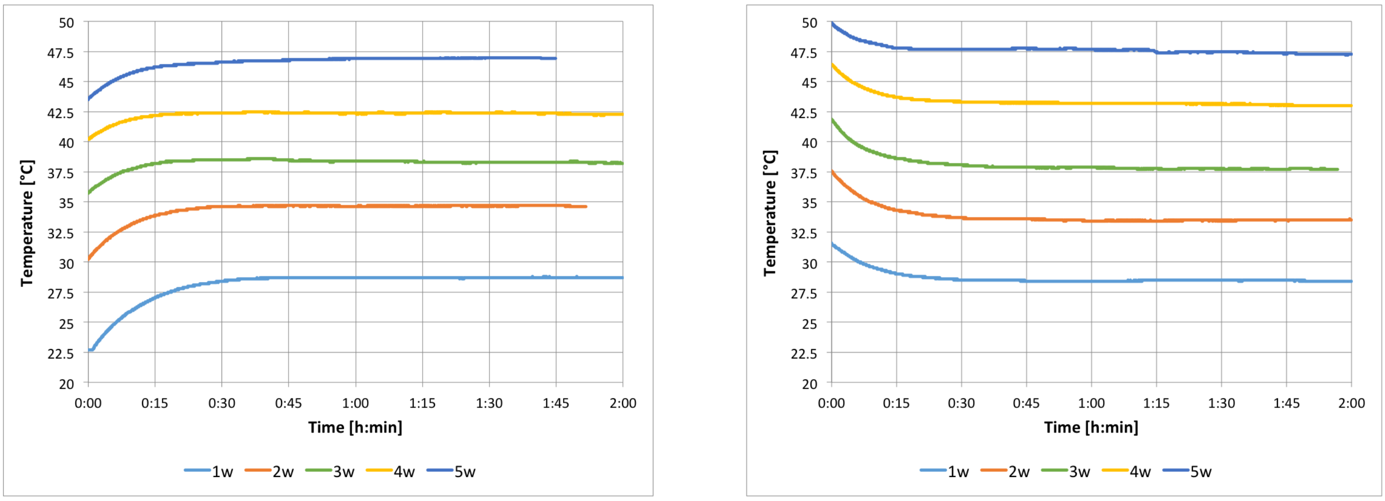

(a) Incerasing power

(b) Decerasing power

Figure 7.2: Temperature development in heat sink in vertical position over a time span of two hours

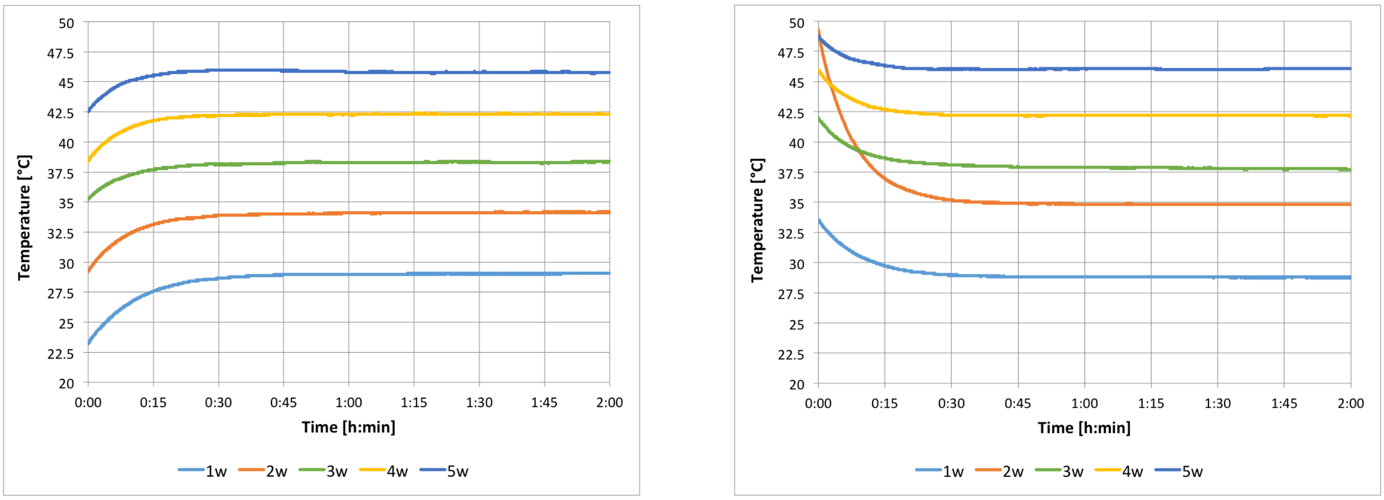

(a) Incerasing power

(b) Decerasing power

Figure 7.3: Temperature development in heat sink in horizontal position over a time span of two hours

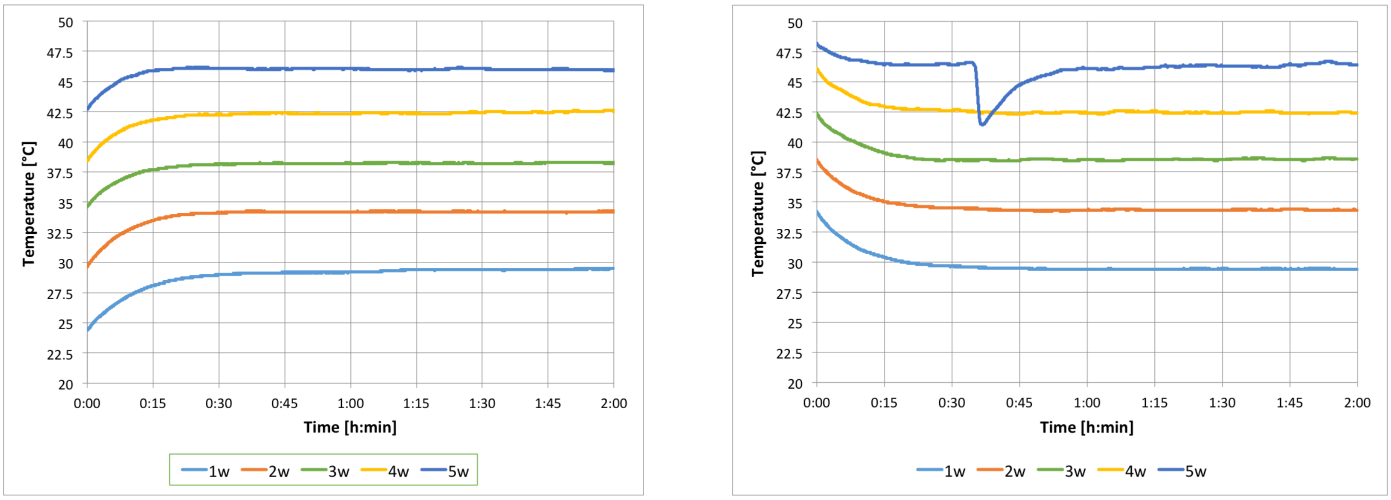

(a) Incerasing power

(b) Decerasing power

Figure 7.4: Temperature development in heat sink in 45° position over a time span of two hours

The 2w experiment, in figure 7.3b started at 50℃ instead of starting at the temperature 3w ended on. This was due to a mistake made in the initial experiment, resulting in a new experiment being conducted. The 5w experiment, shown in figure 7.4b, has a sudden decrease in temperature 35 minutes into the experiment. However, the temperature stabilized afterwards, allowing those data to be used in later comparisons.

Notice that all of the experimental temperatures were at a steady state 45 minutes after the experiment began. The average of the temperatures measured between 1:30 and 2:00 (Table 7.1-7.3) was used when comparing experiments to simulations in the next chapter. The ambient temperature in the simulations will be constant, while in the experiment, it will vary. Therefore, the average air temperature was subtracted from the average temperature between the HS and HE to create a new temperature measurement that does not depend on ambient air temperature. This new measurement was compared to the same measurement taken from the simulation and is shown in tables 7.1, 7.2, and 7.3. Additionally, the previously mentioned tables display the average temperatures in the air, between HS and HE, as well as the standard deviation for each experiment. "up" mean increasing power experiment, while "down" mean decreasing power experiment.

Table 7.1: Experimental Results for Heat Sink in Vertical Position

Power(up/down)	Average HS Junction Temp. ℃	Average Air Temp ℃	Average Difference ΔT ℃	SD	Samples included in Average
1w (up)	28.70	22.61	6.09	0.106	1800
2w (up)	34.68	23.42	11.26	0.119	1301
3w (up)	38.29	23.10	15.18	0.128	1800
4w (up)	42.35	22.93	19.42	0.129	1800
5w (up)	46.98	22.90	24.08	0.156	900
1w (down)	28.46	22.62	5.85	0.117	1800
2w (down)	33.49	22.58	10.91	0.118	1301
3w (down)	37.73	22.61	15.12	0.132	1611
4w (down)	43.06	22.98	20.08	0.152	1800
5w (down)	47.37	23.85	23.52	0.136	900

Table 7.2: Experimental Results for Heat Sink in Horizontal Position

Power(up/down)	Average HS Junction Temp. ℃	Average Air Temp ℃	Average Difference ΔT ℃	SD	Samples included in Average
1w (up)	29.06	22.93	6.13	0.135	1800
2w (up)	34.12	23.21	10.91	0.127	1800
3w (up)	38.33	23.28	15.04	0.128	1800
4w (up)	42.30	23.24	19.07	0.150	1800
5w (up)	45.81	23.18	22.64	0.090	1800
1w (down)	28.78	22.79	5.99	0.118	1800
2w (down)	34.80	24.59	10.21	0.043	1800
3w (down)	37.79	22.93	14.87	0.108	1800
4w (down)	42.20	23.05	19.15	0.117	1800
5w (down)	46.06	23.04	23.02	0.139	1800

Table 7.3: Experimental Results for Heat Sink in 45° Position

Power(up/down)	Average HS Junction Temp. °C	Average Air Temp °C	Average Difference ΔT °C	SD	Samples included in Average
1w (up)	29.42	23.27	6.16	0.120	1800
2w (up)	34.20	23.33	10.88	0.123	1800
3w (up)	38.25	23.21	14.95	0.130	1800
4w (up)	42.48	23.28	19.20	0.129	1800
5w (up)	46.00	23.08	22.93	0.129	1800
1w (down)	29.41	23.28	6.13	0.141	1800
2w (down)	34.33	23.28	11.05	0.123	1800
3w (down)	38.58	23.28	15.30	0.155	1800
4w (down)	42.44	23.23	19.21	0.124	1800
5w (down)	46.39	23.09	23.30	0.181	1800

After the experiments were executed, the thermocouple was moved from between the aluminum plates to one of the fins via a piece of tape as seen in figure 7.5. This was done to see if the difference between experiments and Comsol would be the same at two different locations. This is time, the experiment was only conducted with the heat sink in a vertical position and only once at each interval from 1W to 5W. The temperature development can be seen in figure 7.6

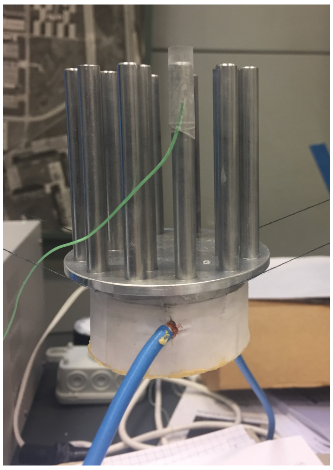

Figure 7.5: Fin measurement

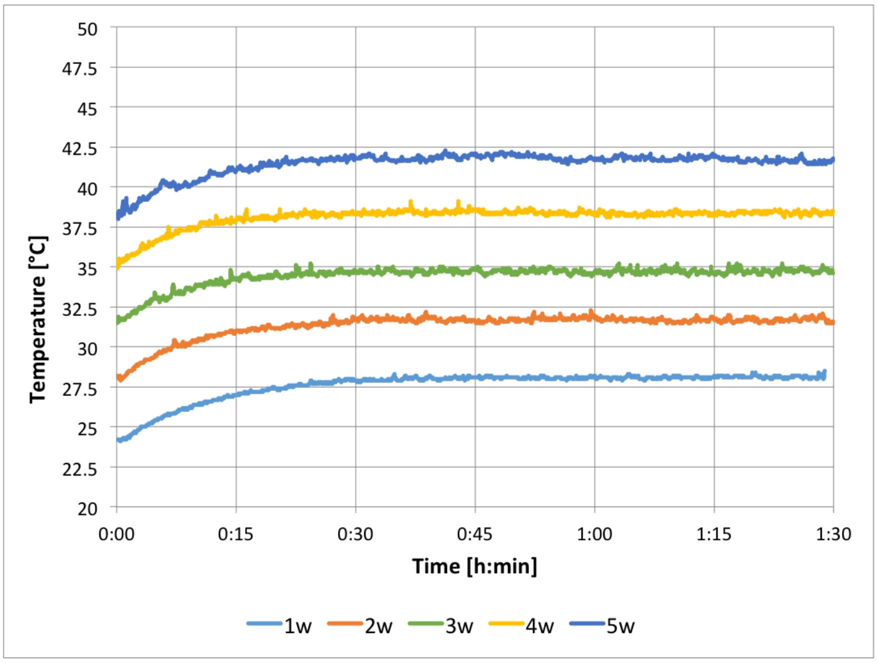

Figure 7.6: Temperature development at the top of fin when heat sink is in vertical position

Based on the fin measurement chart in figure 7.6 , the temperature was greatly affected by its surroundings and not as stable as the temperatures measured in between the aluminum plates. This is also reflected in the standard deviation, which is slightly higher compared the other tests, though still around 0.2. Each of the experiments in this portion of the project were conducted in 1 hour and 30 minutes. The last 15 minutes of this timespan were used to calculate the average temperature, average difference, and standard deviation. The values can be seen in table 7.4

Table 7.4: Experimental Results of Fins in Vertical Position

Power(up/down)	Average HStemp.	Average air temp	Average difference	SD	Samples included in average
1w	28.13	23.56	4.57	0.144	900
2w	31.70	23.49	8.21	0.164	900
3w	34.73	23.46	11.27	0.168	900
4w	38.38	24.13	14.25	0.202	900
5w	41.64	24.06	17.58	0.199	900

7.1.1 Infrared camera

Pictures of the heat sink in the vertical position were taken with an infrared camera. The aluminum was shiny with an emissivity between 0.04 and 0.2. This is too low for the camera to pick up when the other materials in the picture have a much higher emissivity. Paper tape was put on one fin to increase emissivity and highlight how hot the fins became. The emissivity setting on the camera was set to the default at 1. An infrared picture of heat sink in vertical position at 3w can be seen below. Pictures of other powers can be seen in Appendix E

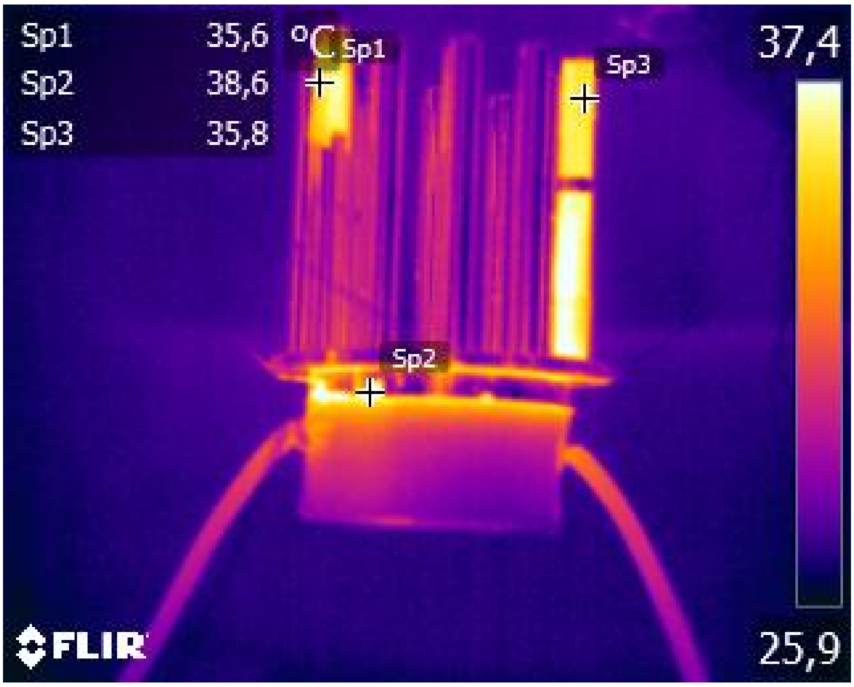

Figure 7.7: Infrared picture of heat sink in vertical position at 3w

As seen in the photo, there are two fins that produce a temperature output, while the others are "cold". In both cases, tape attached to the fin can be attributed to the increased output. On one fin, paper tape was used to increase the emissivity for the infrared camera, while the other fin had the thermocouple taped to it. The tape is an extra resistance, causing more heat flux to go out to the other fins that do not have tape. Therefore, these results are unreliable, though the temperatures in the picture fit relatively well with the temperatures in Table 7.4. Additionally, the picture shows that some of the heat disappears out through the electric cables. It is also possible to see some heat in the junctions between parts, like between the aluminum plates as well as between the isolation foam and heat element aluminum plate.

7.2 Simulations

Each simulation was conducted over a period of 45 minutes and new results were calculated and displayed every minute, giving a development of the temperature in the heat sink over time. In this section, the development will be displayed for the five power inputs in the three heat sink positions. In figures 7.8, 7.9, and 7.10, the heat and velocity distribution is displayed within the control volume.

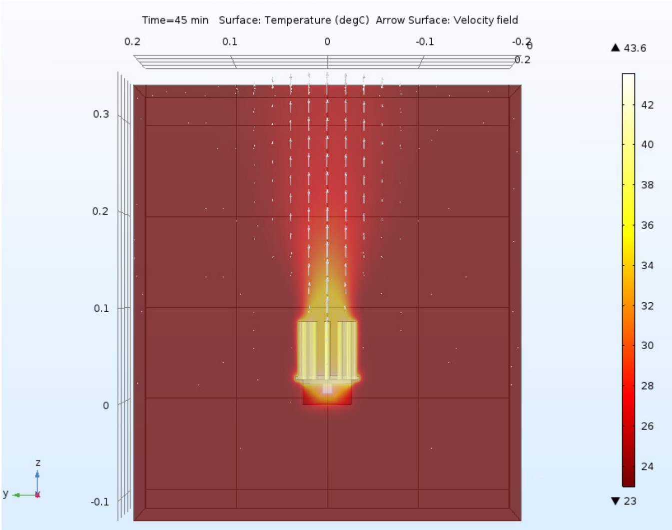

(a) Temperature

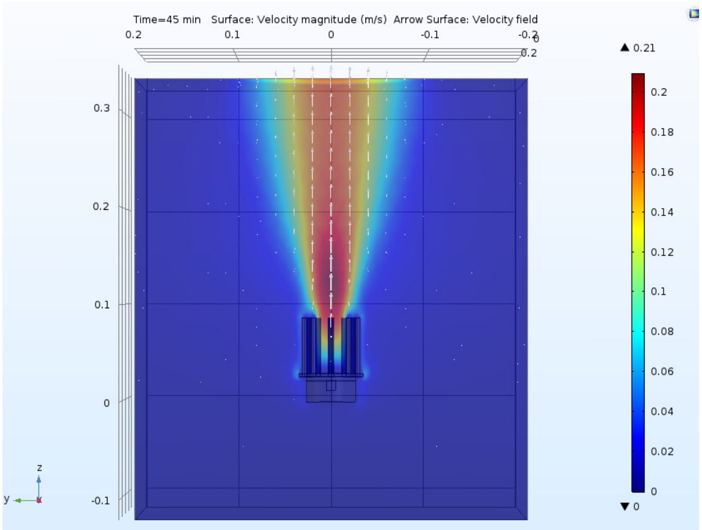

(b) Velocity

Figure 7.8: Result for heat sink at vertical position with 4 w input and fine mesh

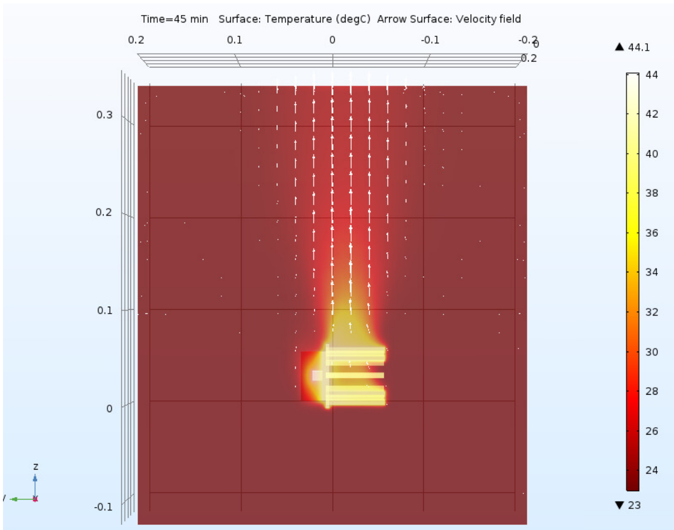

(a) Temperature

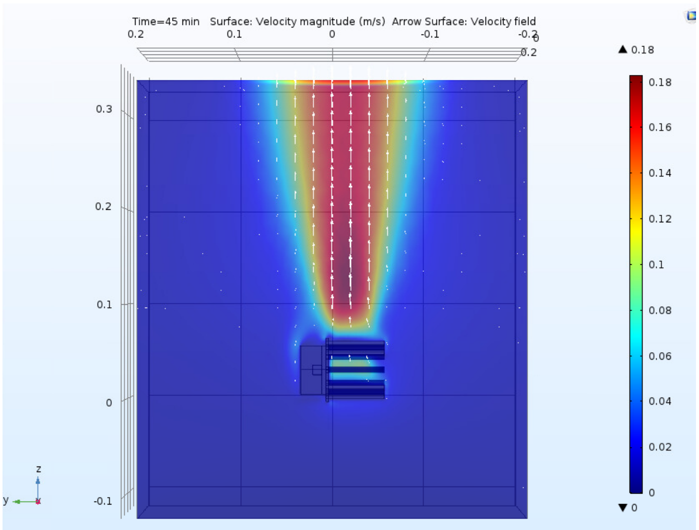

(b) Velocity

Figure 7.9: Result for heat sink at horizontal position with 4 w input and fine mesh

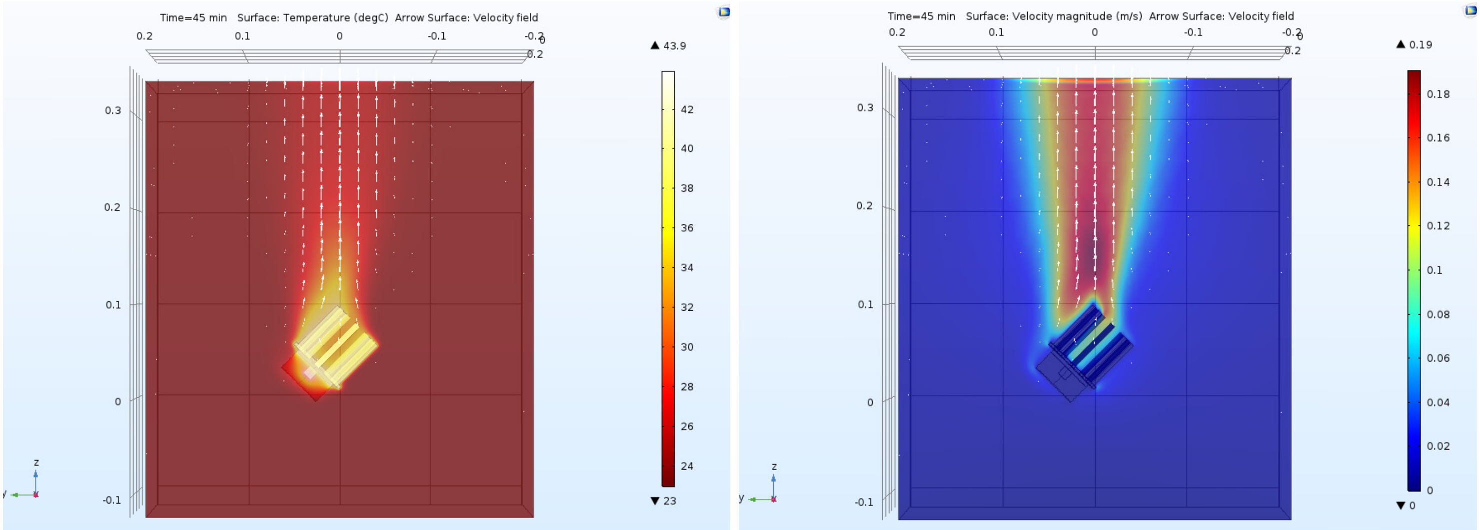

(a) Temperature **(b)** Velocity

Figure 7.10: Result for heat sink at 45 °position with 4 w input and fine mesh

The figures above show that the heat generated in the resistor gets directed towards the heat sink, while the lower part of the isolation foam stays close to ambient temperature. The heat appears to be well distributed to all the fins, generating an airflow where the warmer air becomes less dense and floats above of the colder, heavier air. To make up for the air that disappears out of the control volume at the top, new air at ambient temperature will be dragged in from the side boundaries. The white arrows in all the figures above, illustrate the velocity field and are proportionally distributed in terms of velocity, meaning that the bigger the arrow, the higher flow velocity. In these figures, the bigger arrows above the heat sink are pointing upwards, indicating that the velocity in this position is highest and in a vertical direction. Around and under the heat sink, the arrows are smaller, which means that the velocity is much lower in these areas. To clearly see the direction the flow and where there are low velocities, a figure is created with arrows that are not dependent on the velocity itself, only on its direction. Figure 7.11 shows that air comes in from the sides and then flows vertically up under the heat sink, around it, and in between the fins, before the flow catches some speed when the air gets warmed up and disappears at the top. All of the figures shown are using 4 watts, but the same pattern will occur

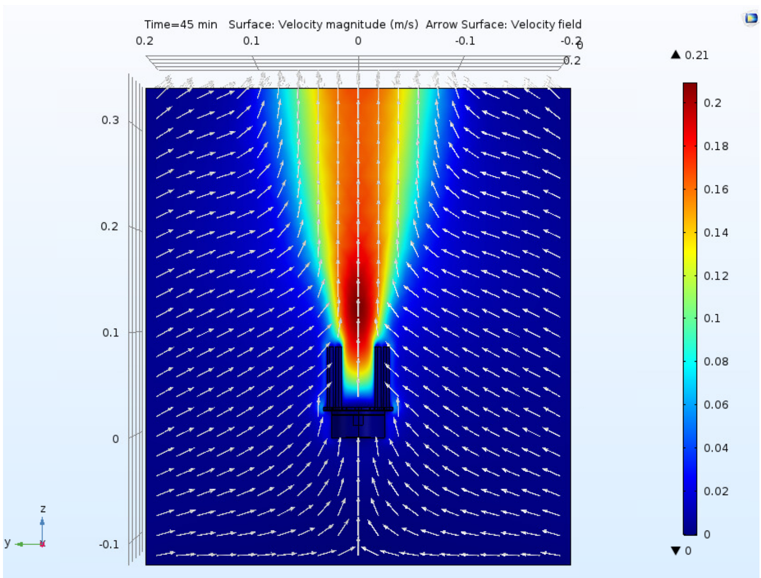

Figure 7.11: Result for 4w with arrows

at all power inputs with minor differences in the temperature and velocity. In the charts below, the temperature development for all 5 power inputs is plotted over a time span of 45 minutes.

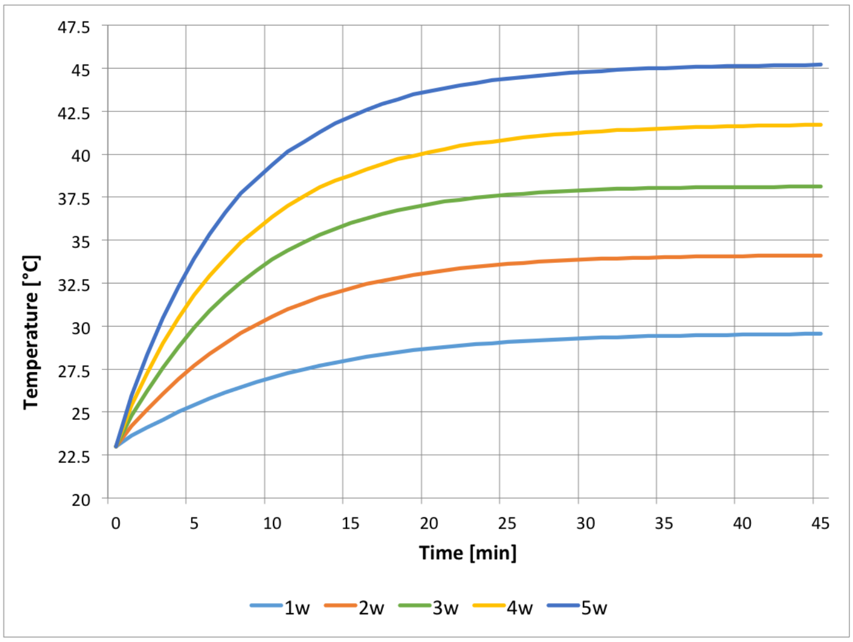

Figure 7.12: Temperature development for simulation of vertical heat sink with fine mesh

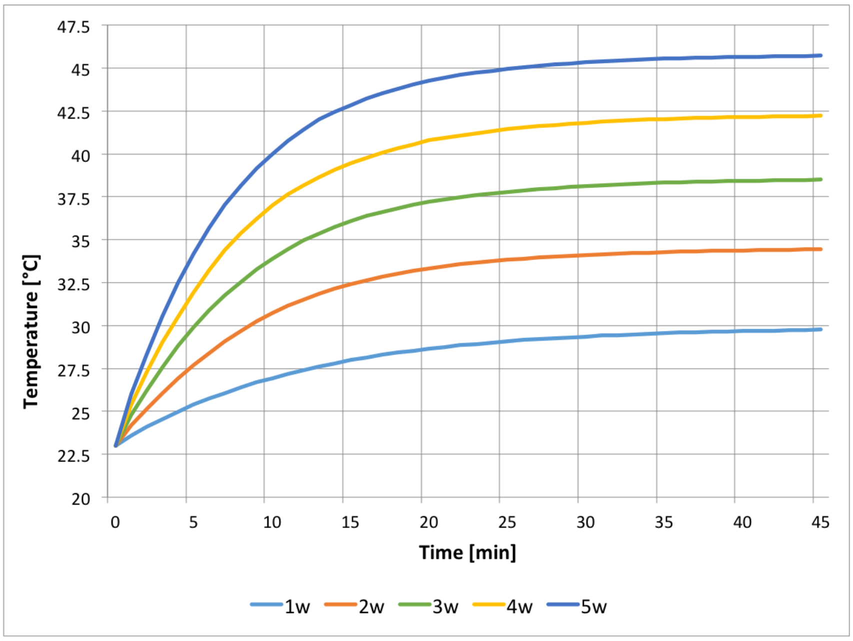

Figure 7.13: Temperature development for simulation of horizontal heat sink with fine mesh

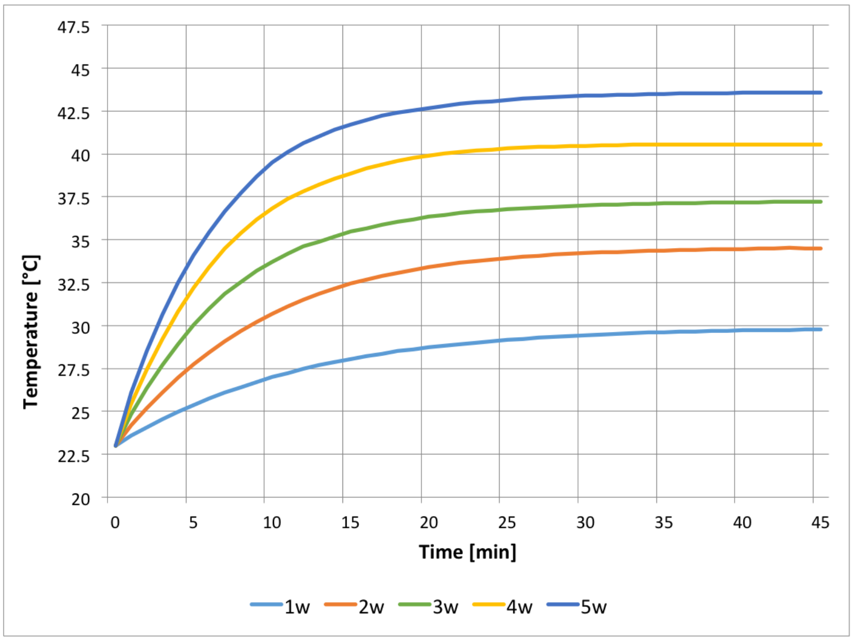

Figure 7.14: Temperature development for simulation of heat sink in 45° position with fine mesh

For the Comsol models, steady state is defined as achieving a temperature change that is less 0.1℃ within the last 5 minutes of a 45 minute simulation. The charts above show that the temperature rises the most in the start, and even out after approximately after 35 minutes.

8 Comparison and Discussion

In this section, three different comparisons are made. First, the results obtained in the real life experiments are compared to the results obtained through Comsol simulations. Then, variations in the Comsol setup, including mesh type and air box dimensions, are compared to investigate how each will alter the results. Lastly, different heat sink variables, such as fin height and diameter, are compared to one another in Comsol using parametric shape optimization.

8.1 Comsol Simulations and Experiments

To assess Comsol's ability to accurately predict real life heat transfer and natural convection in and around a heat sink, the experimental temperatures taken at the HS junction (Figure 4.1) and at the fins are compared to the results for the same geometry found in Comsol simulations (Figure 7.1).

8.1.1 Comparison of Temperature Development

The results chapter showed that a steady state condition in both in the experimental and simulated results was achieved, but do they have a correlation? If yes, how strong is this correlation? In the charts in Figure 8.2, the temperature developments for both situations are plotted for the three positions with 1 watt power trials in a 45 minute time span.

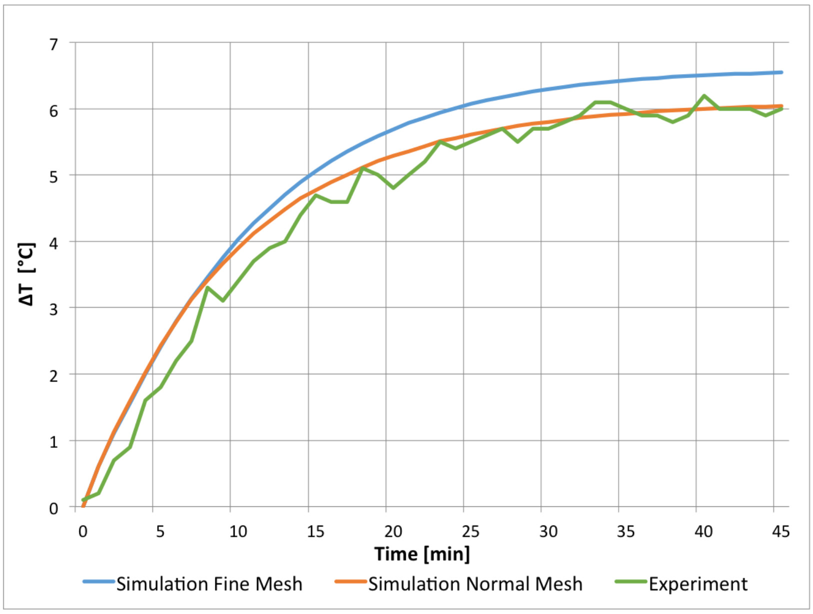

Figure 8.1: Temperature development in heat sink over 45 minutes at 1 w input in vertical position

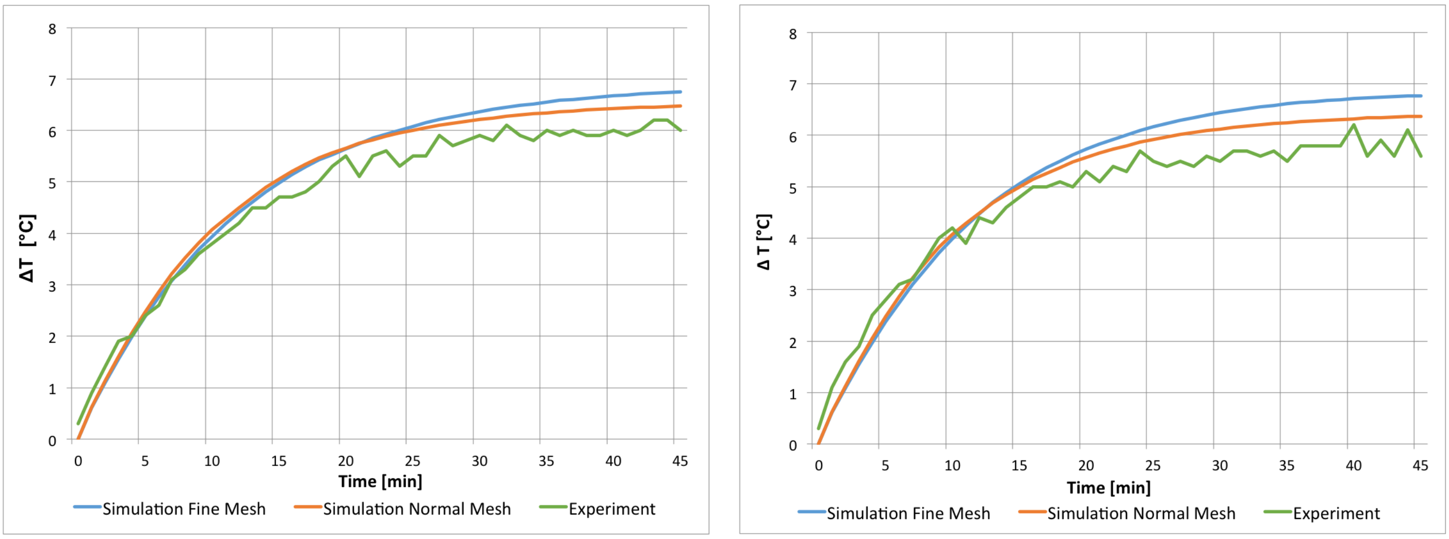

(a) Horizontal position **(b)** 45° position

Figure 8.2: Temperature development in heat sink over 45 minutes at 1 w input

As expected, the Comsol results have a strong correlation to the real life experiments. The linear dependence measured using Pearson's correlation method(Appendix F) gives a correlation coefficient of over 0.99 (out of 1) for both meshes in all three HS positions. Pearson's correlation value describes how the graphs have the same shape, but not how similar the temperatures are. In the beginning of the simulation, temperatures were consistent with one another but as time went on, they diverged. The real life experiment had the lowest steady state temperature, the fine mesh simulation had the highest steady state temperature, and the normal mesh simulation fell in the middle. The exception to this pattern was the vertical heat sink, in which the normal mesh simulation and the real life experiment had the same steady state temperature.

8.1.2 Comparison at Steady State Temperature

In Comsol, the ambient temperature was subtracted from the steady state temperatures and compared with the same measurements taken from the experiments at all power inputs, in all positions. In other words, the average temperature difference in the experiments, shown in Tables 7.1, 7.2, and 7.3, was compared to the last temperature achieved at each power in Comsol minus 23°C (ambient temperature in simulations). There are three charts, one for each HS position, and three graphs in each chart. One graph represents the experiment and consists of the mean of the two temperatures at each power level. The two other graphs are each based on simulations with normal mesh and fine mesh. This is done not only to gain a better understanding of the correlation between Comsol simulations and real life experiments, but also to see which mesh best predicts the experimental results.

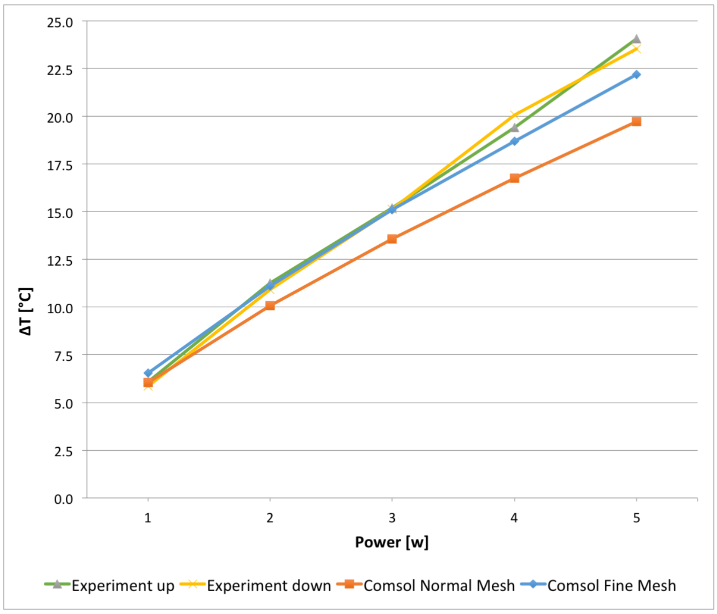

(a) Vertical position

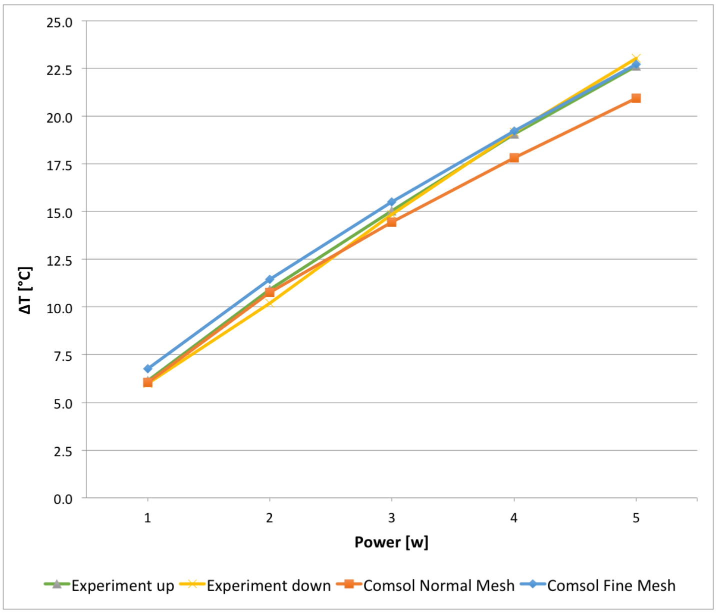

(b) Horizontal position

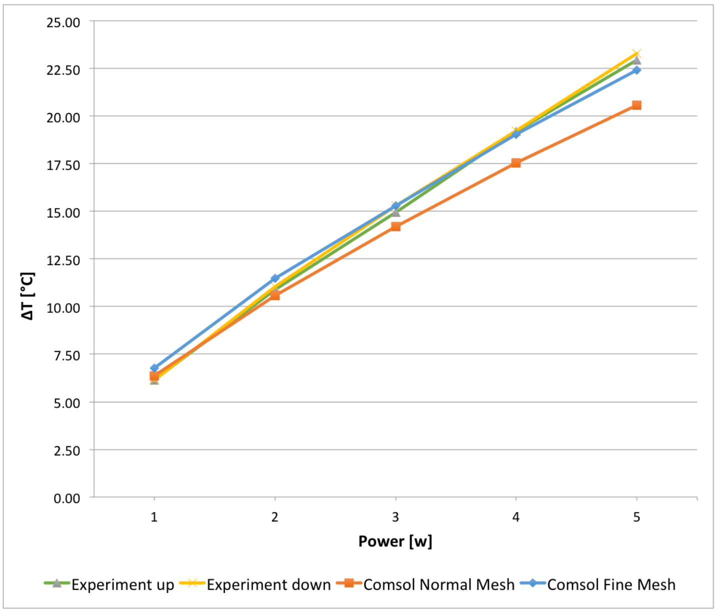

(c) 45°position

Figure 8.3: Comsol Simulation vs Real Life Experiment

The charts indicate that the normal mesh realistically predicts the experimental results at the low power inputs, while the fine mesh is better at high input powers. The normal mesh matches the real life experiments accurately at 1 watt and only has a 0.07℃ difference compared to the experiment in vertical position. However, the difference grows larger and larger and at 5 watts, the normal mesh is 4.06℃ lower than the temperature found in the vertical experiment. Overall, the fine mesh gives a more precise picture of the experimental temperatures than the normal mesh. The fine mesh has an average percentage difference of 4.4%, 4.88% and 4.0% for the vertical, horizontal, and 45° HS, respectively. The difference, percentage difference, and average percentage difference can be seen in the Tables G.1,G.2, and G.3 in Appendix G.1.

8.2 Small changes in Comsol setup

In this project, numerous rounds of testing were conducted before the Comsol model used became a reliable tool for producing accurate simulation. In this section, some of the comparisons are shown as well as some extra tests that may be used for further optimization of the model. For this section, all of the simulations were done in a vertical position with a power of 4 w. These conditions were chosen at random, and the results may have been different if another position or power level was chosen. Normal mesh was used because of lack of time. The red values in the following charts are what all the other simulations in this project is simulated with.

8.2.1 Comparison of Meshes

Normal and *fine* mesh types were included as a part of the comsol verification portion in 8.1.2, but in this section, the results for four different meshes were tested. All four meshes were physics controlled by Comsol and were defined as *Coarser*, *Coarse*, *Normal*, and *Fine*. They can all be seen in Figure 6.4.

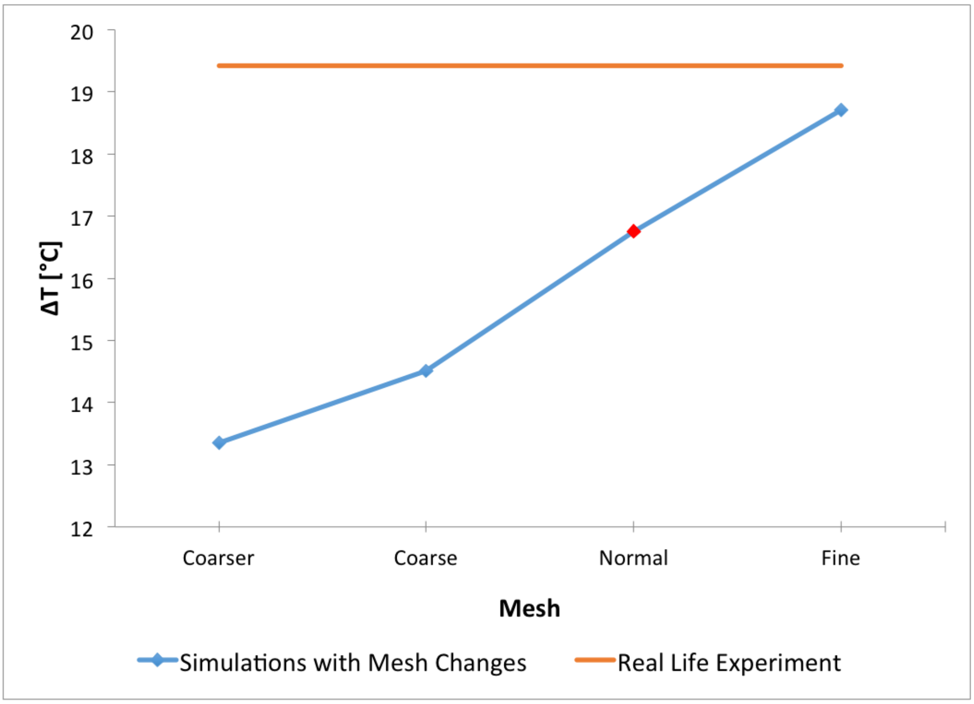

Figure 8.4: Change in Mesh, Vertical 4w

The finer meshes gave a result that is closer to the experimental results, but the coarser meshes used significantly less simulation time. The *coarser* mesh had a simulation time of 4 minutes and a temperature 31% lower when compared to experimental temperatures. The *coarse* mesh had a temperature that was 25% lower and took 9 minutes to simulate. The *normal* mesh had a temp that was 14% lower and used 45 minutes, and the *fine* mesh was only 3.7% lower in temperature, but took 8 hours and 32 minutes to simulate. The simulation time is determined by the amount of degrees of freedom (DOF) the different models have. The more DOF, the longer the simulation time will be and the more unknown variables there will be affecting the results. This pattern is reflected in the results, as the *coarser* mesh had 40 000 DOF, *coarse* mesh had 68 000 DOF, *normal* mesh had 195 000 DOF, and *fine* mesh had 900 000 DOF.More data can be seen in Figure G.1 in the appendix.

8.2.2 Comparison of Airbox Dimensions

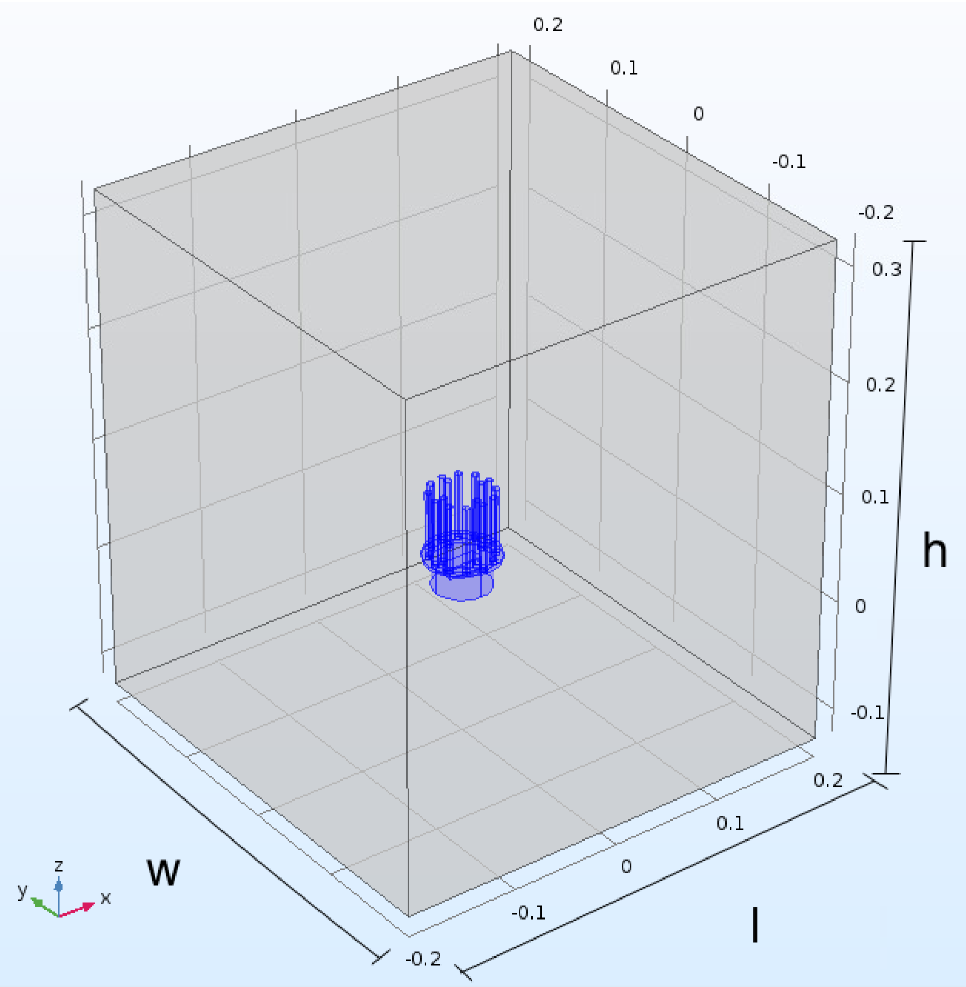

Figure 8.5

The airbox dimension comparison was done to see what kind of impact the open boundary conditions had on the fluid flow and heat transfer. The expectation was that the heat sink would be less affected by the boundary conditions with a larger box, therefore producing more realistic results. These results can be seen in Figure 8.6, and the h x w x l can be seen in Figure 8.5

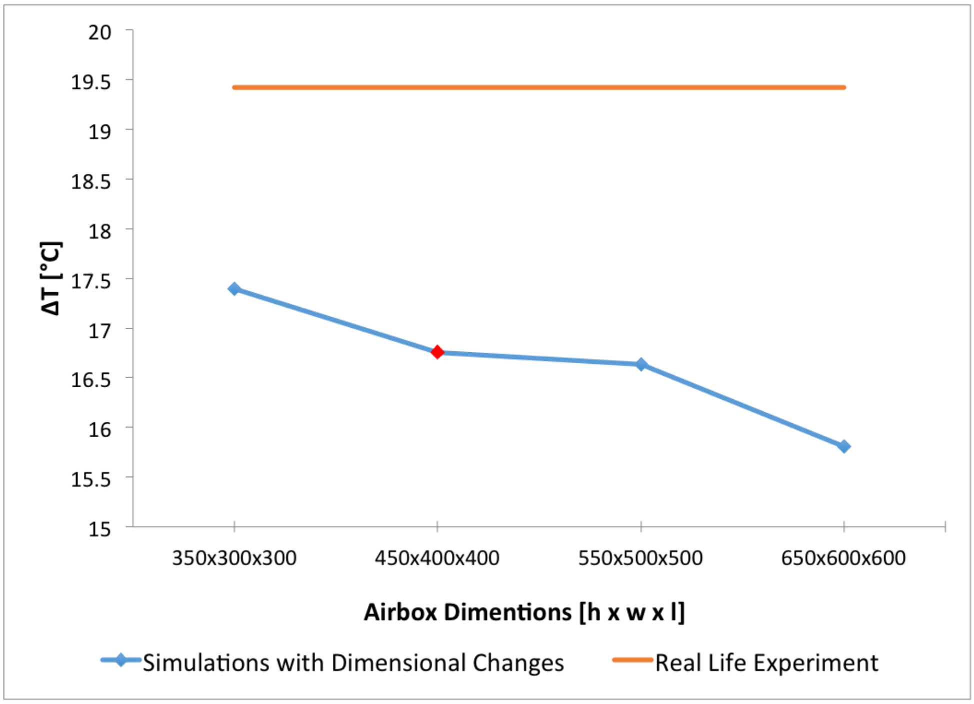

Figure 8.6: Change of Airbox Dimentions, Vertical 4w

The data indicates that the bigger the airbox, the lower the temperature. When the airbox dimensions increased, the mesh element size also increased, causing the mesh to become coarser and the temperature to decrease. Coarser mesh also results in lower and less accurate temperatures when compared to real life experiments, which is the opposite of what was expected. The 350x300x300 airbox had approximately 270,000 DOF and was 2.2℃ from the experimental temperature, while the 650x600x600 airbox had 130,000 DOF a temperature of 3.61℃ from the experimental temperature. The other data can be seen in Figure G.2 in the appendix.

8.2.3 Incompressible, weakly compressible or compressible flow

The density for all fluids depends on temperature and absolute pressure through a thermodynamic relation, $\rho = \rho(p, A, T)$ [42]. In Comsol, compressible flow means that the fluid density relies on temperature and absolute pressure. In weakly compressible flow, the fluid density only depends on pressure, while in incompressible flow, the density is constant. Assuming weakly or incompressible flow reduces the Navier-Stokes equations (see 5.8) and makes the calculations easier for Comsol to solve.

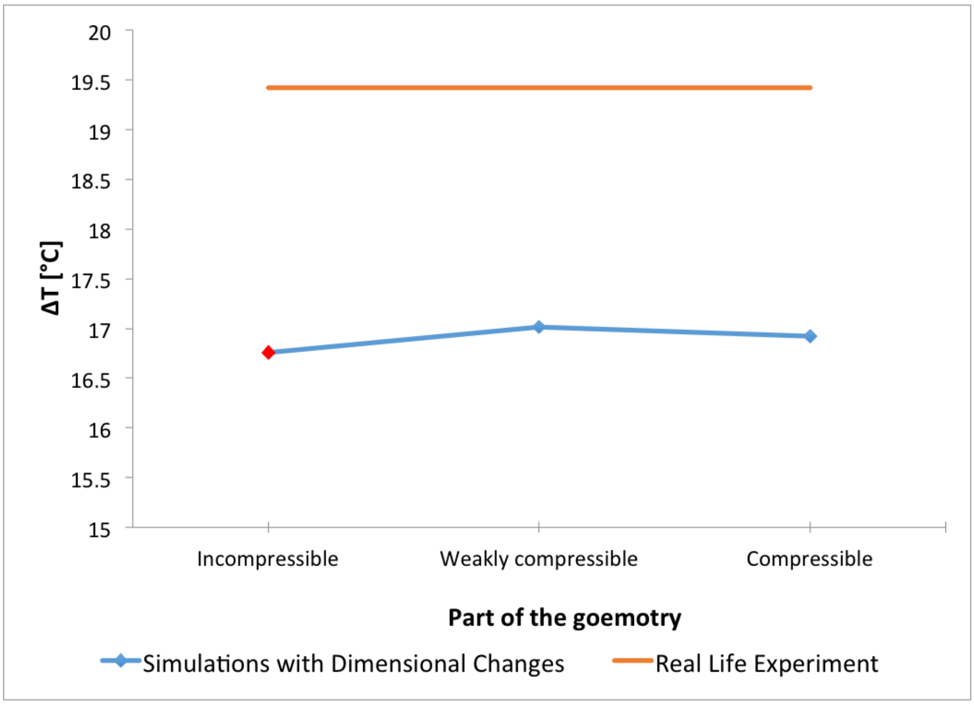

Figure 8.7: Change in flow nature, Vertical 4w

Figure 8.7 shows an insignificant difference between the three possible density assumptions, so the assumption of constant density and incompressible flow was acceptable. All of the simulations had 195,000 DOF. However, the compressible flow simulation only used 15 minutes compared to the 1 hour and 8 minutes used for the weakly compressible and the 43 minutes used for the incompressible flow. This was highly unexpected, as the initial expectation was that the compressible flow simulation would use the most time. More data in Figure G.3

8.2.4 Full geometry, half geometry or quarter geometry

Reducing the size of the model using symmetry is an efficient tool for solving large problems in Comsol. By doing this, the DOF are reduced and the simulation finishes faster. Our model is symmetric both over the xz plane and the yz plane as shown in Figure 8.5. This means that the model size can be reduced to 1/4 of its original size. The figure below shows the temperatures achieved in the simulations with a quarter of the model compared to a half model and a full model. Figure 8.5 and C.13 shows the full and quarter model.

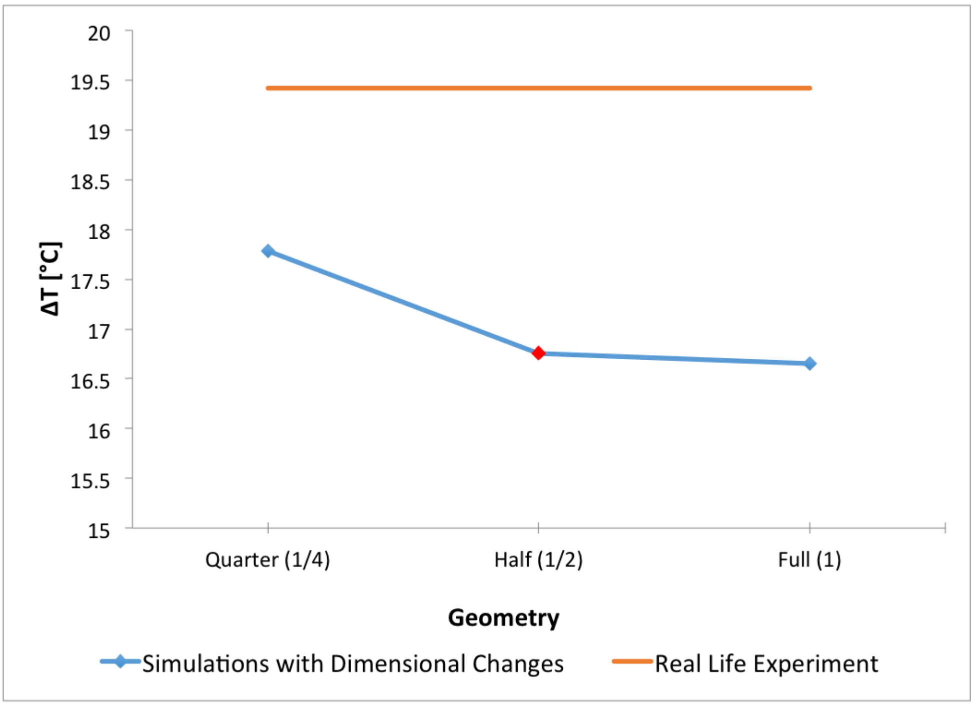

Figure 8.8: Change in geometry, Vertical 4w

The quarter model had a temperature of 17.78°C, which was closest to the experimental temperature of 19.42°C. The half and full models had similar temperatures of 16.75°C and 16.72°C ,neither of which were close to the experimental temperature. A limitation of the quarter model was that it was only usable in vertical position. In the horizontal and 45° positions, the quarter model was no longer symmetric over one axis plane because of the direction of gravity. The half model, on the other hand, was usable for all heat sink positions. A benefit of using the half model was that the simulation time was shorter than for the full model, taking 42 minutes for the half model and approximately 3 hours for the full model. In addition, the full geometry model started to oscillate and collapse after a while, as shown in Figure C.14.

8.2.5 Does a more realistic geometry give better results?

In making the Comsol simulation model, numerous features from the real life experiment were overlooked to make a simpler model and reduce the computation time. The overlooked features include the screws, electric cables, and the thermal grease between the aluminum plates. In this section, the effect of adding some of the overlooked features will be compared to the results of the simplified model. The results can be seen in Figure 8.9 below:

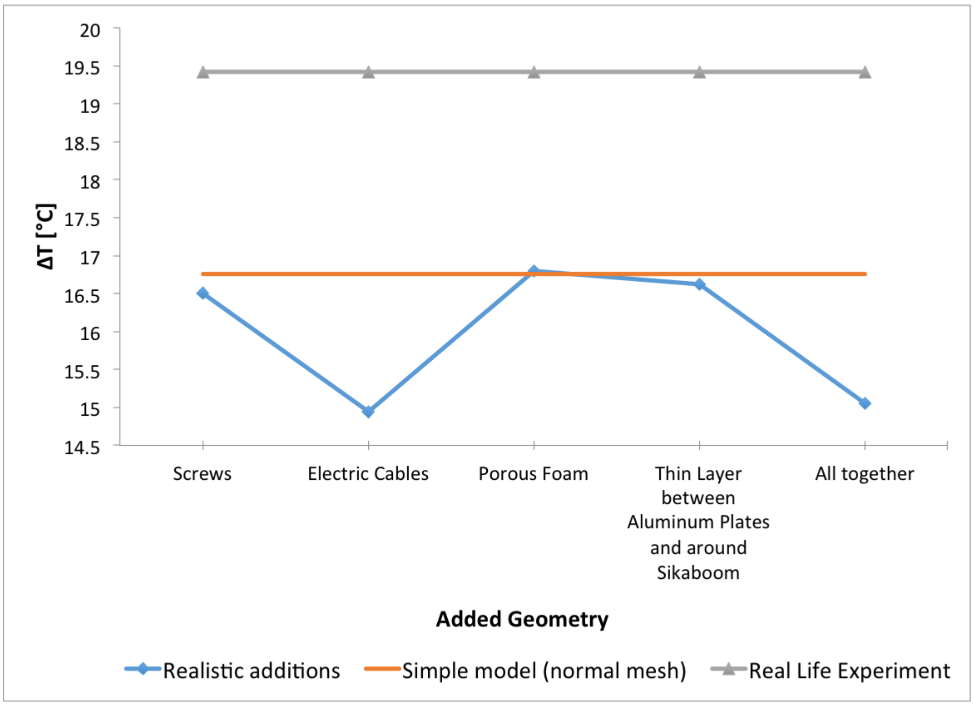

Figure 8.9: Realistc simulation, Vertical 4w

Looking at the chart, the majority of the additions did not greatly affect the results. The one exception to this was the addition of the electric cables, which caused the temperature in the heat sink to fall approximately 2 °C. This same phenomenon was reflected in the infrared picture in Figure 7.7, where a significant amount of heat left the resistor through the electric cables.

There are a lot of uncertainties attached to these new features:

- The makeup of the isolation foam is uncertain it terms of the Sikaboom to air ratio. Additionally, the cleanliness of the air is unknown and may contain chemicals.
- The diameter of electric cables was measured, but there is a plastic layer round that cables that was not accounted for.
- The screws are simplified so there is no thread on them and they may not be the right material.
- The tape around the isolation foam is assumed to be paper, though this may be incorrect.
- The thickness of the thermal grease layer is not accurate. Even with the thermal grease, there may be some air bubbles and gaps in the coupling between the heat element and heat sink.

In addition to creating extra uncertainties and producing results that are farther away from the experimental data, the new features also used more computational time. "All together", the simulation including all the additions, had 225000 DOF and took 1 hour and 6 minutes to simulate, while the simplified geometry had 194 000 DOF and took 45 minutes.

8.2.6 The Importance of Resistor Material

Since the resistor material was unknown the significance of material was also investigated to determine if material effects the simulation results. Resistors are usually made out of more than one material, but the resistor material itself (where the heat is produced) is usually made out of either carbon, metal, or metal-oxide film [43]. For all of simulations in this project, the heat source was made out of one constant material, which was predetermined to be carbon. However, other simulations were conducted with other materials to see if the material properties would have an effect on how much heat flux the resistor emits.

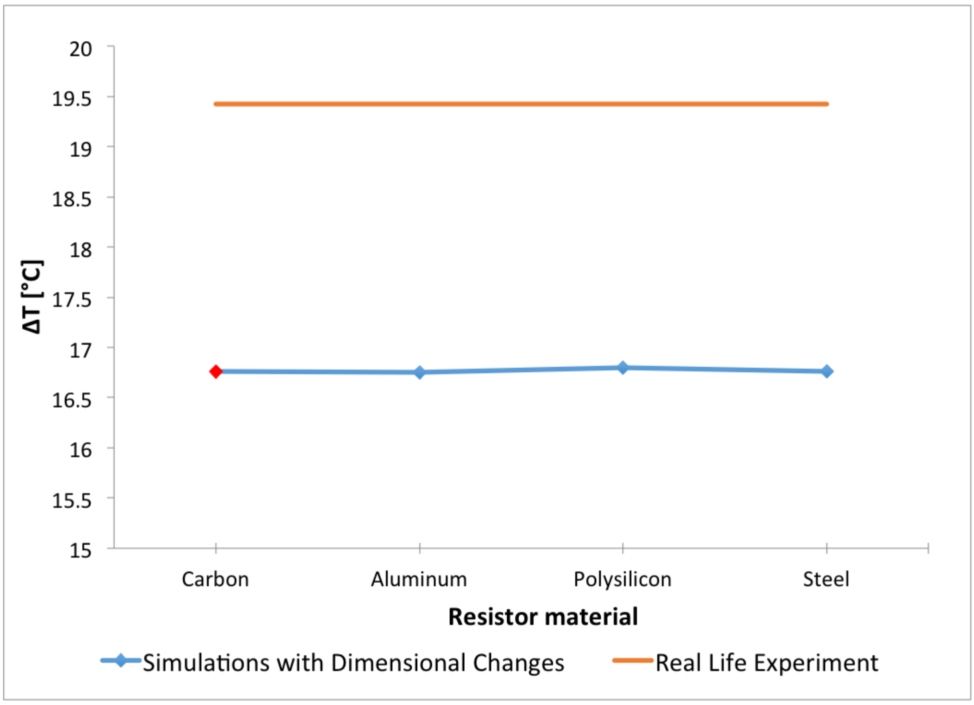

Figure 8.10: Resistor Material, Vertical 4w

In conclusion, the resistor material did not have an effect on the simulation of heat transfer in the heat sink. Although, due to conduction within the heat source itself, there might have been a greater difference in the results if the heat sink was bigger.

8.3 Optimization

Different heat sink parameters were compared to one another in Comsol to create a parametric shape optimization. Considering that Comsol results will be compared with other Comsol results, the actual temperature found in the HS junction was used. Be aware that the y-axis scales in Figures 8.11 to 8.14 below are not equal. The red values in the following charts are the dimensions of the manufactured heat sink in chapter 4

8.3.1 Fin Height

The figure below shows that the the higher fins allowed for more heat transfer between the heat sink and the ambient air.However, the improvement seems to decrease the longer the fins get. By increasing the fins in the manufactured HS from 60 mm to 80 mm we can increase performance by 4.85%. More data can be seen in Figure G.7.

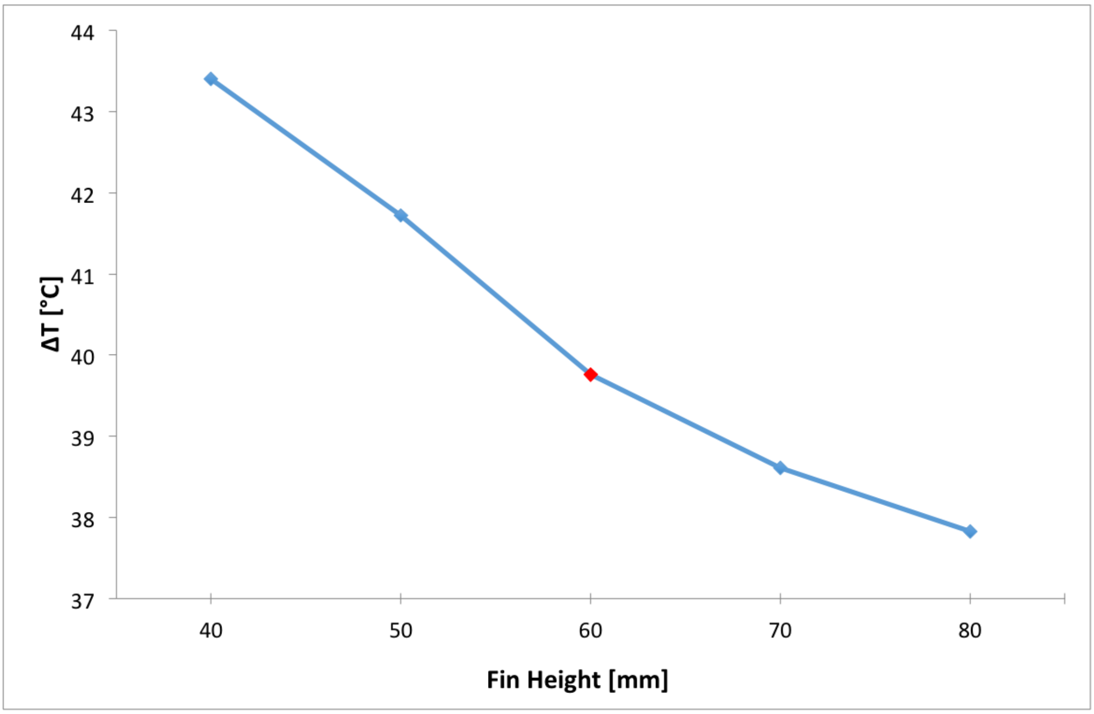

Figure 8.11: Optimization of Fin Height

8.3.2 Fin Diameter

Figure 8.12 below shows that the optimal fin diameter is between 7 and 8.2mm. By changing the diameter from 5.98 mm to 7 mm, the temperature at the HS junction decreased from 39.76 to 39.45, which is an improvement of 1.86% . When the diameter was over 8 mm, the inner fin and outer fin grew together, acting as one fin. The fins growing together was neither an advantage nor a big disadvantage, as the temperature found with 9 mm fins was only 0.05℃ higher than the temperature with 8.2 mm fins.

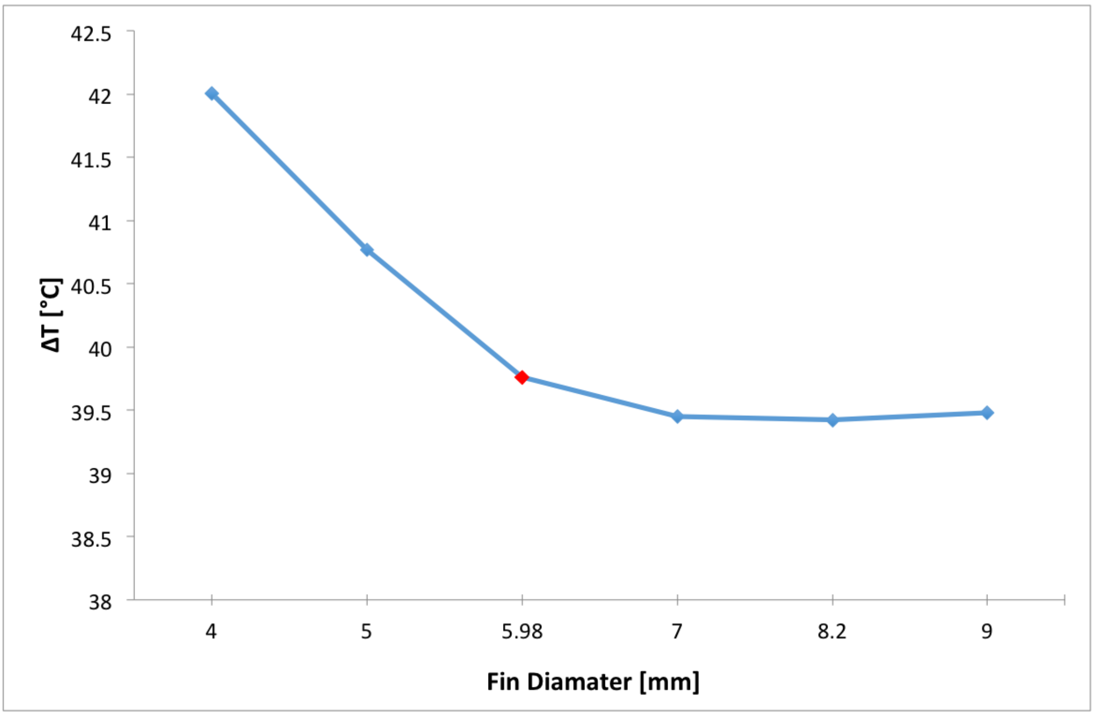

Figure 8.12: Optimization of Fin Diameter

8.3.3 Number of Fins in Outer Circle

Based on Figure 8.13, the optimal number of fins in the outer circle is 16. At 16 fins, the HS junction temperature was 39.1℃, 0.65℃ lower than with 12 fins and 1.2℃ lower than with 20 fins. The reason for this could be attributed to the fact that there was not enough space between the fins for "cold" ambient air to get into the center of the heat sink. The ambient air warmed up when flowing in between the fins, reducing the chimney effect inside the cooling geometry. This means that the fins were only cooled from the outside and that the plate would not be cooled down as much.

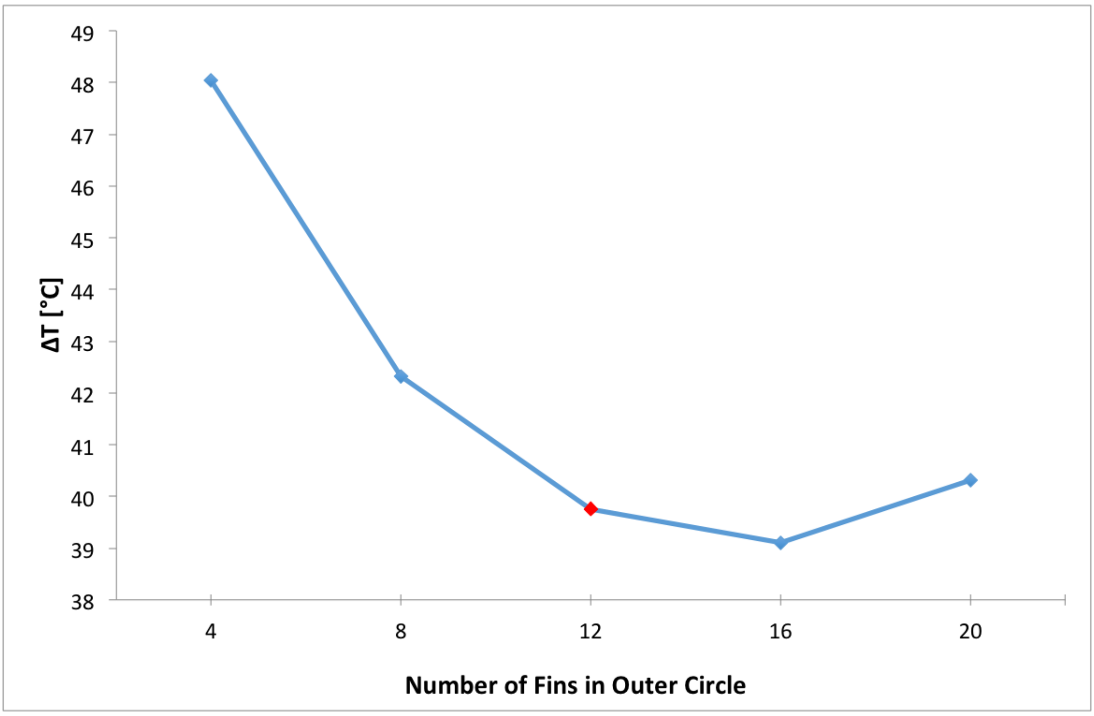

Figure 8.13: Optimization of Number of fins in outer Circle

8.3.4 Number of Fins in Inner Circle

The Figure 8.14 below shows that in order to optimize the heat sink, six fins should be used in the inner circle instead of four. Eight fins are too many, possibly because there would be less space for cold air to flow in between the hot fins like explained in the outer circle fins section above. One factor of error was that in all simulations except the 8 fin simulation, the inner fins were aligned with an outer fin. In the 8 fin simulation, the fins were evenly distributed with 4 out of 8 aligning with outer fins and 4 fins in-between two outer fins. Compared to the other optimization charts, change in number of inner fins did not have a big effect on temperature. There was less than 0.6℃ between the highest temperature at 0 fins and lowest temperature at 6 fins in the inner circle.

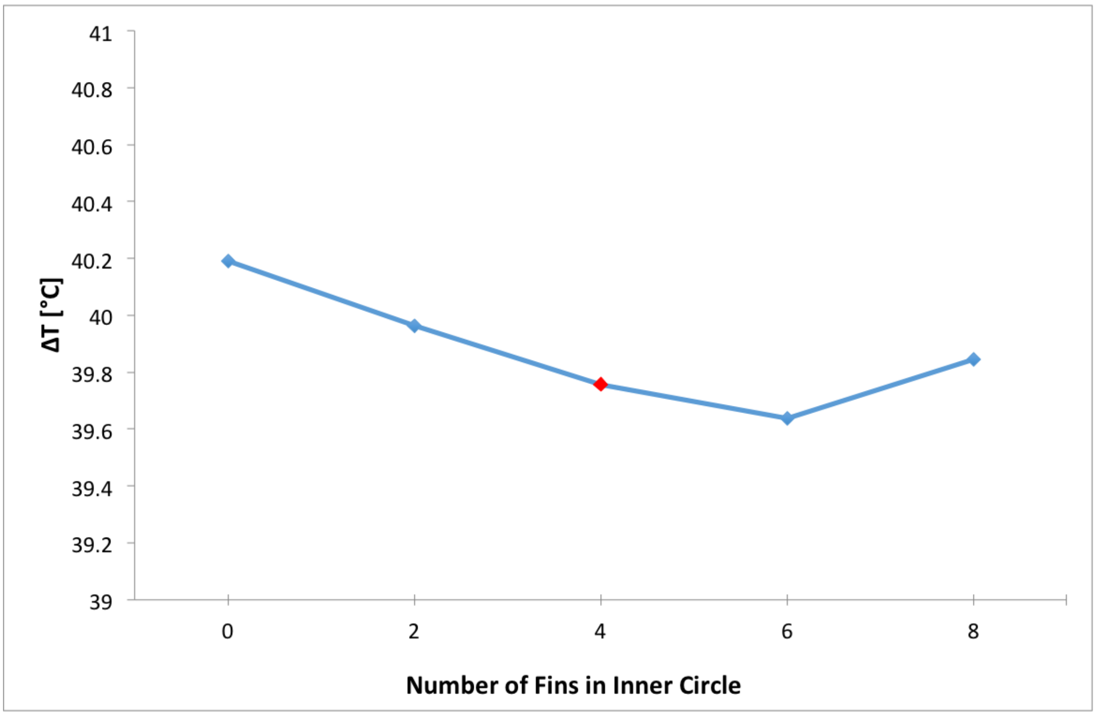

Figure 8.14: Optimization of Number of fins in inner Circle

8.4 Discussion

Maximum velocity achieved in the simulations was 0.23 m/s for the 5w experiment in the vertical position. By looking at Reynolds number, our assumption of laminar flow was verified. The kinematic viscosity of air at 50℃ is $17.9 \cdot 10^{-6} m^2/s$ and the critical Reynolds number, where flow changes from laminar to turbulent, is $5 * 10^5$.

$$Re = \frac{uL}{\nu} \Rightarrow L = \frac{Re \cdot \nu}{u} = \frac{5 \cdot 10^5 \cdot 17.9 \cdot 10^{-6}\ m^2/s}{0.23\ m/s} = 38.91m \tag{8.1}$$

The characteristic length has to be over 38.91 meters for the flow to be turbulent. The heat sink and the heat element had a total height of 86mm and a maximum diameter of 65mm, meaning that the characteristic length was significantly lower than 38.91 meters, causing the flow will be laminar.

Comsol's ability to accurately predict real life heat transfer and natural convection in and around a heat sink was investigated, with results shown in section 8.1.2. The fine mesh simulation had an average percentage ΔT difference of between 4% and 5% compared to the experiments, where the temperature predictions were a bit too high for 1w and too low for 5w. On a larger scale, simulation temperatures get farther and farther away from the real life experiment temperatures the more power input there is to the resistor. However, the normal mesh simulation was more precise for 1 w, both when it came to the steady state temperature and when it came to the temperature development, indicating that finer meshes are needed when higher power inputs are used.

A typical engineering problem is to find a balance between performance and price.

Finding a middle ground, where both cost and performance are optimized is key. Normal mesh took 45 minutes per simulation to get a temperature that was 7.09% away from the real life temperature, while fine mesh took 8 1/2 hours to get a temperature that differed 4.4% from real life. In the making of this project, hundreds of simulations were conducted, yet only 65 were used. Five simulations could run at the same time. 15 of the 65 simulations ran with a fine mesh, 1 with a *coarser* mesh, 1 with coarse mesh, and 48 with a normal mesh. Based on the times recorded in the mesh comparison section 8.2.1, total simulation time was 6 days and 20 hours and 43 minutes. If all the simulations were conducted with *fine* mesh, the total simulation time would have been 23 days and 30 minutes, which is 70 % longer than before.

Considering the results and comparisons in the optimization section, a heat sink with 22 fins, 16 in the outer circle and 6 in the inner, with a height of 80 mm and a diameter of 8.2 mm would perform the best. In comparison to the Comsol model used in all of the other simulations, the optimization by

- lengthening the fins from 60mm to 80mm would reduce the temperature with 1.93°C,
- increasing the diameter from 5.98mm to 8.2mm would reduce the temperature 0.34°C,
- increasing the number of fins from 12 to 16 in the outer circle would reduce the temperature 0.65°C
- increasing the number of fins from 4 to 6 in inner circle would reduce the temperature 0.12°C

All of these optimizations produced a total of 3.04°C, which reduced the heat sink temperature from 39.76°C to 36.72°C, an improvement from 9.2%. However, none of the optimization comparisons are cross tested and may be dependent on each other, meaning that changing one parameter may ruin the optimization of another.

Based on the optimization comparison, larger surfaces result in better performances, but cold air getting into the middle of the heat sink is also important so that the chimney effect works effectively.

The accuracy of these optimization comparisons is also essential when considering the heat sink design. When comparing the temperatures found in the HS junction to the temperature of the fins at 4w in the vertical position (figure G.11 and G.12), the fins have a higher temperature than the real life experiment while the HS junction has a lower temperature. This indicates that the resistance between the aluminum plate and the fins is bigger than Comsol predicted and/or that the resistance in the aluminum is higher than expected. With this in mind, let's look at the fin length optimization again. If the fins were not as warm as Comsol calculated, the heat transfer from the fins to the surrounding air would not be as large. Therefore, the effect of extending the fins would not be as efficient as Comsol predicts that it would be.

8.4.1 Errors

In the experiments, there were several error factors. The air flow in experiment was affected by the presence of computer, slabs, equipment, in addition to people walking by the experiment, and doors being opened into the experimental lab. Small gaps between the heat sink and heat element also changed the outcome of temperature, as well as the thread used to hang the HS.

In the compassion of simulation elements and optimization, the simulation was only conducted for one position and one wattage level, which means that other positions with other power inputs would need to be investigated.

When fin diameter was compared in section 8.3.2 the distance between the compared diameter was varying. It should have been 4 mm, 5 mm, 6 mm, 7 mm, 8 mm, and 9 mm, but the mesh caused some problems when the space between the inner and outer fin became small. It was chosen to used 8.2 instead.

9 Summary and Conclusion

In this project, a new heat sink was modeled and manufactured. Comsol models were also developed for verification of the FEM solver Comsol as a tool to predict temperature in and around a LED heat sink. Based on temperatures measured between the heat sink and the heat element (heat sink junction), comparisons between simulations and real life experiments were made. The temperature was measured with thermocouples. The experiments were carried out at 1 watt, 2 watts, 3 watts, 4 watts, and 5 watts power inputs, in vertical, horizontal, and 45° heat sink positions. The compared values were calculated as the difference between ambient temperature and the temperature measured at the heat sink junction.

In Comsol, the heat sink was modeled as a 3D axis-symmetric domain, but the simulations were only conducted for half of the heat sink geometry to reduce computational time and to get more stable results. Results were solved numerically using the Navier-Stokes equation in tandem with specific boundary conditions. To find the most compatible model that accurately reflected real life experiments, numerous features was tested. Assuming that the air around the HS was incompressible produced the same results as the compressible situation. Surprisingly, the simulation for compressible flow only took 15 minutes compared to 43 minutes for the incompressible flow. Resistor material did not affect the the simulations, and a simpler model, without electric cables and screws, is more consistent with real life experimental results.

Two models were used in the verification of Comsol, one with physics defined *fine* mesh and the other with the physics defined *normal* mesh. The *fine* mesh gave the most accurate results overall, while the *normal* mesh was more accurate at 1w in all HS positions. At the 2w vertical HS position, the *fine* mesh model predicted a temperature of 11.099℃ compared to the 11.08℃ obtained from the experiments. This 0.02℃ difference is the lowest temperature difference conducted. The highest difference for the *fine* mesh was 1.61℃ and was at the 5w vertical HS position. This time, the experiment had a temperature of 23.8℃, while Comsol gave a temperature of 22.193℃. On average, there was a 0.52℃ difference between the temperatures obtained in the *fine* mesh model versus the experimental temperatures. There was an average difference of 1.20℃ between the experiments and the *normal* mesh.

Optimization of the manufactured heat sink design was also investigated in Comsol. Fin height, fin diameter, and number of fins were the parameters that were investigated. Simulation results showed that increasing the fin length would increase performance the most. By increasing the fin length from 60mm to 80mm, the HS junction temperature was reduced 1.93℃ from 39.76℃ to 37.83℃. Comparisons between fin temperatures in Comsol and the experiments show that the temperatures in Comsol are, on average, 2.35℃ higher than in the experiments. This means that increasing fin height would not be as effective as the Comsol simulations predict. However, the optimization comparisons also show that more and thicker fins perform better, concluding that the heat sink needs more surface area to optimize results.

10 Further Work

First of all, simulations from more than one position and wattage level must be conducted. More simulations would make the Comsol model more reliable and the optimization trends clearer.

To make a better Comsol model, new comparisons of airbox dimensions could also be conducted with the same box dimensions but this time, when the simulations have same amount of degrees of freedom.

In terms of optimization, a lot of new simulations could be carried out. Comparing differently shaped fins, like oval fins or fins that are thicker at the base and gradually becomes thinner. This would be harder to manufacture but not impossible. Other things could be comparing different plate thicknesses or cross comparing the simulations already done. For example, higher and thicker fins, or thicker and more fins in outer circle.

Optimizing for another heat sink position could also be interesting. Another position or another power input may have given other results. It would also be possible to compare the new results with the results obtained in this thesis.

Another really interesting direction for future research would be to use the elaborated Comsol model on another heat sink to investigate whether or not it works on other heat sinks, or even manufacture a new heat sink based on the optimization factors found, and see if it actually performs better than the current heat sink.

Lastly, it would also be interesting to look at the air velocity over the heat sink, and compare it to Comsol results, as well as to the results obtained by Nissen and Arentfiled [19, 20]

11 References

[1] W. T. Megan Watzke *et al.*, "About light," *Light Beyond the Bulb*, 2015. [Online]. Available: http://lightexhibit.org/aboutlight.html

[2] M. Denchak, "Are the effects of global warming really that bad?" *NRDC*, 2016. [Online]. Available: https://www.nrdc.org/stories/are-effects-global-warming-really-bad

[3] European Commision, "Paris agreement," 2017. [Online]. Available: http://ec.europa.eu/clima/policies/international/negotiations/paris_en

[4] United Nations, "Historic paris agreement on climate change," 2015. [Online]. Available: http://newsroom.unfccc.int/unfccc-newsroom/finale-cop21/

[5] European Commision, "Paris agreement," 2017. [Online]. Available: http://ec.europa.eu/clima/policies/strategies/2020_en

[6] Eurostat, "Climate change the eu," December 2015. [Online]. Available: http://ec.europa.eu/eurostat/documents/10186/7087616/COP21+infograph+EU.pdf

[7] European Commision, "Europe 2020 targets," 2015. [Online]. Available: http://ec.europa.eu/europe2020/europe-2020-in-a-nutshell/targets/index_en.htm

[8] ——, "Green paper lighting the future accelerating the deployment of innovative lighting technologies," 2011. [Online]. Available: http://eur-lex.europa.eu/legal-content/EN/ALL/?uri=celex:52011DC0889

[9] ——, "Action 72: Launch green paper on solid state lighting (ssl)," 2014. [Online]. Available: https://ec.europa.eu/digital-single-market/en/content/action-72-launch-green-paper-solid-state-lighting-ssl

[10] ——, "Commission regulation (ec) no 244/2009," *Official Journal of the European Union*, 2009. [Online]. Available: http://eur-lex.europa.eu/LexUriServ/LexUriServ.do?uri=OJ:L:2009:076:0003:0016:en:PDF

[11] D. C. Giancoli, *Physics for scientists and engineers with modern physics.* Pearson Education, 2008, vol. 2.

[12] T. Whitaker, "Fact or fiction: Leds don't produce heat," *LEDs Magazine*, pp. 1–4, 2005.

[13] J. Cooper, "Driving led lamps-some simple design guidelines," *LEDs Magazine*, vol. 4, pp. 26–28, 2007.

[14] T. L. Bergman, F. P. Incropera, D. P. DeWitt, and A. S. Lavine, *Fundamentals of heat and mass transfer*, 7th ed. John Wiley & Sons, 2011.

[15] A. T. Morrison, "Optimization of heat sink fin geometries for heat sinks in natural convection," in *Thermal Phenomena in Electronic Systems, 1992. I-THERM III, InterSociety Conference on.* IEEE, 1992, pp. 145–148.

[16] R. Bahadur and A. Bar-Cohen, "Thermal design and optimization of natural convection polymer pin fin heat sinks," *IEEE Transactions on Components and Packaging Technologies*, vol. 28, no. 2, pp. 238–246, 2005.

[17] S. Jang and M. W. Shin, "Thermal analysis of led arrays for automotive headlamp with a novel cooling system," *IEEE Transactions on Device and Materials Reliability*, vol. 8, no. 3, pp. 561–564, 2008.

[18] X.-J. Zhao, Y.-X. Cai, J. Wang, X.-H. Li, and C. Zhang, "Thermal model design and analysis of the high-power led automotive headlight cooling device," *Applied Thermal Engineering*, vol. 75, pp. 248–258, 2015.

[19] B. S. Nissen, "Natural convection for leds," Master's thesis, Technical University of Denmark, 2015.

[20] F. Arenfeldt, "Passive cooling of led," Master's thesis, Technical University of Denmark, 2016.

[21] J. Alexandersen, O. Sigmund, and N. Aage, "Large scale three-dimensional topology optimisation of heat sinks cooled by natural convection," *International Journal of Heat and Mass Transfer*, vol. 100, pp. 876–891, 2016.

[22] J. Alexandersen, N. Aage, C. S. Andreasen, and O. Sigmund, "Topology optimisation for natural convection problems," *International Journal for Numerical Methods in Fluids*, vol. 76, no. 10, pp. 699–721, 2014.

[23] J. Goldstein, "Episode 534: The history of light," *NPR*, 2014.

[24] N. Khan and N. Abas, "Comparative study of energy saving light sources," *Renewable and Sustainable Energy Reviews*, vol. 15, no. 1, pp. 296–309, 2011.

[25] J. M. Kusterer, "What wavelength goes with a color?" *Atmospheric Science Data Center*, vol. 28, 2007.

[26] N. Kumar, *Comprehensive physics XII.* Laxmi Publications, 2008.

[27] G. H. Smith, *Camera lenses: from box camera to digital.* SPIE Press, 2006.

[28] A. Umer and A. Umer, "An overview of laser technology in dentistry," in *Electronics, Communications and Photonics Conference (SIECPC), 2011 Saudi International.* IEEE, 2011, pp. 1–6.

[29] Sparkfun, "Light-emitting diodes." [Online]. Available: https://learn.sparkfun.com/tutorials/light-emitting-diodes-leds

[30] I. Moreno and C.-C. Sun, "Modeling the radiation pattern of leds," *Optics express*, vol. 16, no. 3, pp. 1808–1819, 2008.

[31] T. R. Kuphaldt, "Lessons in electric circuits, volume iii-semiconductors," 2007.

[32] L. Magazine, "What is an led?" 2005. [Online]. Available: http://www.ledsmagazine.com/articles/2004/01/what-is-an-led.html

[33] E. Star, "Learn about led bulbs." [Online]. Available: https://www.energystar.gov/products/lighting_fans/light_bulbs/learn_about_led_bulbs

[34] F. Manuals, "Color theory and basic shapes." [Online]. Available: http://write.flossmanuals.net/digital-foundations/color-theory/

[35] C.-C. Hsieh and Y.-H. Li, "The study for saving energy and optimization of led street light heat sink design," *Advances in Materials Science and Engineering*, vol. 2015, 2015.

[36] N. INSTRUMENTS, "Ni tb-9214." [Online]. Available: http://sine.ni.com/nips/cds/view/p/lang/da/nid/211280

[37] ——, "cdaq-9171." [Online]. Available: http://www.ni.com/da-dk/support/model.cdaq-9171.html

[38] M. Spiegelman, "Myths and methods in modeling," *Columbia University Course Lecture Notes, available online at http://www. ldeo. columbia. edu/˜ mspieg/mmm/course. pdf, accessed*, vol. 6, p. 2006, 2004.

[39] Comsol, "Navier-stokes equation." [Online]. Available: https://www.comsol.dk/multiphysics/navier-stokes-equations

[40] Sika, "Sika boom®-s." [Online]. Available: http://www.izonet.com.tr/uploads/1228466615_en.pdf

[41] D. CORNING, "Dow corning® 340 heat sink compound." [Online]. Available: http://www.dowcorning.com/applications/search/default.aspx?R=104EN

[42] B. Carasi, "Compressibikity options and buoyancy forces for flow simulation," *COMSOL BLOG*, 2016. [Online]. Available: https://www.comsol.com/blogs/compressibility-options-and-buoyancy-forces-for-flow-simulations/

[43] R. guide, "Welcome to the resistor guide." [Online]. Available: http://www.resistorguide.com

Appendix

A Abbreviation list

Table A.1: Abbreviation list

Abbreviation	Explanation
LED	Light Emitting Diode
FEM	Finite Element Method
HS	Heat Sink (see Figure 1.1)
HE	Heat Element (see Figure 1.1)
SD	Standard Deviation
ΔT	Measured temperature subtracted with ambient air temperature
DOF	Degree's of freedom

B Engineering Drawings

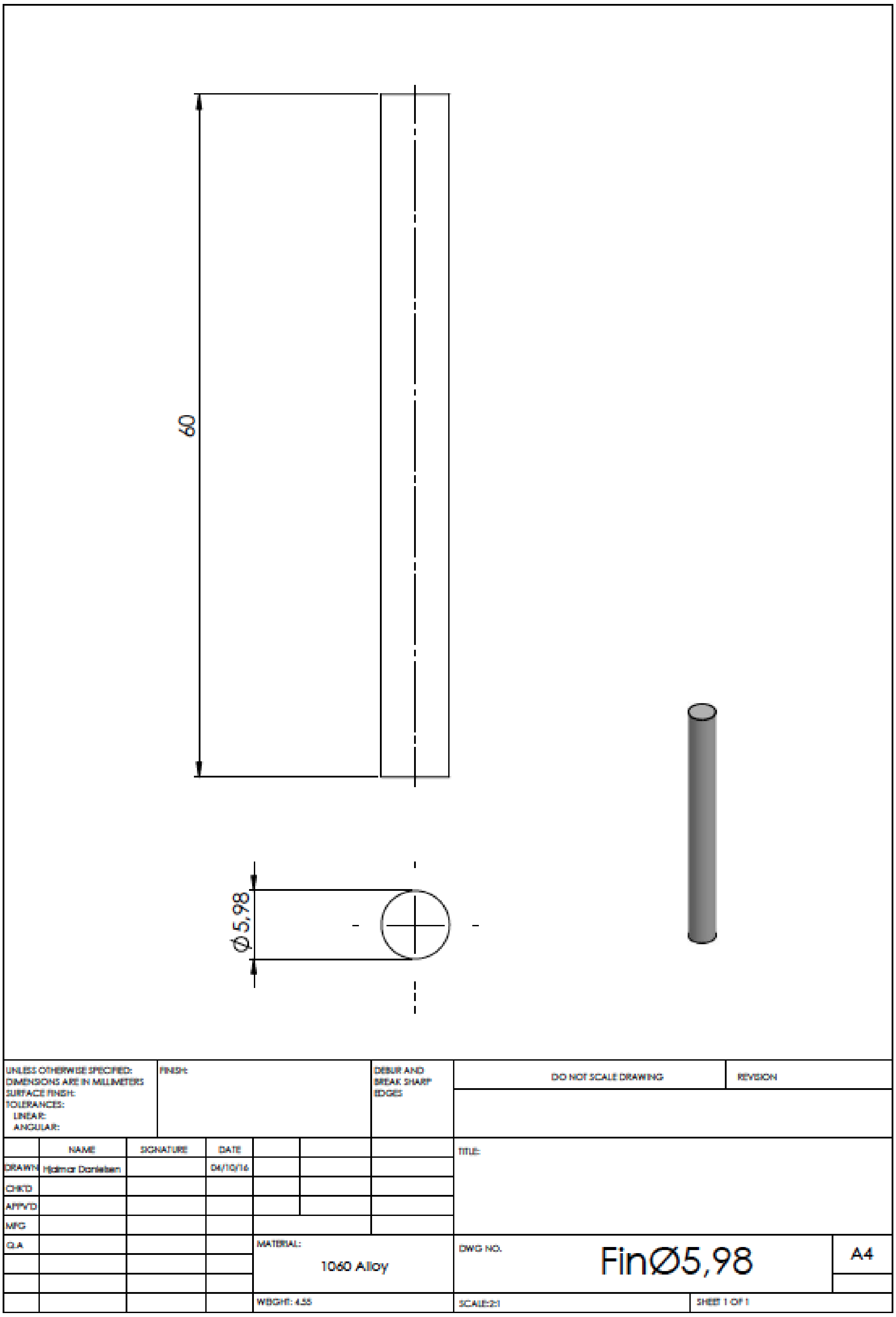

Figure B.1: Engineering drawing for Fins

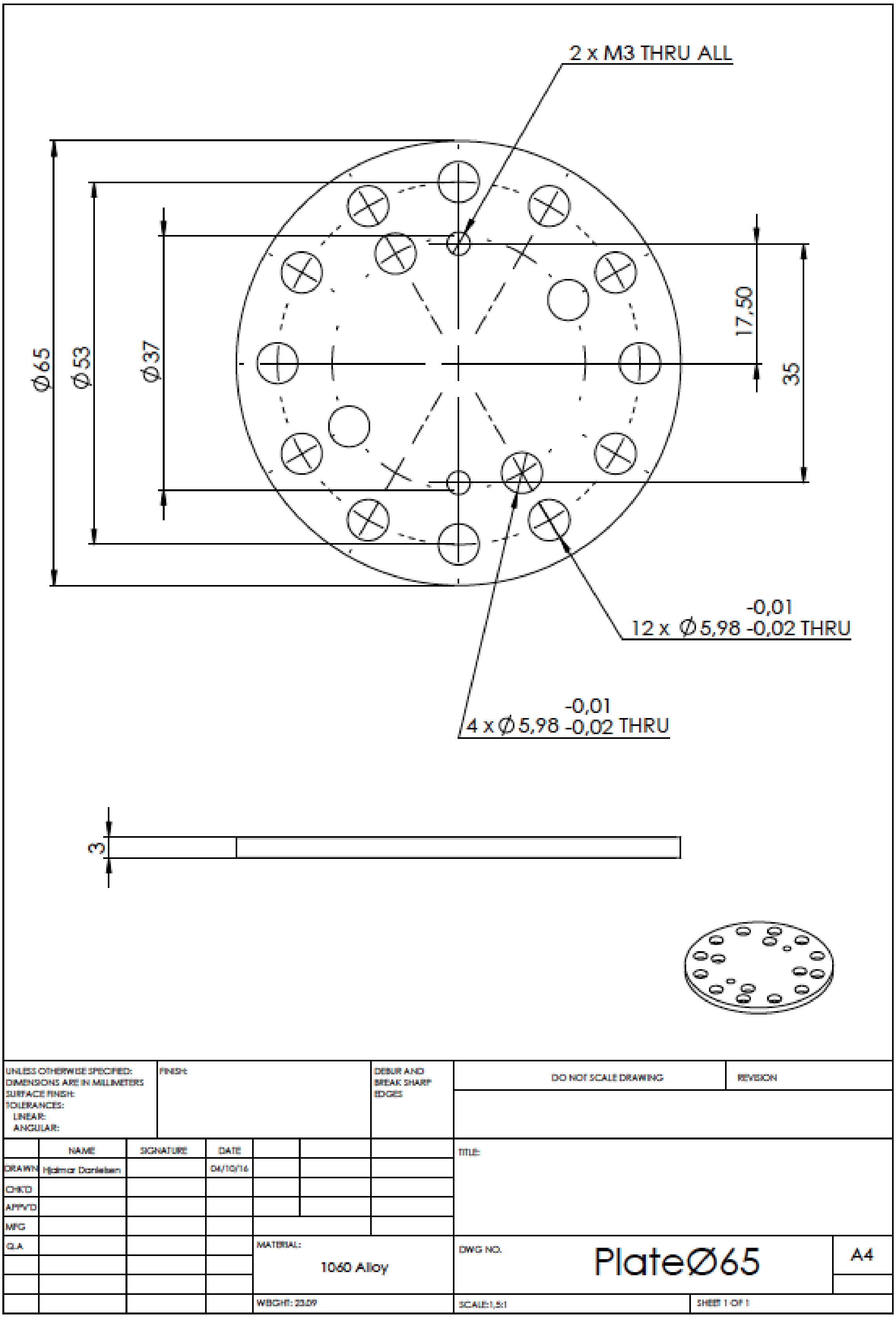

Figure B.2: Engineering drawing for aluminum plate

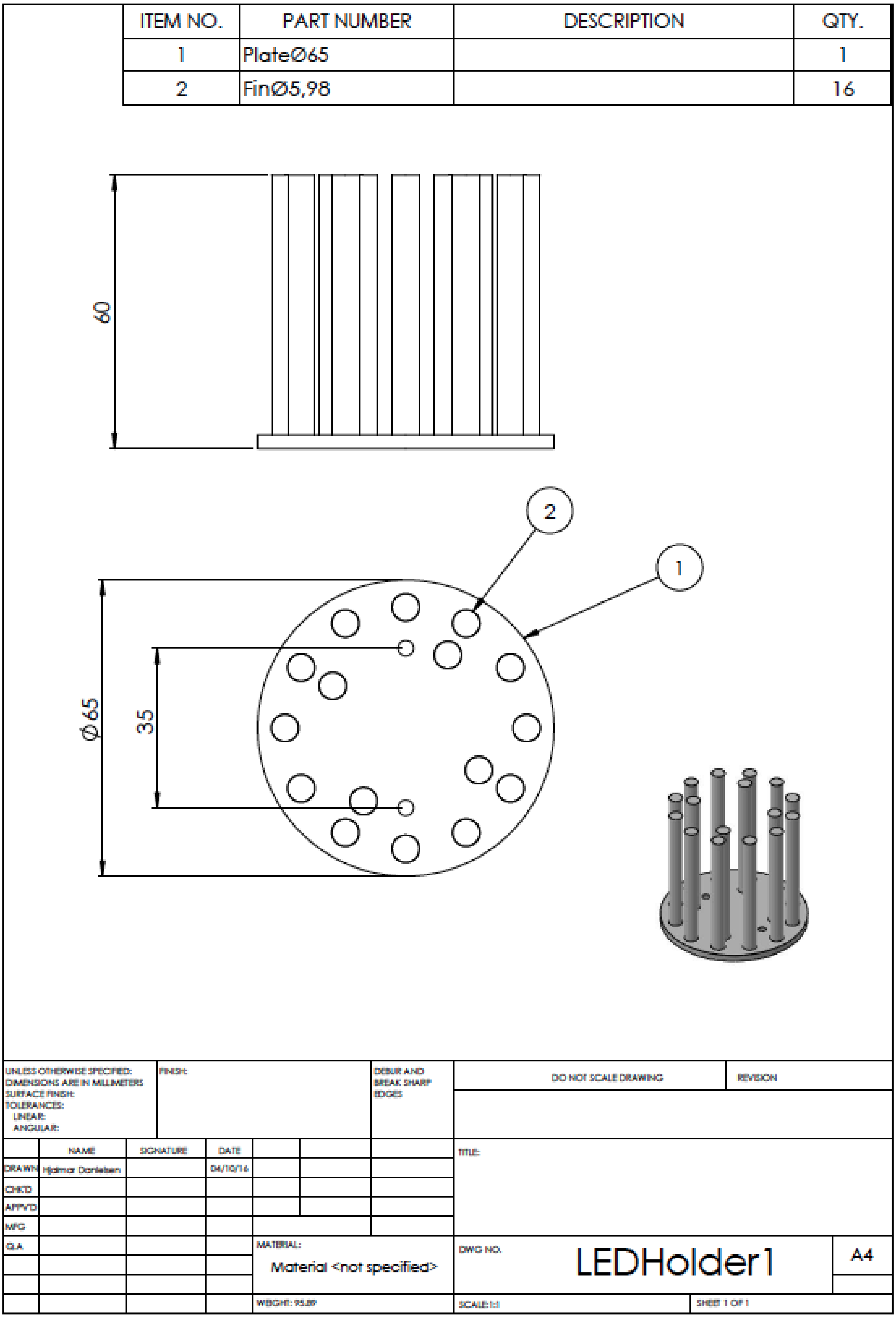

Figure B.3: Engineering drawing for heat sink assembly

In the air domain does conservation of mass, conservation of momentum and conservation of energy all apply, while in the solids does only conservation of energy apply.

C Comsol Setup

C.1 Parameter list

Settings

Parameters

Parameters

Name	Expression	Value	Description
d_plate	65[mm]	0.065 m	Plate diameter
d_fin	5.98 [mm]	0.00598 m	Fin diameter
h_plate	3[mm]	0.003 m	hight/thickness of plate
h_fin	60[mm]	0.06 m	hight of fin
d_fouter	53 [mm]	0.053 m	Outer placement diameter of fins on plate
d_finner	37 [mm]	0.037 m	Inner placement diameter of fins on plate
d_bolt	3 [mm]	0.003 m	Bolt hole diameter
d_bplace	35[mm]	0.035 m	Bolt placement diameter
d_he	50 [mm]	0.05 m	Diamater of heat element system
h_plate2	4 [mm]	0.004 m	Hight of plate between heat block and holder
h_hb	1[cm]	0.01 m	Hight of heat block
w_hb	1[cm]	0.01 m	Width of heat block
l_hb	3[cm]	0.03 m	Length of heat block

Name:

Figure C.1: Parameters part 1

d_he_2	50 [mm]	0.05 m	Diamater of heat element system
h_foam	22 [mm]	0.022 m	Hight of foam
T_amb	23 [degC]	296.15 K	Ambient temperature
r_air	400[mm]	0.4 m	Surrounding air length and width
h_air	450[mm]	0.45 m	Surrounding air height
p0	1 [atm]	1.0133E5 Pa	Initial and absolute pressure
h_table	120[mm]	0.12 m	Hight from desk to heat sink

Figure C.2: Parameters part 2

C.2 Air properties

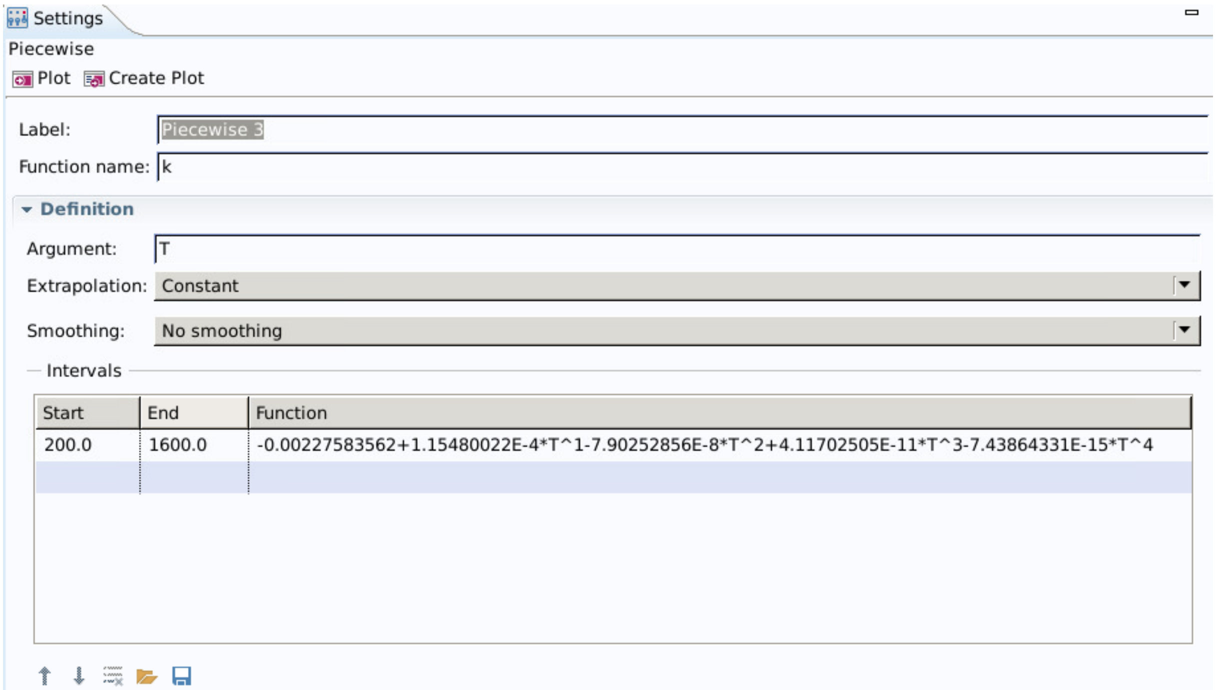

Figure C.3: Airs thermal conductivity

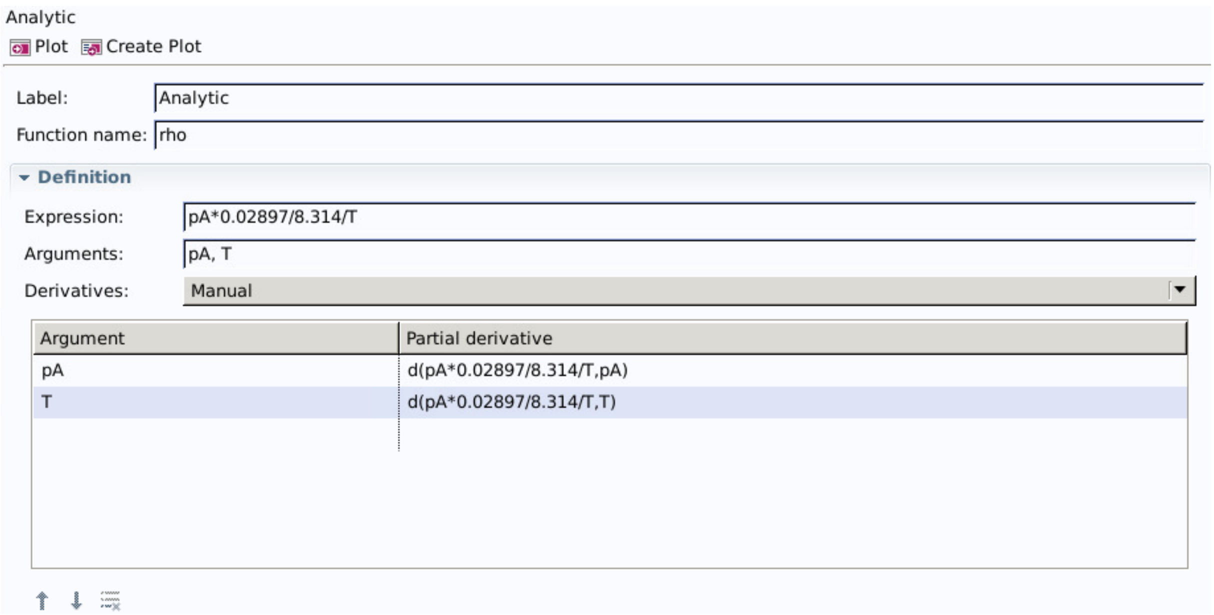

Figure C.4: Airs density

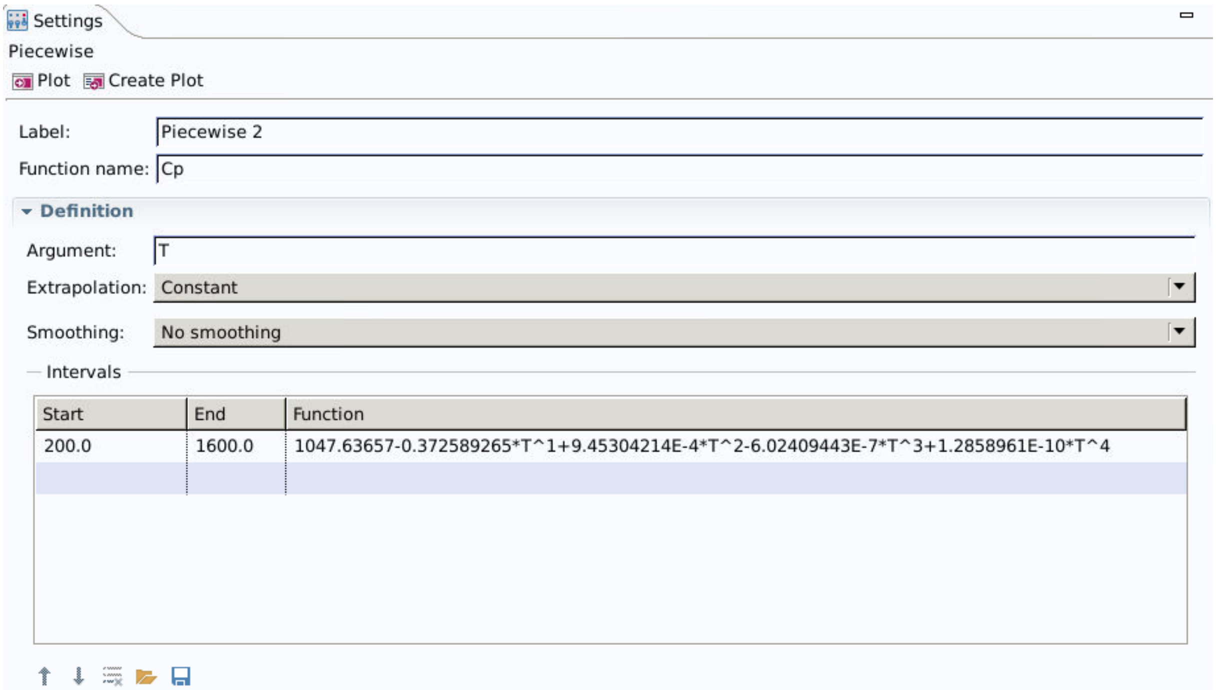

Figure C.5: Airs heat capacity

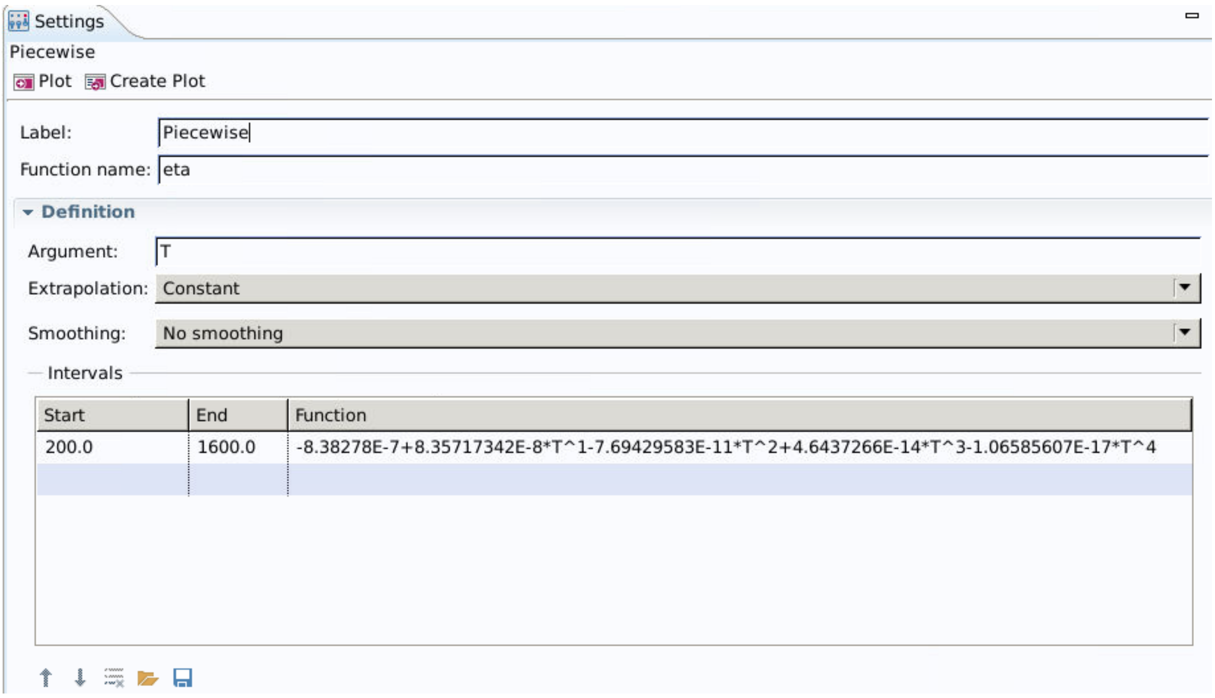

Figure C.6: Airs dynamic viscosity

C.3 Features used in Comsol

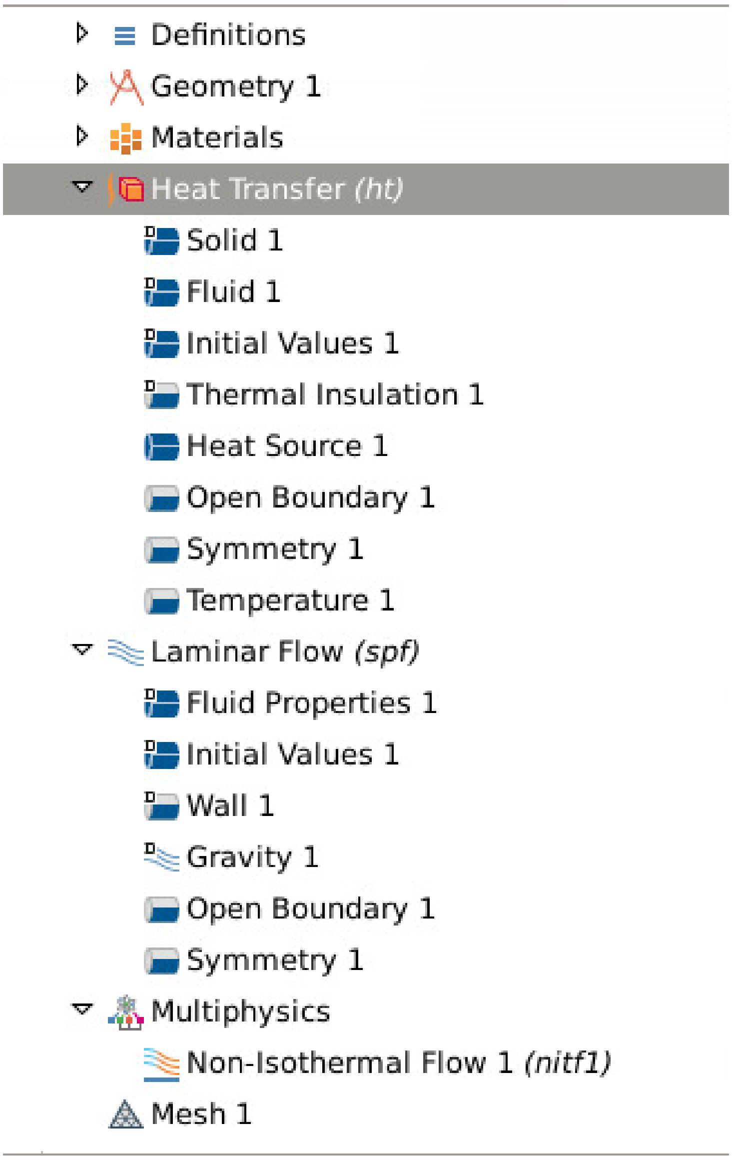

Figure C.7: Comsol nodes used

C.3.1 Heat Transfer (ht)

Solid

In this node we'll choose what part of the geometry that should behave as solids when it comes to heat transfer. We can also set the thermodynamic properties of the solid. The equations that are used

$$\rho C_p \frac{\delta T}{\delta t} + \rho C_p u * \nabla T + \nabla q = Q \tag{C.1}$$

$$q = -k \nabla T \tag{C.2}$$

The thermal conduction k describes the relationship between the heat flux vector q and the temperature gradient ∇T in $q = -k\nabla T$

Fluid

In this section we'll decide what domain that is a fluid. It's possible to change w

$$\rho C_p \frac{\delta T}{\delta t} + \rho C_p u * \nabla T + \nabla q = Q \tag{C.3}$$

$$q = -k\nabla T \tag{C.4}$$

Initial Values

Here, the initial temperature is set. Different domains can have different initial temperature. In this experiment the initial temperature is the same for all domains, which is room temperature, which is defined as $T_a mb = 23$ in the parameters.

Heat source

Heat generation is described by this feature. The heat source can be specified as heat per volume in the domain, a total heat source (power), or a linear heat source. In this experiment the resistor generates heat and we decide the amount of power (watts) into it. The heat rate is then calculated by

$$Q_0 = \frac{P_0}{V} \tag{C.5}$$

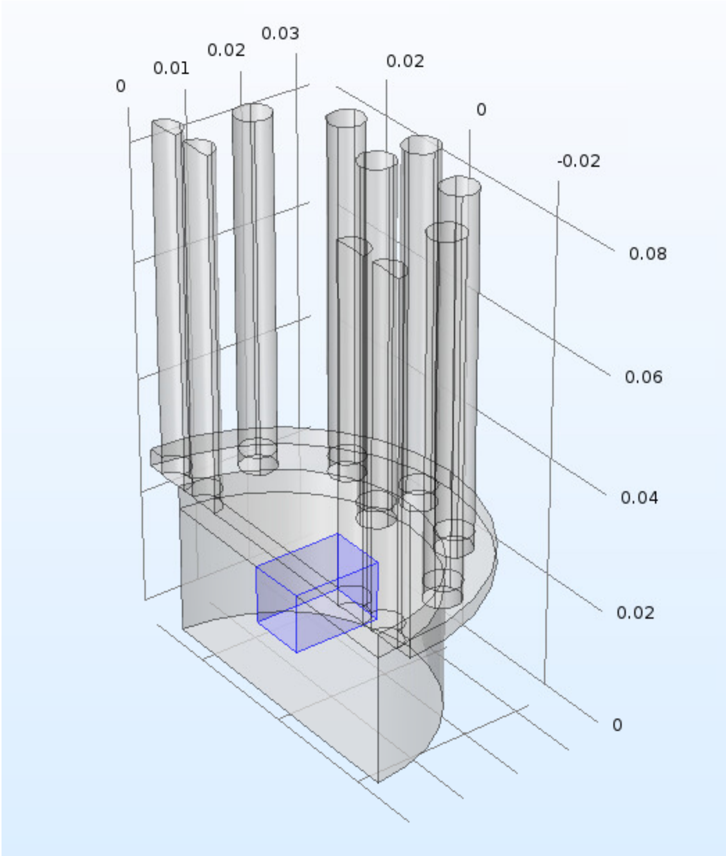

Figure C.8: Heat source

Open Boundary

With this boundary condition the heat can flow into the domain or out of the domain with a specified exterior temperature. The exterior temperature T_0 is decided to be 23℃ in the simulations

Symmetry

This boundary condition means that there is a "mirrored" part that's not included in the geometry. The exact thing will happen on the "other side, and the boundary condition is therefore that no heat flux across this boundary

Temperature

This node is used to specify the temperature of the desk at the bottom of Airbox. Here, the temperature is set to 23℃

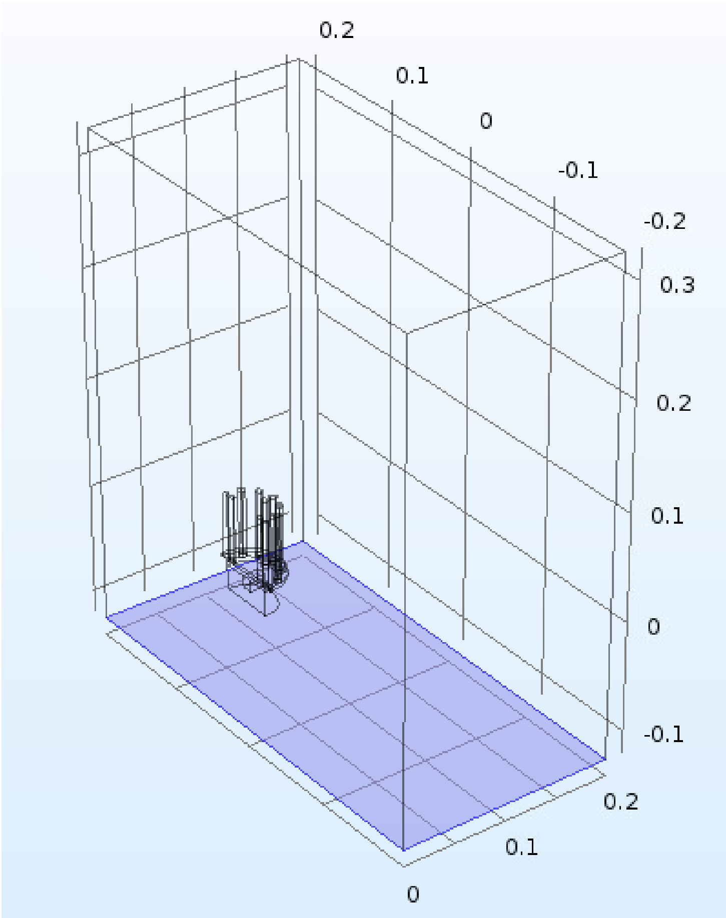

Figure C.9: Temperature bondary condition

C.3.2 Laminar Flow

Fluid properties

All the momentum equations solved by the interface are added with this feature, except volume force.

$$\rho \frac{\delta u}{\delta t} + \rho(u \cdot \nabla)u = \nabla \cdot \left[-pl + \mu(\nabla u + (\nabla u)^T) \right] + F \tag{C.6}$$

and

$$\rho \nabla \cdot = 0 \tag{C.7}$$

There is also an option to input temperature, absolute pressure, density, and material to the fluid in the model.

Initial Values

Here, the initial values for the velocity filed is stated, in addition to the pressure that serves as an initial guess for a nonlinear solver or as an initial condition for transient simulations.

Wall

This tells the solver that there is a wall. In our case we have a table under the heat sink, that works as a wall. With this condition we describe the fluid flow at the wall. Our table has a no slip condition, that means that the air-velocity is zero at the table

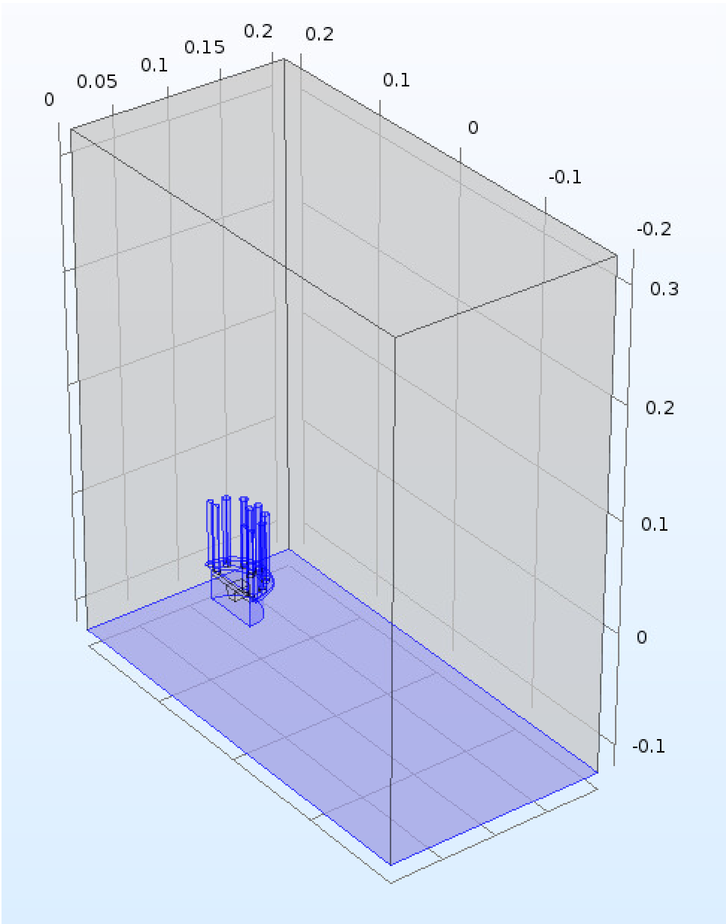

Figure C.10: Wall bondary

Open Boundary

With this condition can fluids both enter and leave the domain; the boundary is open to large volumes of fluids. It is possible to choose if there is *normal stress* or *no viscous stress* at the boundary. If choosing *normal stress* you'll have to input the amount of stress, f_0, there is at the boundary, and this will be put into the formula

$$\left[-pl + \mu(\nabla u + (\nabla u)^T\right] n = -f_0 n \tag{C.8}$$

If *no viscous stress* is selected does the viscous stress vanishes

$$\left[\mu(\nabla + (\nabla u)^T)\right] n = 0 \tag{C.9}$$

Symmetry

This node prescribes no penetration and vanishing shear stress at the boundary selected. It is a combination of Dirichlet and Neumann condition.

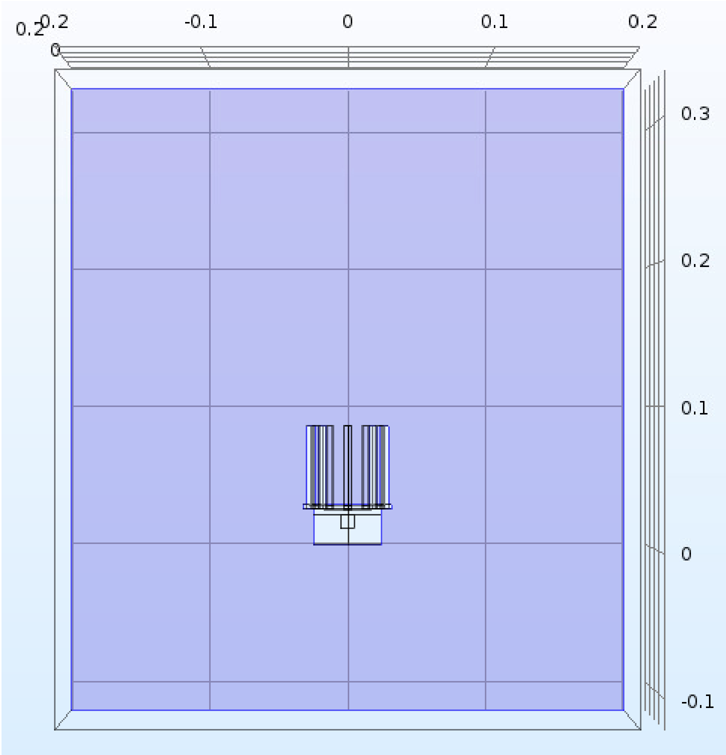

Figure C.11: Symmetry bondary in fluid

C.3.3 Non-Isothermal flow

The density definition in the Non-Isothermal Flow node ensure that the same definition of the density is used on the fluid flow and heat transfer interfaces.

C.4 How Comsol simulations where run

Simulations were run through Thinlinc in the terminal with a code like this

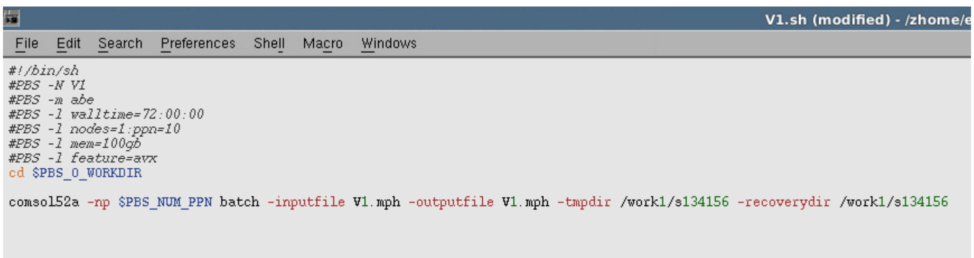

Figure C.12: Simulation run code

C.5 Geometry

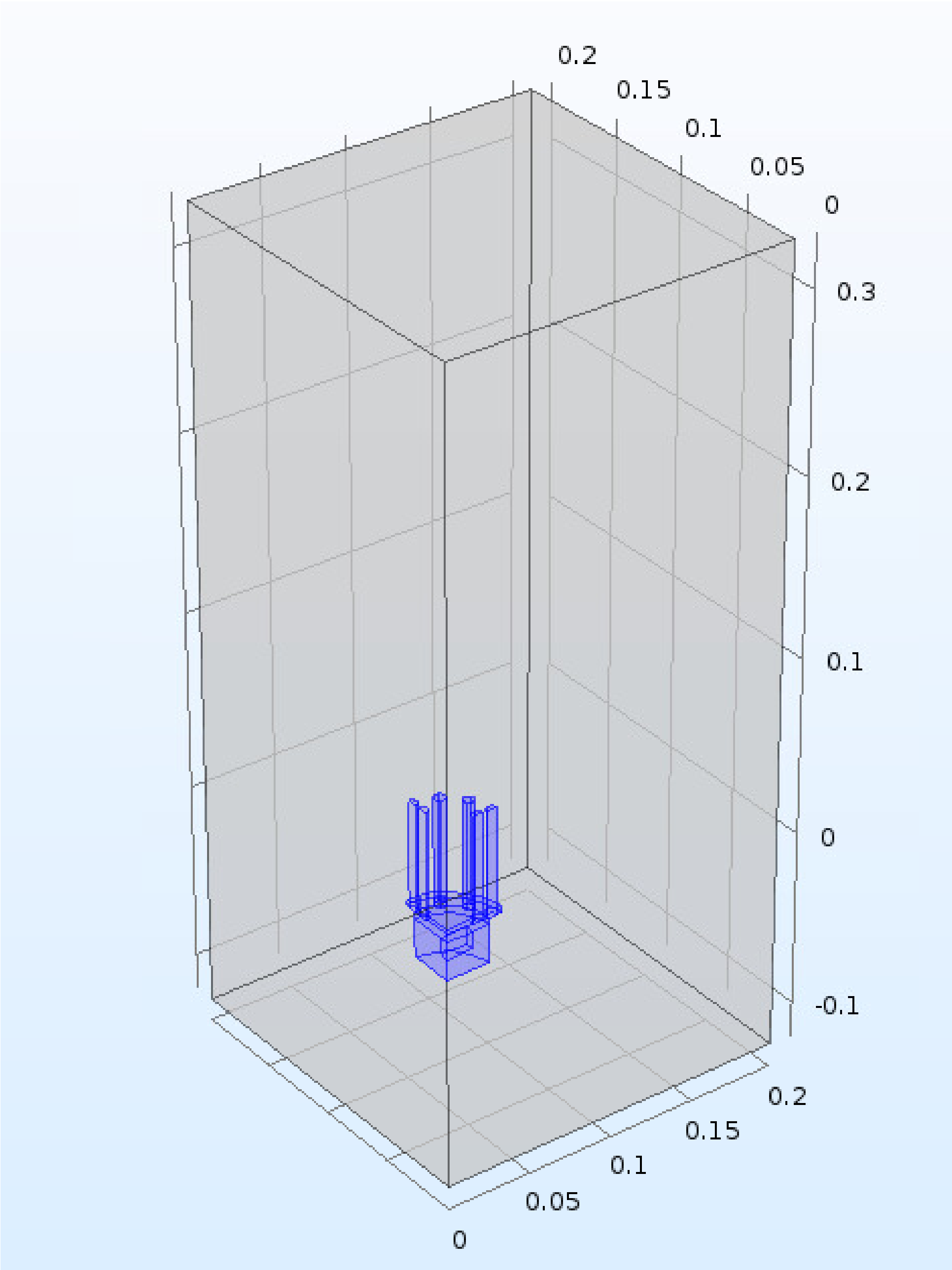

Figure C.13: Quarter geometry

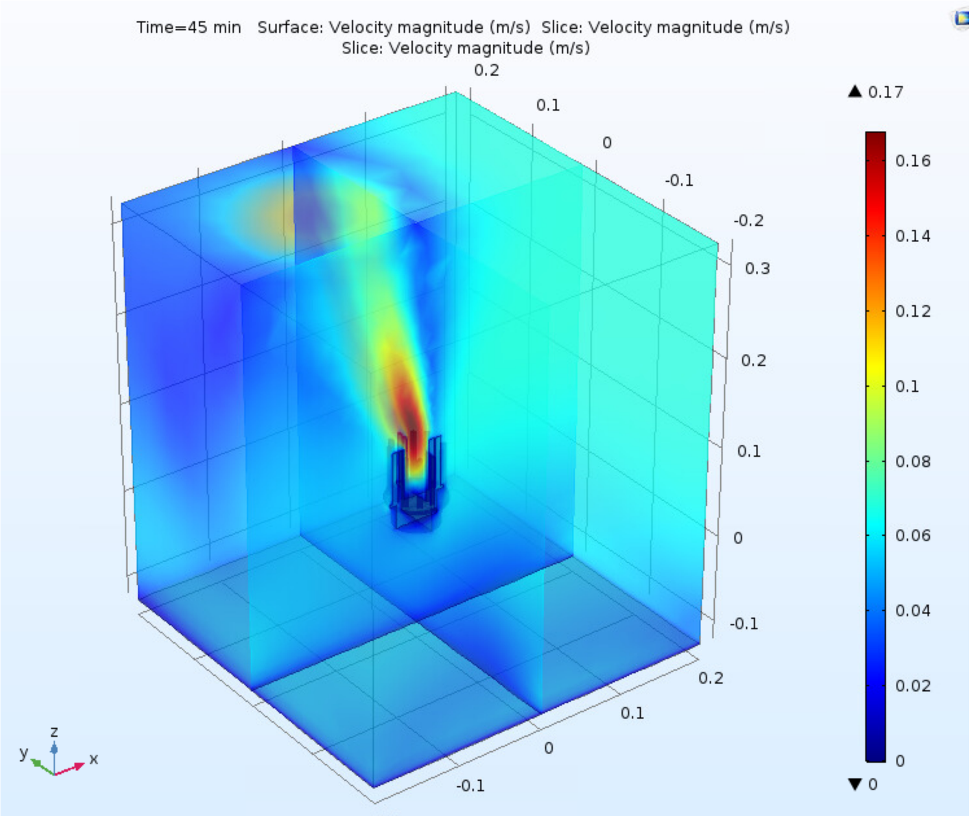

Figure C.14: Full geometry simulation fail

D Result

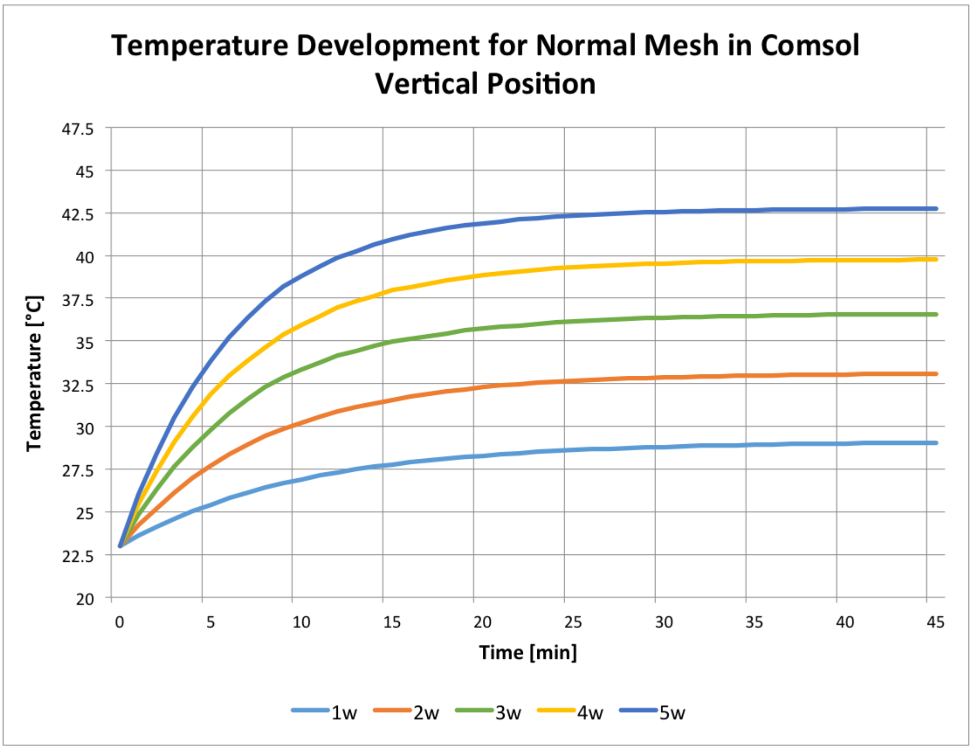

Figure D.1: Tempertue development for normal mehs in vertical position in Comsol

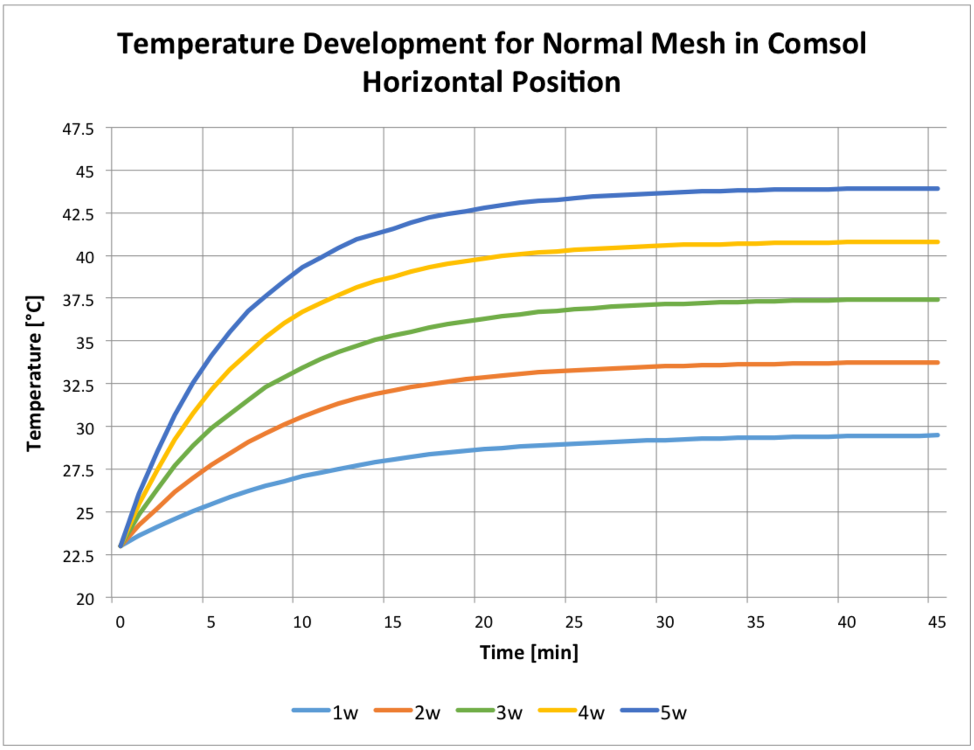

Figure D.2: Tempertue development for normal mehs in horizontal position in Comsol

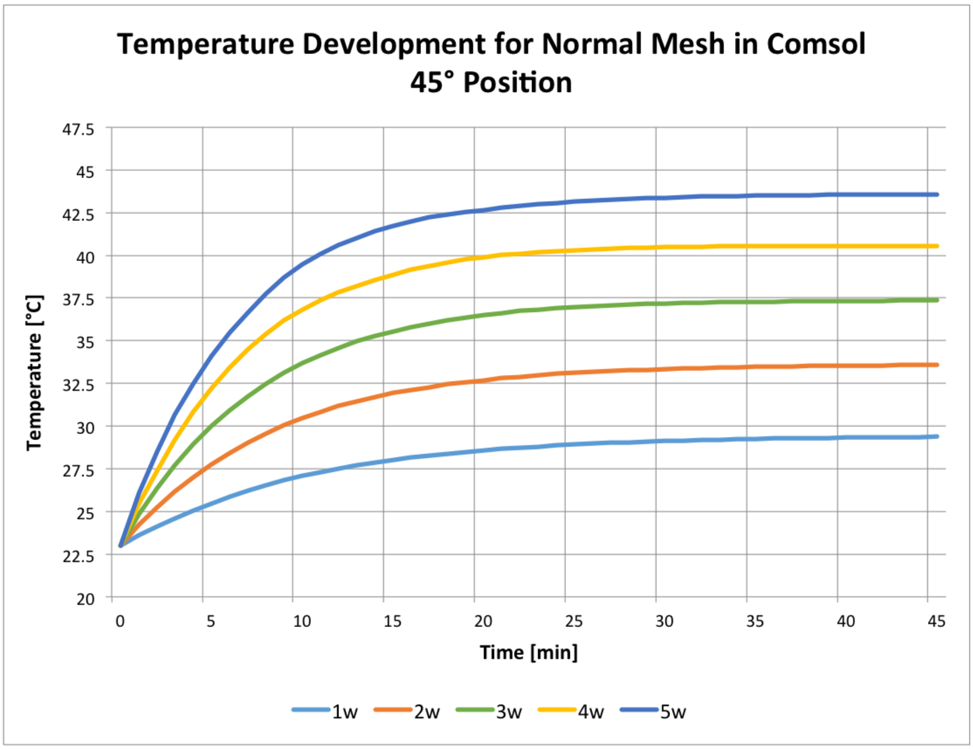

Figure D.3: Tempertue development for normal mehs in 45° position in Comsol

E Infrared Pictures

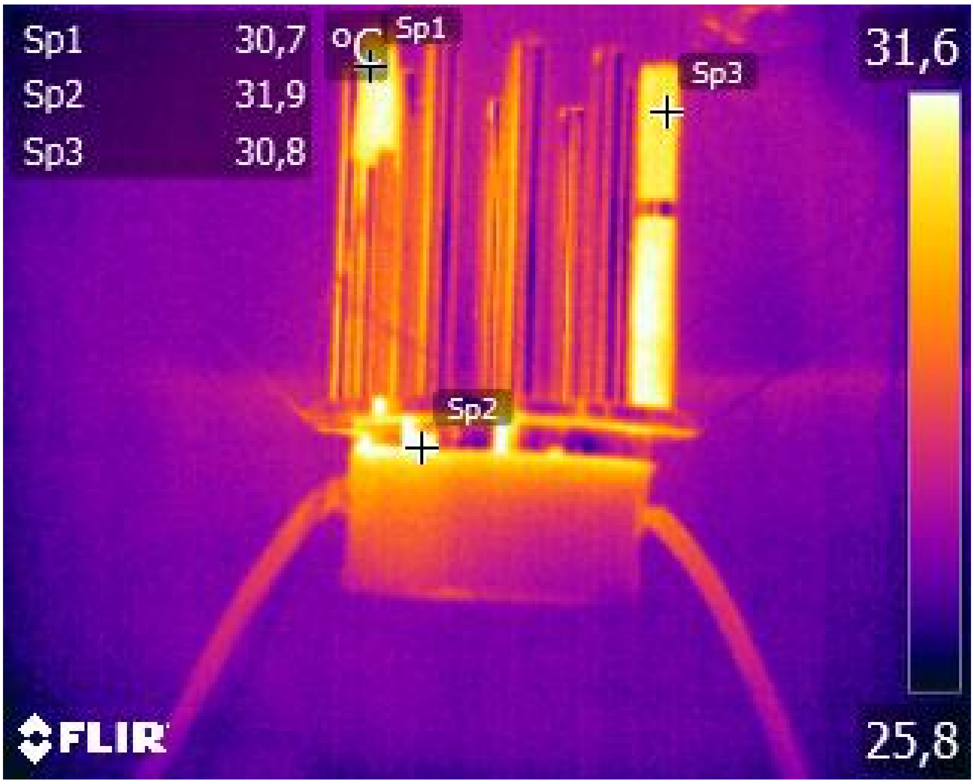

Figure E.1

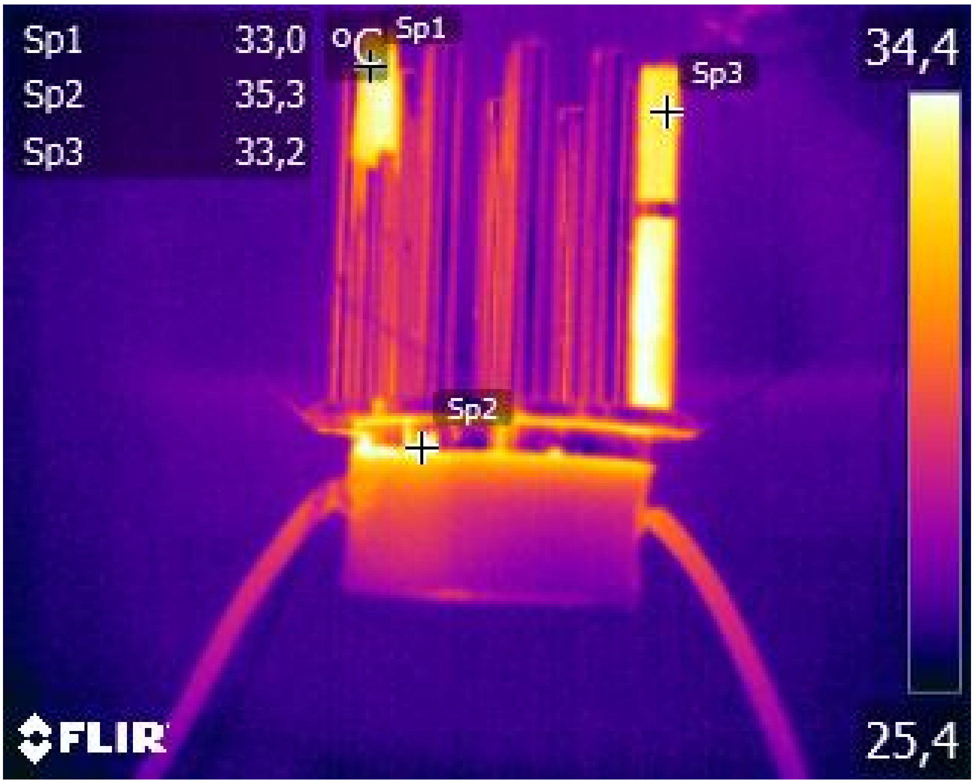

Figure E.2

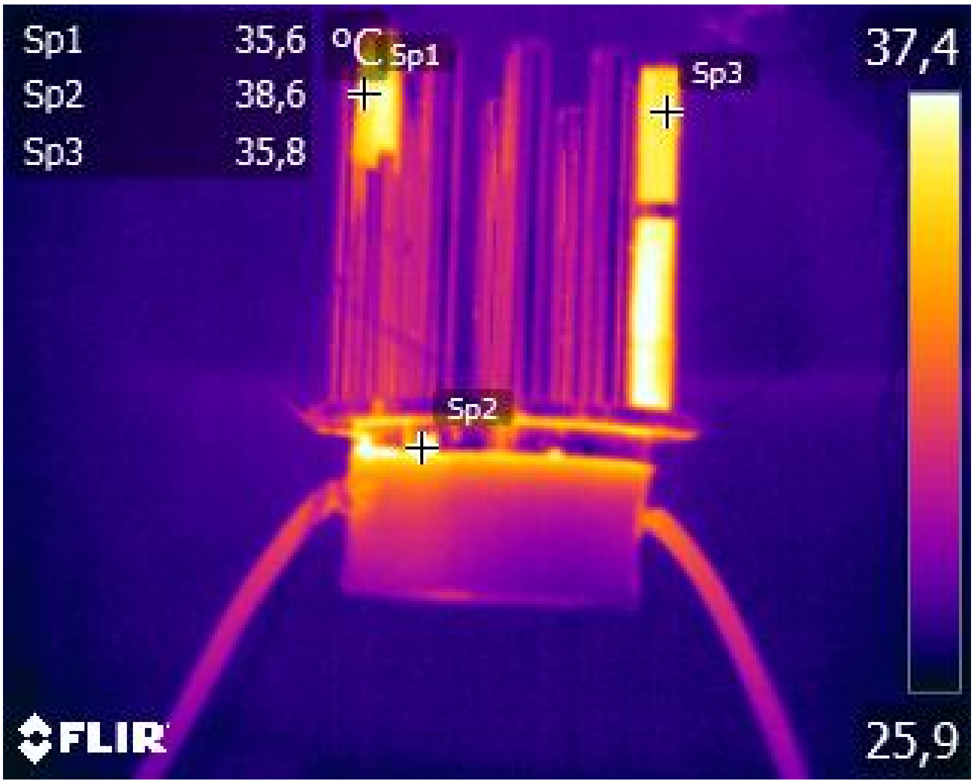

Figure E.3

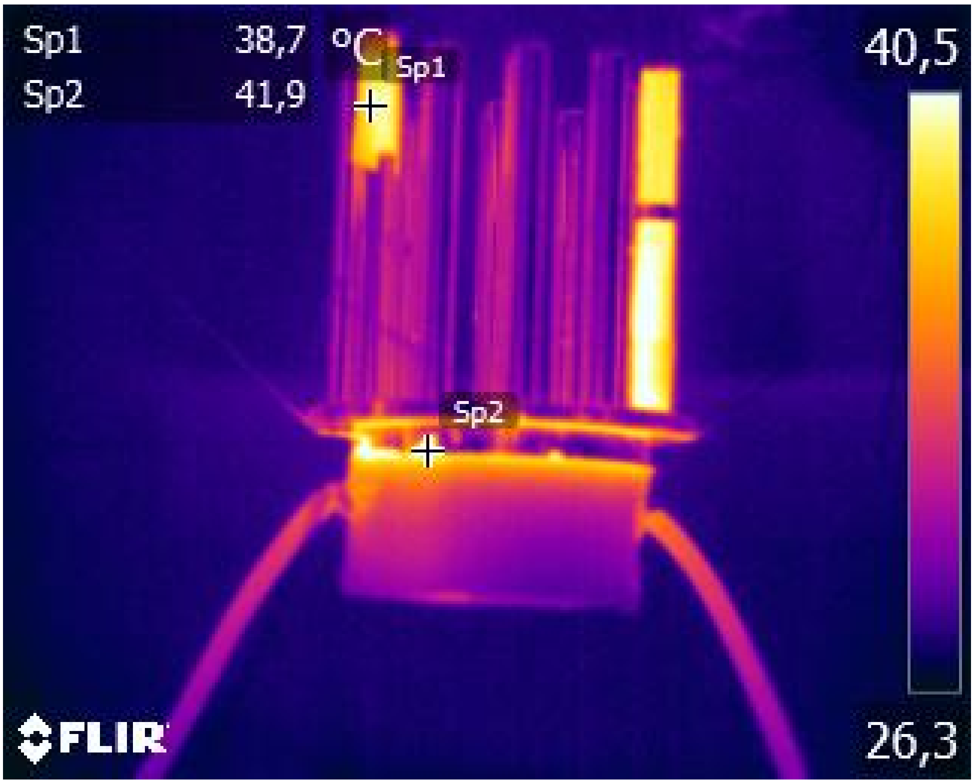

Figure E.4

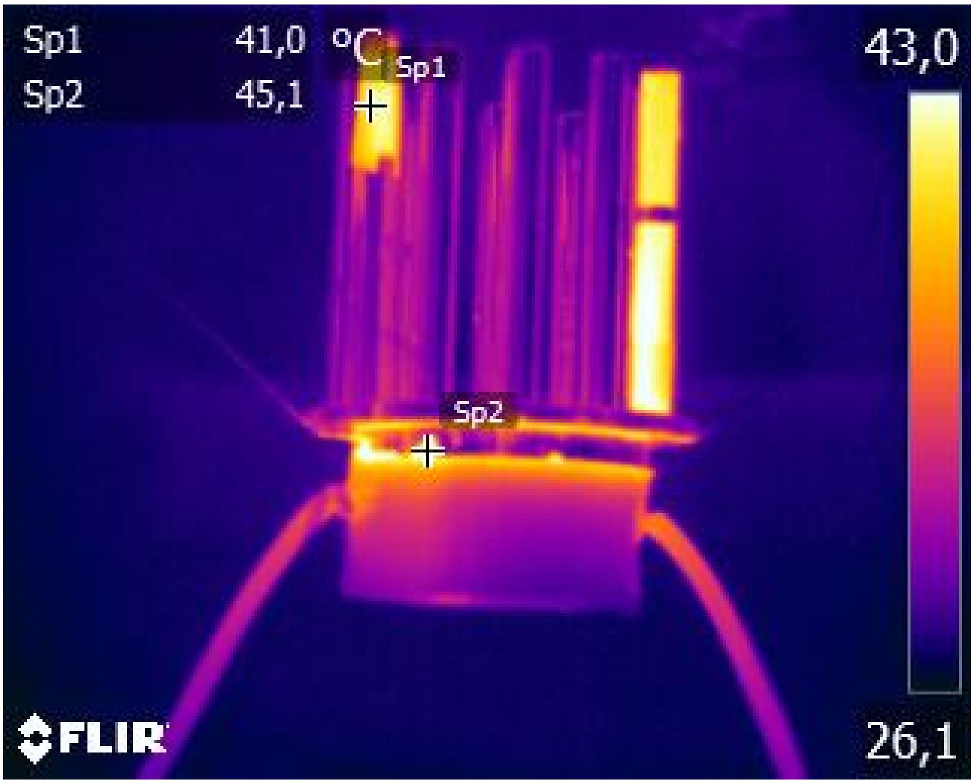

Figure E.5

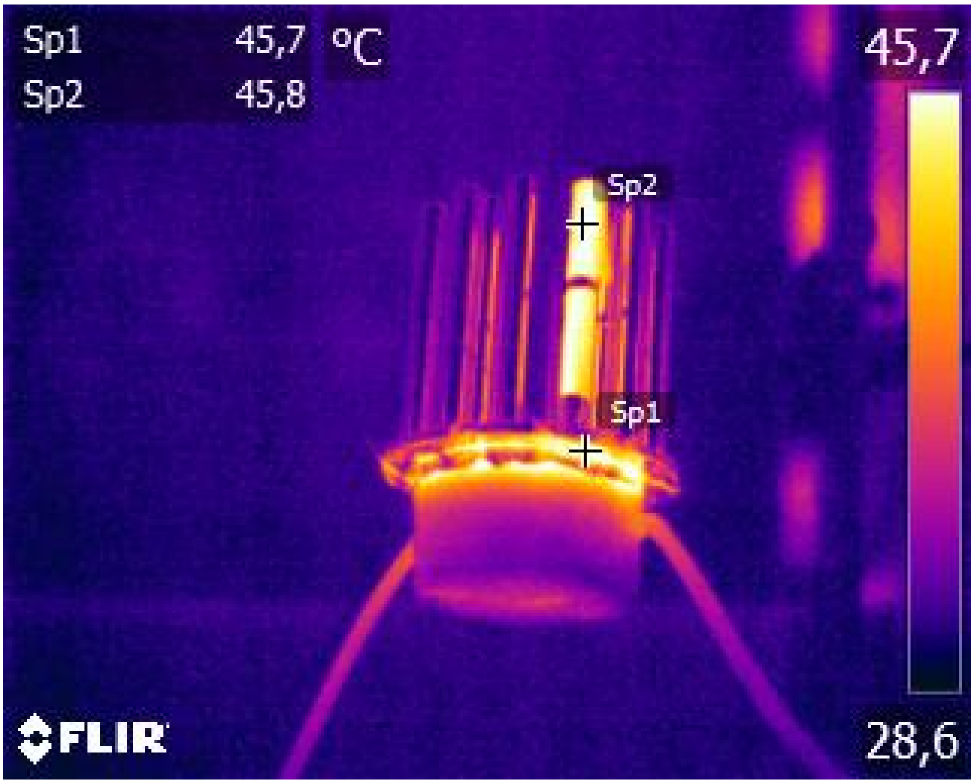

Figure E.6

F Pearson Correlation

The Pearson correlation measures the strength of linear dependence between two variables. In other words how strongly they are related to each other. The correlation coefficient has a range from -1 to 1, where 1 indicates a perfect positive correlation, -1 indicates a negative correlation, and 0 indicates no correlation. It is calculated like this:

$$r = \frac{\sum(x - \bar{x})(y - \bar{y}}{\sqrt{\sum(x - \bar{x} \sum(y - \bar{y}}} \tag{F.1}$$

Found by $(= PEARSON(array1, array2))$ or $(= CORREL(array1, array2))$ in excel

G Comparisons

G.1 Comparison of Steady State Temperature

In this section are all the comparisons shown in numbers. There are four tables below, one for each HS position and one for all of the positions all together. The tables show how good the Comsol simulations are compared to the results found in the real life experiments. The tables show four values for each experiment/simulation; 1) Experimental ΔT subtracted by *normal* mesh simulation ΔT, 2) Experimental ΔT subtracted by *fine* mesh simulation ΔT, 3) *normal* mesh simulation ΔT divided by experimental $DeltaT$, and 4) *fine* mesh simulation ΔT divided by experimental ΔT.

The "Average" is calculated by adding the absolute temperatures for all the wattage levels and dividing by number of temperature samples. Example for vertical *normal mesh*;

$$\frac{0.07 + |-1| + |-1.58| + |-2.99| + |-4.06|}{5} = 1.94$$

The same is done for the percentages.

For the "Overall" calculations the same is done as with the "Average", just will all HS positions all together.

Table G.1: Simulation results compared to expermental results in verical position

	Difference between Experiment and Simulation with *normal* mesh °C	Difference between Experiment and Simulation *fine* mesh °C	Percentage Difference *normal* mesh	Percentage Difference *fine* mesh
1w	0.07	0.58	1.25	9.71
2w	-1.00	0.02	-9.05	0.14
3w	-1.58	-0.05	-10.43	-0.30
4w	-2.99	-1.04	-15.15	-5.27
5w	-4.06	-1.61	-17.06	-6.75
Average (absolute)	1.94	0.66	10.59	4.44

Table G.2: Simulation results compared to expermental results in horzontal position

	Difference between Experiment and Simulation with *normal* mesh ℃	Difference between Experiment and Simulation *fine* mesh ℃	Percentage Difference *normal* mesh	Percentage Difference *fine* mesh
1w	-0.02	0.69	-0.26	11.42
2w	0.20	0.87	1.88	8.28
3w	-0.51	0.54	-3.41	3.61
4w	-1.29	0.11	-6.75	0.55
5w	-1.89	-0.12	-8.27	-0.53
Average (absolute)	0.78	0.47	4.11	4.88

Table G.3: Simulation results compared to expermental results in 45° position

	Difference between Experiment and Simulation with *normal* mesh ℃	Difference between Experiment and Simulation *fine* mesh ℃	Percentage Difference *normal* mesh	Percentage Difference *fine* mesh
1w	0.23	0.63	3.75	10.25
2w	-0.39	0.53	-3.53	4.82
3w	-0.91	0.16	-6.05	1.05
4w	-1.66	-0.16	-8.62	-0.82
5w	-2.53	-0.71	-10.94	-3.07
Average (absolute)	1.14	0.44	6.58	4.00

Table G.4: Simulation results compared to expermental results overall

	Difference between Experiment and Simulation with *normal* mesh ℃	Difference between Experiment and Simulation *fine* mesh ℃	Percentage Difference *normal* mesh	Percentage Difference *fine* mesh
Overall	1.29	0.52	7.09	4.44

G.2 Small changes in Comsol

In this section are small changes in Comsol compared to the temperature obtained by real life experiment. All the simulations is for vertical heat sink position at 4 W

G.2.1 Mesh Comparison

The table below show 1)the ΔT obtained by simulation, 2)the difference between the obtained ΔT and the temperature obtained by experiment, 3) the percentage difference between the obtained ΔT and the temperature obtained by experiment.

Column1	Coarser	Coarse	Normal	Fine
ΔT obtained by Comsol simulation	13.35	14.51	16.76	18.71
ΔT from experiment subtracted with simulation ΔT	6.07	4.91	2.66	0.71
Percentage difference	-31.24	-25.27	-13.71	-3.66

Figure G.1: Mesh Comparison

G.2.2 Airbox Comparison

Column1	350x300x300	450x400x400	550x500x500	650x600x600
ΔT obtained by Comsol simulation	17.40	16.76	16.73	15.81
ΔT from experiment subtracted with simulation ΔT	2.02	2.66	2.69	3.61
Percentage difference	-10.42	-13.71	-13.87	-18.60

Figure G.2: Airbox comparison

G.2.3 Flow Comparison

Column1	Incompressible	Weakly Compressible	Compressible
ΔT obtained by Comsol simulation	16.76	17.01	16.92
ΔT from experiment subtracted with simulation ΔT	2.66	2.41	2.50
Percentage difference	-13.71	-12.38	-12.87

Figure G.3: Flow comparison

G.2.4 Geometry Comparison

Column1	Quarter	Half	Full
ΔT obtained by Comsol simulation	17.78	16.76	16.65
ΔT from experiment subtracted with simulation ΔT	1.64	2.66	2.77
Percentage difference	-8.43	-13.71	-14.24

Figure G.4: Geometry comparison

G.2.5 Realistic Comparison

Column1	Screws	Electric Cables	Porous Foam	Thin Layer	All Together
ΔT obtained by Comsol simulation	16.50	14.94	16.80	16.62	15.05
ΔT from experiment subtracted with simulation ΔT	2.92	4.48	2.62	2.80	4.37
Percentage difference	-15.01	-23.07	-13.48	-14.42	-22.50

Figure G.5: Realistic comparison

G.2.6 Resistor Material Comparison

Column1	Carbon	Aluminum	Polysilicon	Steel
ΔT obtained by Comsol simulation	16.76	16.75	16.80	16.76
ΔT from experiment subtracted with simulation ΔT	2.66	2.67	2.62	2.66
Percentage difference	-13.71	-13.75	-13.50	-13.70

Figure G.6: Resistor material comparison

G.3 Optimization

In this section is a optimization comparison. The temperatures obtained for the "new" parameters are compared to the manufactured heat sink. Negative values means that the parameter is a better optimized heat sink. All the simulations is for vertical heat sink position at 4 W

G.3.1 Fin Height

Fin length	40	402	60	70	80
Temp. obtained by Comsol simulation	43.40	41.72	39.76	38.61	37.83
ΔT between manufactured HS and new trial	3.65	1.96	0.00	-1.14	-1.93
Percentage difference	9.17	4.94	0.00	-2.88	-4.85

Figure G.7: Fin height/lenght

G.3.2 Fin Diameter

Fin Diameter	4	5	5.98	7	8.2	9
Temp. obtained by Comsol simulation	42.00	40.77	39.76	39.45	39.42	39.48
ΔT between manufactured HS and new trial	2.25	1.01	0.00	-0.31	-0.33	-0.28
Percentage difference	5.65	2.54	0.00	-0.78	-0.84	-0.70

Figure G.8: Fin diameter

G.3.3 Fins in Outer Circle

Number of Fins in Inner Circle	0	2	4	6	8
Temp. obtained by Comsol simulation	40.19	39.96	39.76	39.64	39.85
ΔT between manufactured HS and new trial	0.43	0.20	0.00	-0.12	0.09
Percentage difference	1.08	0.52	0.00	-0.31	0.22

Figure G.9: Fins in Outer Circle

G.3.4 Fins in Inner Circle

Number of Fins in Inner Circle	0	2	4	6	8
Temp. obtained by Comsol simulation	40.19	39.96	39.76	39.64	39.85
ΔT between manufactured HS and new trial	0.43	0.20	0.00	-0.12	0.09
Percentage difference	1.08	0.52	0.00	-0.31	0.22

Figure G.10: Fins in Inner Circle

G.4 Other comparisons

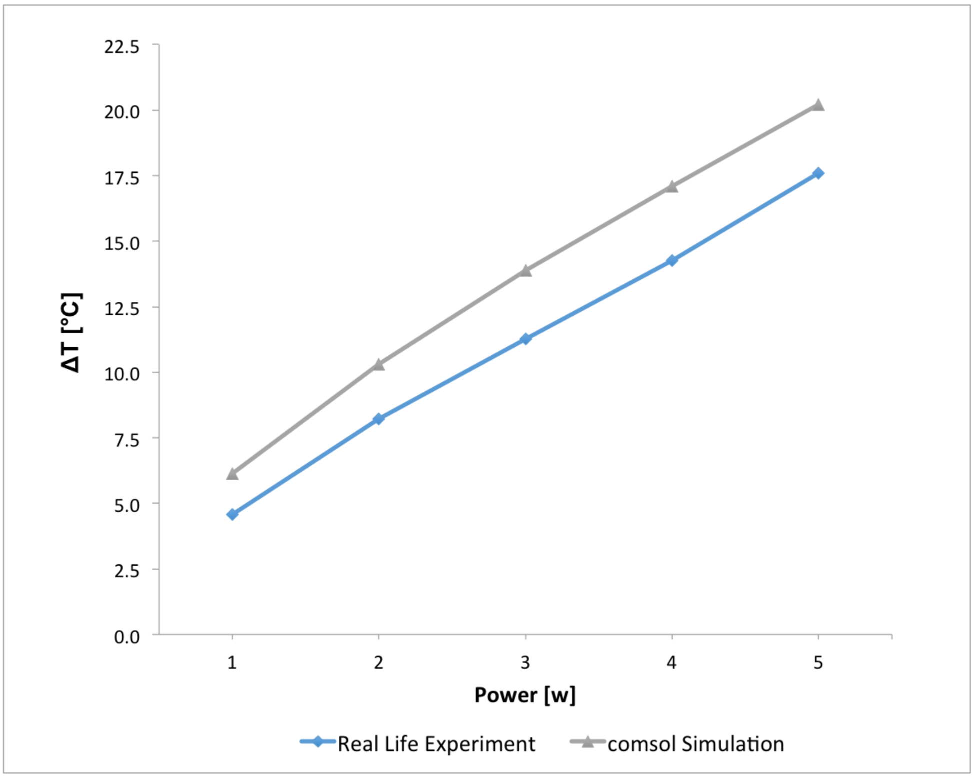

Figure G.11: Fin temperature comparison, Experiment vs Simulation (fine mesh)

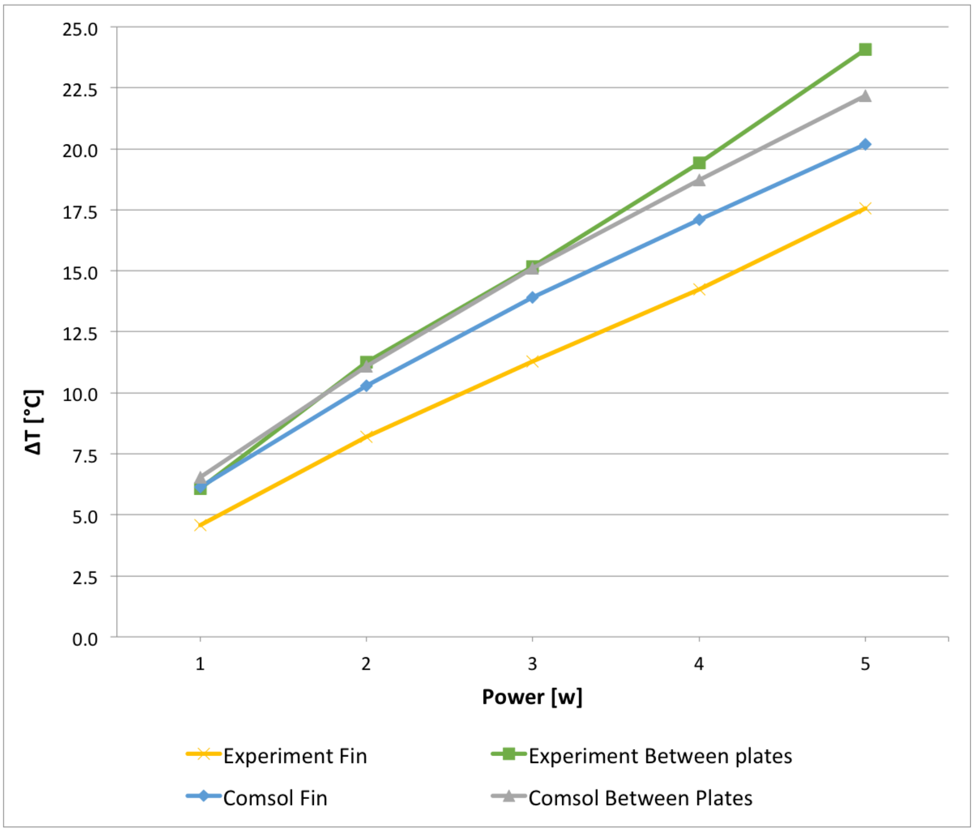

Figure G.12: Comparison of temperature development in HS vs fins in Comsol and Experiment

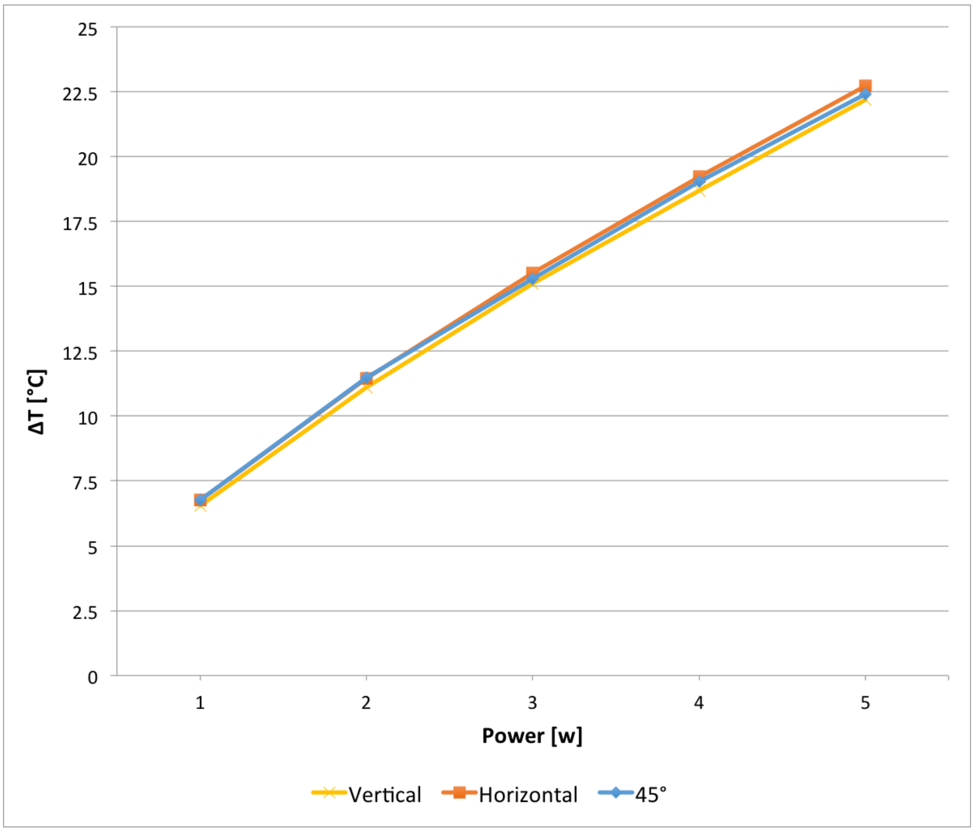

Figure G.13: Comparison between Vertical, Horizontal and 45°position in Comsol

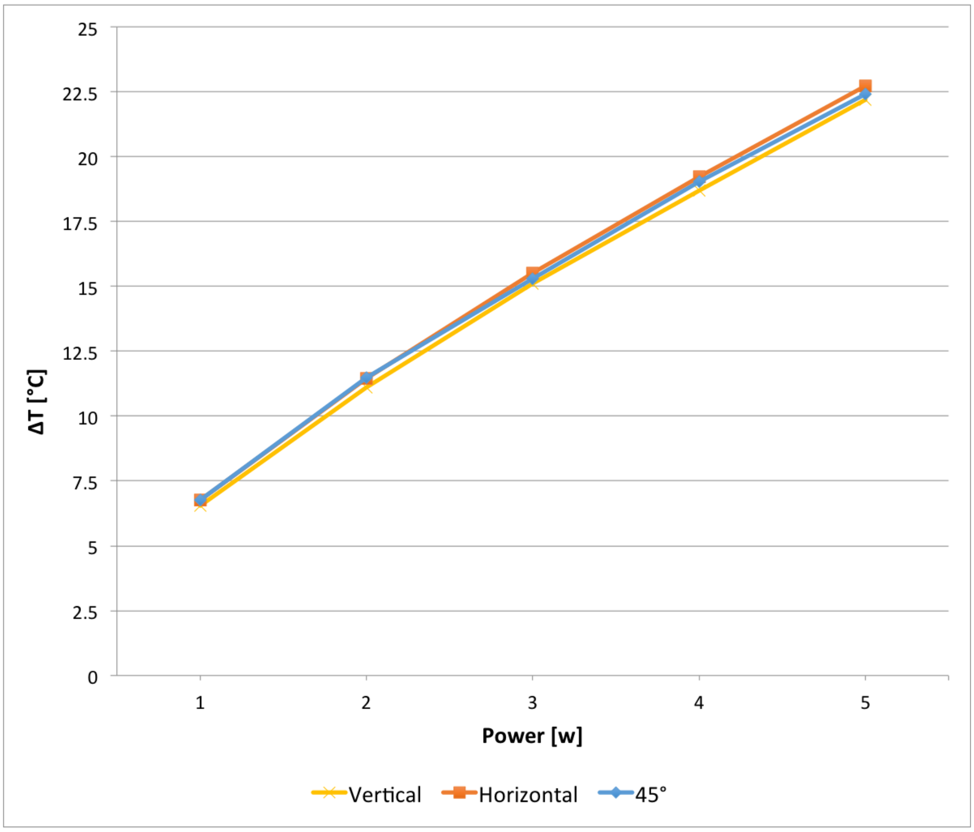

Figure G.14: Comparison between Vertical, Horizontal and 45°position in Experiments

H Fin Measurement

When doing the temperature measurement on the fin, the temperature is given as a chart showing the temperature distribution from the base of the fin to the tip. In the figures below, the charts can be seen, but first a figure of where the measurement are conducted.

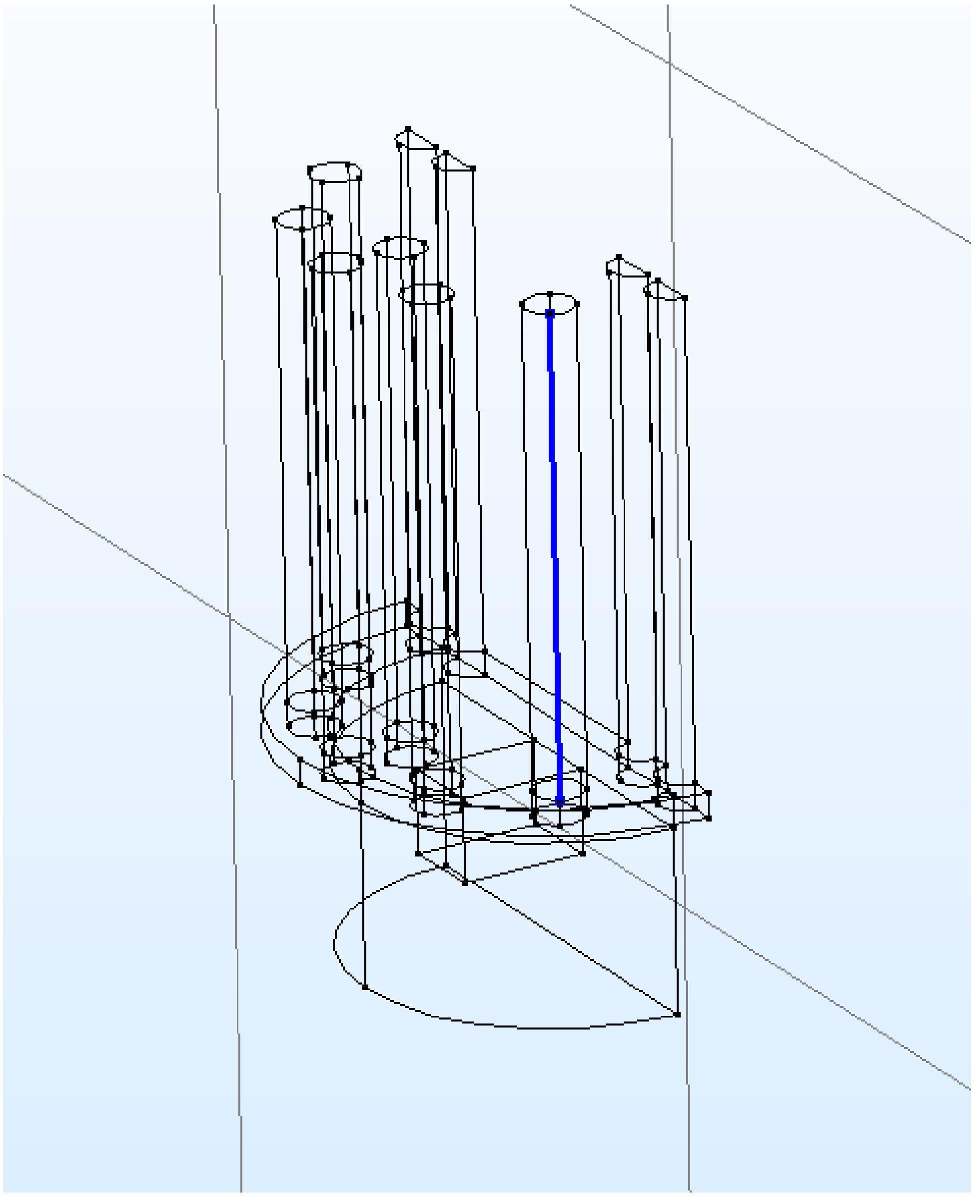

Figure H.1: Measurement point in comsol fin

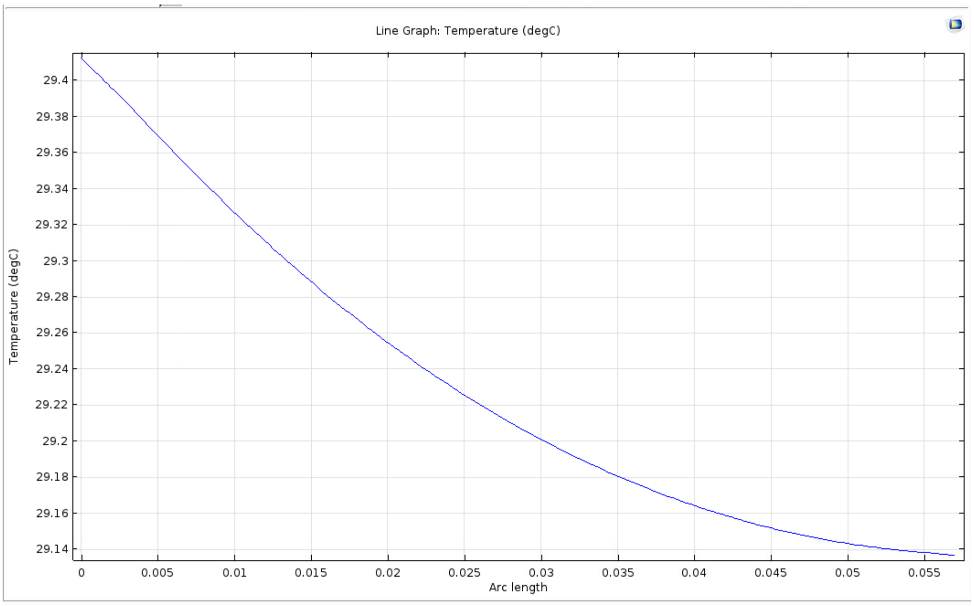

Figure H.2: Temperature distribution at 1w, fine mesh

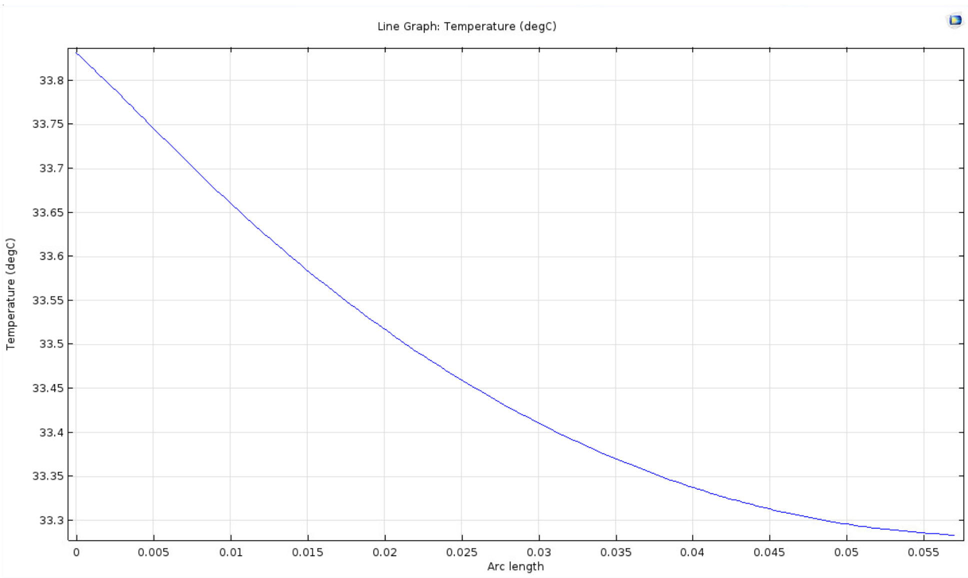

Figure H.3: Temperature distribution at 2w, fine mesh

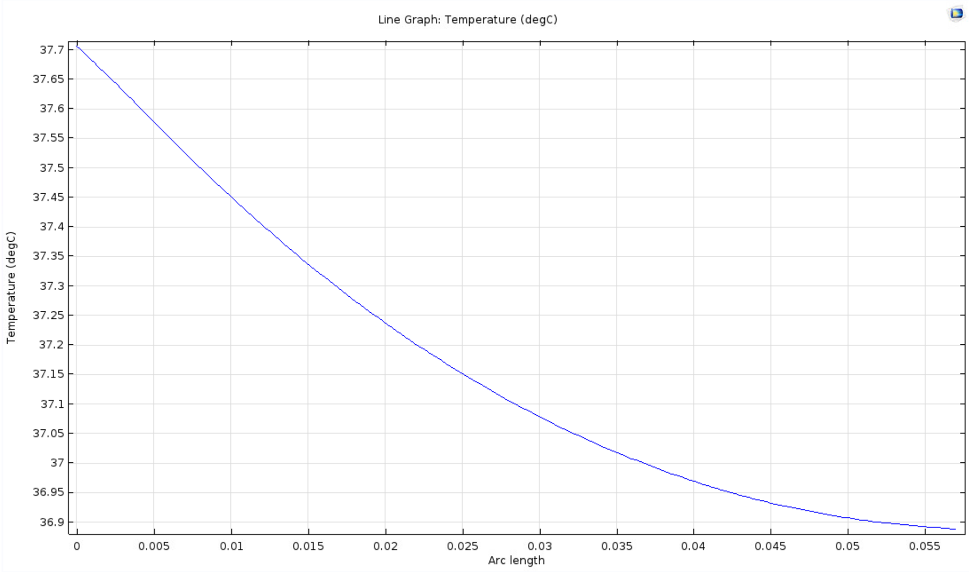

Figure H.4: Temperature distribution at 3w, fine mesh

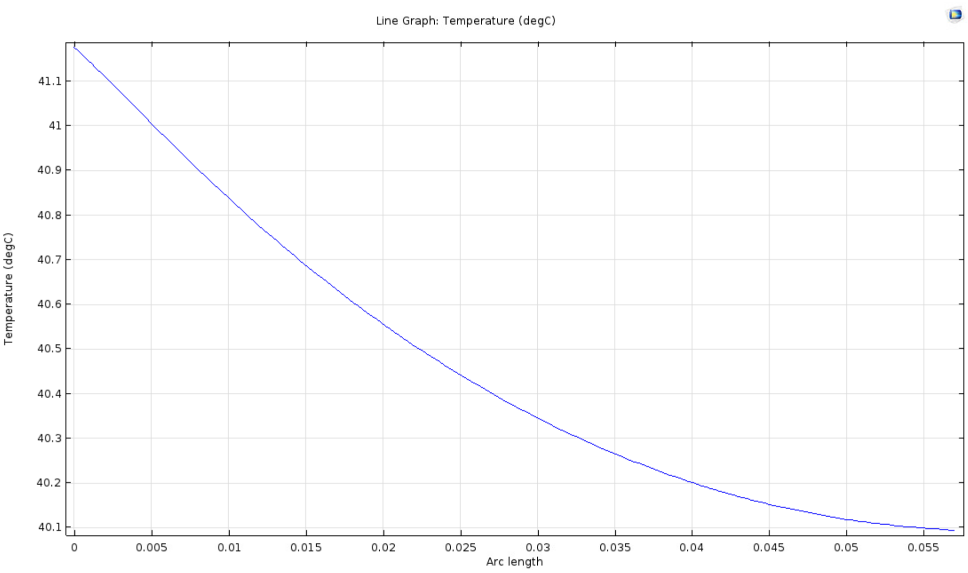

Figure H.5: Temperature distribution at 4w, fine mesh

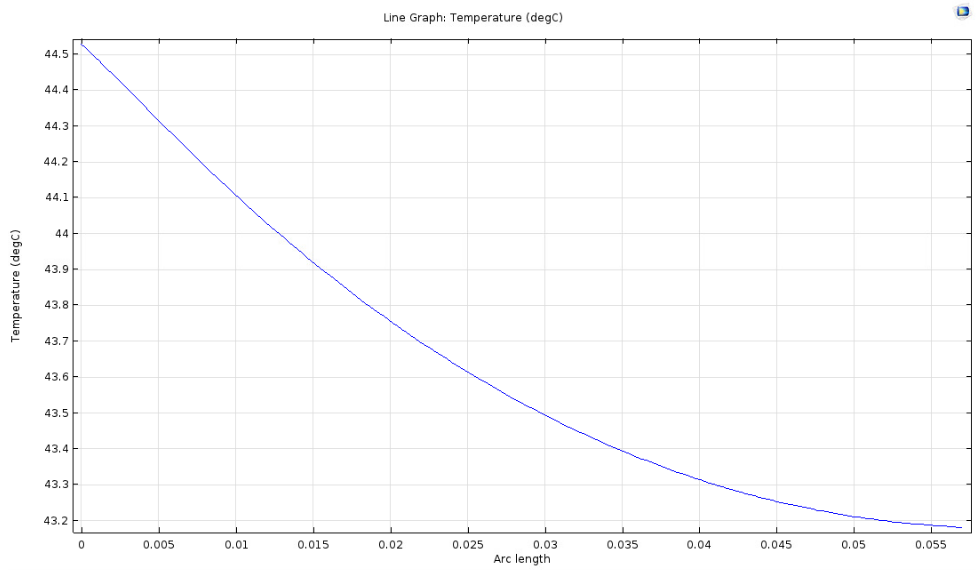

Figure H.6: Temperature distribution at 5w, fine mesh